# Protein diffusion in the cytoplasm of *Escherichia coli*

**Dissertation**

zur Erlangung des Grades eines

Doktor der Naturwissenschaften

(Dr. rer.nat.)

des Fachbereichs Biologie der Philipps-Universität Marburg

Vorgelegt von

**Nicola Bellotto**

Aus Feltre, Italien

Marburg, 2022

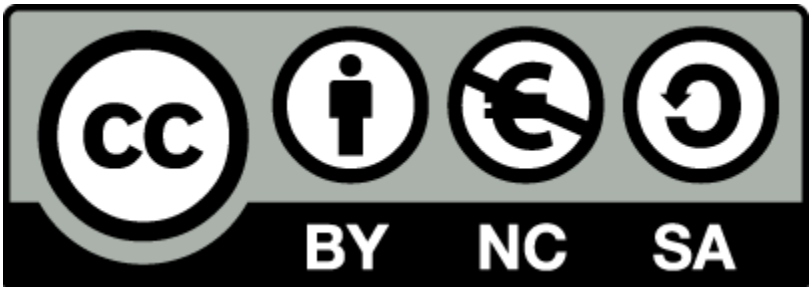

Die vorliegende Dissertation wurde von August 2018 bis Oktober 2022 am Max-Planck-Institut für terrestrische Mikrobiologie in Marburg unter Leitung von Prof. Dr. Victor Sourjik angefertigt.

Vom Fachbereich Biologie der Philipps-Universität Marburg (Hochschulkennziffer 1180) als Dissertation angenommen am _____

Erstgutachter: Prof. Dr. Victor Sourjik

Zweitgutachter: Prof. Dr. Martin Thanbichler

Weitere Mitglieder der Prüfungskommission:

Prof. Dr. Michael Bölker

Dr. Andreas Diepold

Tag der Disputation: _____

Die während der Promotion erzielten Ergebnisse wurden in folgend Originalpublikation veröffentlicht:

**N. Bellotto**, J. Agudo-Canalejo, R. Colin, R. Golestanian, G. Malengo, V. Sourjik (2022). Dependence of diffusion in *Escherichia coli* cytoplasm on protein size, environmental conditions and cell growth. *bioRxiv*, 2022.02.17.480843.
(Under revision)

# Contents

# Abbreviations

| | |
|---|---|
| GFP | Green fluorescent protein |
| FCS | Fluorescence correlation spectroscopy |
| FRAP | Fluorescence recovery after photobleaching |
| SPT | Single-particle tracking |
| MSD | Mean squared displacement |
| DNA | Deoxyribonucleic acid |
| RNA | Ribonucleic acid |
| MM | Molecular mass |
| Da | Dalton |
| IPTG | isopropyl-thiogalactopyranoside |
| OD | Optical density |
| ACF | Autocorrelation function |
| CFX | Cephalexin |
| Rif | Rifampicin |
| DMSO | Dimethyl sulfoxide |
| Cam | Chloramphenicol |
| DNP | Dinitrophenol |
| OU | Ornstein-Uhlenbeck |
| Glu | Glucose |
| CA | Casamino acids |
| ATP | Adenosine triphosphate |
| AMP | Adenosine monophosphate |
| AMP-PNP | Adenylyl-imidodiphosphate |
| CTP | Cytidine triphosphate |
| CMP | Cytidine monophosphate |
| Rpm | Revolutions per minute |
| $ddH_2O$ | Double-distilled water |

## Zusammenfassung

In prokaryontischen Zellen ist die passive translationale Diffusion für die meisten zellulären Prozesse von grundlegender Bedeutung, da sie die Sortierung von Makromolekülen, insbesondere von Proteinen, ermöglicht und die Obergrenze für den Ablauf biochemischer Reaktionen festlegt. In der stark gedrängten, begrenzten und inhomogenen Umgebung einer Bakterienzelle wird die Proteindiffusion normalerweise behindert. Allgemeine Schlussfolgerungen über die Größenabhängigkeit der Proteindiffusion aus früheren Studien zu ziehen, wurde durch die begrenzte Anzahl der untersuchten Proteinproben und durch Unterschiede in den untersuchten Stämmen, den Wachstumsbedingungen und den Messtechniken erschwert. Auch wenn die Auswirkungen verschiedener physiologischer Störungen auf Proteindiffusion bekannt sind, wurden in den meisten früheren Studien entweder große Partikel oder freies GFP als untersuchte Proben verwendet. Wie sich diese Störungen auf die Diffusionseigenschaften des Zytoplasmas über den gesamten physiologischen Größenbereich von Proteinen auswirken, bleibt unbekannt. Hier adressieren wir die vorgenannten Einschränkungen, indem wir die Mobilität einer großen Anzahl verschieden großer zytoplasmatischer fluoreszierender Proteinkonstrukte im Zytoplasma von *Escherichia coli* mittels Fluoreszenzkorrelationsspektroskopie (FCS) unter standardisierten Bedingungen systematisch analysieren. Durch Kombination experimenteller Daten mit Simulationen und theoretischer Modellierung kamen wir zu dem Schluss, dass die Proteinmobilität im Zytoplasma gut durch Brownsche Diffusion in der begrenzten Geometrie der Bakterienzelle und bei hoher Viskosität, bedingt durch makromolekulares Gedränge, beschrieben werden kann. Ausgeprägte Subdiffusion und behinderte Mobilität wurden nur bei Proteinen mit umfangreichen Wechselwirkungen innerhalb des Zytoplasmas beobachtet. Wir stellten fest, dass die Größenabhängigkeit der Proteindiffusion für die Mehrzahl der getesteten Proteine, ob arteigen oder artfremd von *E. coli*, gut mit der Stokes-Einstein-Beziehung übereinstimmt, sobald die spezifische Hantelform von Proteinfusionen berücksichtigt wird. Darüber

hinaus blieb diese Größenabhängigkeit über die verschiedenen räumlich-zeitlichen Skalen erhalten, die durch FCS und FRAP (*fluorescence recovery after photobleaching*) untersucht wurden. Eine Untergruppe von Konstrukten, die ein breites Spektrum physiologisch relevanter Proteingrößen abdeckt, wurde dann verwendet, um die Auswirkungen verschiedener biologisch bedeutsamer physikochemischer Störungen und des Zellwachstums auf die Diffusion zu untersuchen. Insbesondere wurde die Proteindiffusion in aktiv wachsenden Zellen, bei hoher Temperatur oder bei Behandlung mit Rifampicin deutlich schneller und bei hoher Osmolarität langsamer. Wichtig ist, dass alle diese Störungen Proteine unterschiedlicher Größe in denselben Proportionen betrafen, womit diese Störungen als Veränderungen einer genau definierten zytoplasmatischen Viskosität beschrieben werden konnten. Weiterhin haben wir beobachtet, dass die Reaktivierung von ATP-abhängigen Enzymen in diffusionsgestörten Zellen ausreicht, um die zytoplasmatische Bewegung und Diffusion von inertem sfGFP zu fördern. Schließlich haben wir gezeigt, dass eine katalytisch induzierte verstärkte Diffusion, die bisher nur *in vitro* beobachtet wurde, für einige ATP-abhängige Enzyme auch in lebenden Systemen nachgewiesen werden kann.

## Summary

Inside prokaryotic cells, passive translational diffusion is fundamental to most cellular processes because it allows the sorting of macromolecules, proteins in particular, and it sets the upper limit for biochemical reactions to happen. In the highly crowded, confined, and non-homogeneous environment of a bacterial cell, protein diffusion is typically hindered. Drawing general conclusions about the size dependence of protein diffusion from previous studies was hampered by the limited number of protein probes investigated and by the differences in the strain, the growth conditions, or the measurement technique. Furthermore, while the impact of several physiological perturbations on protein diffusion has been established, most of the previous studies used either large particles or free GFP as probes. How these perturbations affect the diffusional properties of the cytoplasm over the entire physiological range of protein sizes remains unknown. Here, we address these limitations by systematically analyzing the mobility of a large number of differently-sized cytoplasmic fluorescent protein constructs in the cytoplasm of *Escherichia coli* by fluorescence correlation spectroscopy (FCS) under standardized conditions. By combining experimental evidences with simulations and theoretical modeling, we concluded that protein mobility in the cytoplasm could be well described by Brownian diffusion in the confined geometry of the bacterial cell and at the high viscosity imposed by macromolecular crowding. Pronounced sub-diffusion and hindered mobility were only observed for proteins with extensive interactions within the cytoplasm. We observed that the size dependence of protein diffusion for the majority of tested proteins, whether native or foreign to *E. coli*, it was well consistent with the Stokes-Einstein relation once the specific dumbbell shape of protein fusions is taken into account. Furthermore, such size dependence was conserved over the different spatiotemporal scales explored by FCS and fluorescence recovery after photobleaching (FRAP). A subset of constructs, spanning over a wide range of physiologically relevant protein masses, was then used to probe the effect on diffusion of diverse, biologically meaningful, physicochemical

perturbations and of cell growth. In particular, protein diffusion became markedly faster in actively growing cells, at high temperature, or upon treatment with rifampicin, and slower at high osmolarity. Importantly, all of these perturbations affected proteins of different sizes in the same proportions, which could thus be described as changes of a well-defined cytoplasmic viscosity. We then observed that the reactivation of ATP-dependent enzymes in diffusionally-impaired cells is sufficient to promote cytoplasmic stirring and diffusion of inert sfGFP. Lastly, we demonstrated that catalytically-induced enhanced diffusion, previously observed only *in vitro*, can be detected for some ATP-dependent enzymes also in living systems.

# 1. Introduction

## 1.1 Theory of diffusion

Diffusion is the spontaneous movement of molecules from a region of higher to one of lower concentration. The diffusion coefficient ($D$) of a spherical molecule in a dilute, unconfined fluid can be predicted by the Stokes-Einstein relation $D \propto {}^{T}/_{(\eta R)}$ (Einstein 1906), where $T$ is the absolute temperature in Kelvin, $\eta$ the viscosity of the medium and $R$ the radius of the diffusing molecule. At the microscale, single molecules typically display thermally-driven random fluctuations of their position over time. Such phenomenon is named Brownian motion and it can be quantified from the mean squared displacement (MSD), a measure of the space "explored" by a randomly-moving molecule in the unit of time. In conditions of equilibrium, the MSD of a molecule is directly related to its diffusion coefficient, that at the spatiotemporal scale relevant for bacterial cells, is conveniently expressed as $\mu m^2/s$. The MSD scales with time as $MSD \propto t^{\alpha}$ (Figure 1.1). $\alpha$ is known as the anomalous diffusion exponent and it quantifies the so-called anomaly of diffusion. In conditions of simple diffusion driven by Brownian motion, the MSD scales linearly with time, and thus $\alpha = 1$. In complex systems, where Brownian motion is altered by the presence of obstacles, inhomogeneities, molecular interactions, or active transport (Bouchaud and Georges 1990; Metzler and Klafter 2000), anomalous diffusion can be observed. In such conditions, the MSD scales non-linearly with time, and thus $\alpha \neq 1$ (Malchus and Weiss 2010). In the anomalous sub-diffusion, the MSD scales less than linearly with time (i.e. $\alpha < 1$), typically due to confinement or crowding (see section 1.4), while in the anomalous super-diffusion the MSD scales more than linearly with time (i.e. $\alpha > 1$), typically due to active transport.

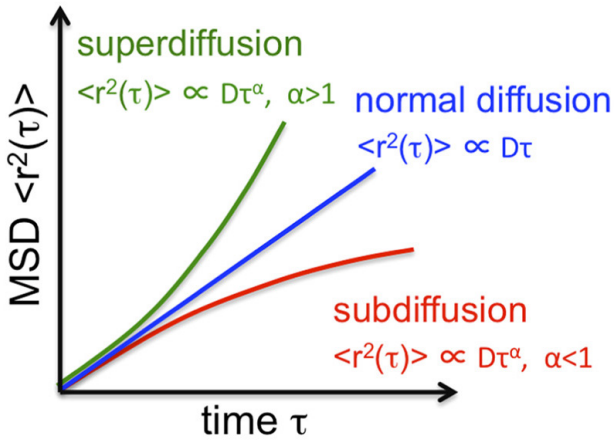


**Figure 1.1** In complex systems, the time-dependence of the mean squared displacement (MSD) is typically non-linear. More details in the sections 1.1 and 1.4. Figure from (Kapanidis, Uphoff, and Stracy 2018).

## 1.2 Diffusion in living systems

Diffusion is a central phenomenon in the physiology of living cells, both eukaryotic and prokaryotic. Primarily, diffusion allows the sorting of (macro)molecules to the locations within the cell where they perform their function. Among the other macromolecules, proteins often need to be sorted at specialized cellular sub-compartments, such as, in bacterial cells, the nucleoid, the flagellum, the different types of secretion systems, or the chemotaxis clusters. Additionally, for the so-called diffusion-limited reactions, such as protein translation (Klumpp et al. 2013), diffusion is necessary to bring the reactants close enough for the reaction to happen (Goldstein, Levine, and Torney 2007).

## 1.3 The bacterial cytoplasm is a complex medium

Bacterial cells were classically represented as membrane-enclosed “bags” where enzymes diffuse freely in a dilute cytoplasm. However, growing evidence accumulated in the past three decades (Luby-Phelps

1999; Luby-Phelps 2013), pointed out that the cytoplasm of a bacterial cell is instead a finite, crowded, complex and inhomogeneous solution (Figure 1.2) and that such properties have important consequences on the reactions happening in the cell. In fact, all the primary models for bacterial cells biology, such as *Escherichia coli*, *Bacillus subtilis*, *Caulobacter crescentus*, or *Staphylococchus aureus*, have individual cell volumes ranging from 0.4 – 3 $\mu m^3$ (Levin and Angert 2015). Such a small size is required to allow efficient nutrient uptake and elimination of waste, but typically limits the absolute number of any type of macromolecule present at one time in the cell. Moreover, the cytoplasm of bacterial cells is characterized by a very high concentration of macromolecules, ranging from 300 to 400 mg/ml (Cayley et al. 1991; Zimmerman and Trach 1991), a phenomenon known as macromolecular crowding. The macromolecular crowding is constituted primarily by proteins (~55% of the total dry weight), RNAs (~20%) and, to a minor extent, DNA (~3%) (van den Berg, Boersma, and Poolman 2017). Overall, macromolecules occupy up to 15-20% of the volume in the *E. coli* cytoplasm. The physiology of bacterial cells is profoundly affected by the macromolecular crowding. On one hand, it restricts protein mobility (Swaminathan, Hoang, and Verkman 1997), but on the other hand it promotes protein folding, protein-protein interactions (Zhou 2013), and the condensation of DNA in the nucleoid (de Vries 2010). Moreover, the great diversity in the size and chemical properties of the solutes makes the cytoplasmic environment highly inhomogeneous (Spitzer and Poolman 2013). The range of masses of cytoplasmic solutes spans over several orders of magnitude, from small molecules (~200 Da) to proteins (5 - 150 kDa), RNAs (40 kDa - 1 MDa), and large macromolecular complexes (~800 kDa for the ClpAP protease, 2.7 MDa for the intact ribosome) and up to the chromosome (~2.5 GDa). The formation of bacterial microcompartments (Yeates, Thompson, and Bobik 2011) and the liquid-liquid phase separation (André 2020) depend on the combined effect of cytoplasmic crowding and inhomogeneity.

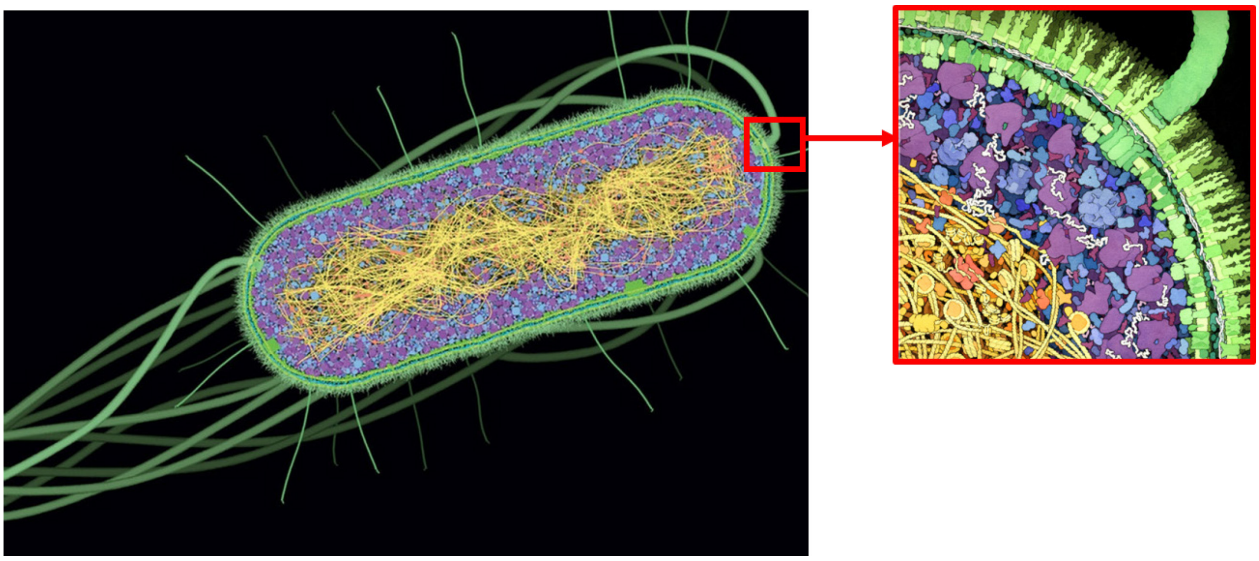

**Figure 1.2** Realistic representation of a bacterial cell. The interior of a bacterial cell is a complex medium: it is highly crowded with macromolecules (yellow: DNA, purple: ribosomes, white: messenger RNAs, blue: proteins) whose sizes and chemical properties are highly inhomogeneous. Figure adapted from (Goodsell 2009).

## 1.4 Protein diffusion in the bacterial cytoplasm

Diffusion in the confined, crowded and inhomogeneous medium of the bacterial cytoplasm is expected to substantially deviate from that in diluted solutions. The size (Muramatsu and Minton 1988), shape (Balbo et al. 2013), and nature of the crowders (Banks and Fradin 2005; Goins, Sanabria, and Waxham 2008) has been shown to affect diffusion *in vitro*. *In vitro* studies, both in solution (Banks and Fradin 2005) and on synthetic membranes (Horton et al. 2010), showed that the presence and concentration of crowders is associated with the onset of anomalous sub-diffusion. Consistently, several studies *in vivo* showed that anomalous sub-diffusion describes diffusion in the cytoplasm and in the nuclei of living eukaryotic cells better than Brownian diffusion, primarily due to the hindering effect of the cytoskeleton or the chromosomes on the diffusing particles at long spatiotemporal scales (Wachsmuth, Waldeck, and Langowski 2000; Di Rienzo et al. 2014; Sabri et al. 2020). Importantly, such effect is conserved for both

small proteins and large particles. In bacterial cells, instead, strong anomalous sub-diffusion appears to be limited to endogenous messenger RNAs and large exogenous multiprotein particles (Lampo et al. 2017; Yu et al. 2018), while small proteins rather show Brownian diffusion (Bakshi, Bratton, and Weisshaar 2011; English et al. 2011). Additionally, evidences both *in vivo* (Etoc et al. 2018) and *in silico* (Saxton 1996), suggest that anomalous sub-diffusion may also arise from the presence of interactions between the diffusing particles and the crowders. Anomalous super-diffusion it is at times observed in eukaryotic cells in presence of active transport by molecular motors (Bruno et al. 2009; Reverey et al. 2015).

## 1.5 Measuring protein diffusion in living cells

The earliest studies of cytoplasmic diffusion *in vivo* were limited to eukaryotic cells, because they required the microinjection of synthetic fluorescent particles in the cell of interest, an operation impractical in the much smaller bacterial cells (Wojcieszyn et al. 1981). It was only with the possibility to clone and endogenously express the green fluorescent protein (GFP) that techniques based on light microscopy became available to study protein mobility also in living bacterial cells. The most widely applied techniques are single-particle tracking (SPT), fluorescence recovery after photobleaching (FRAP) and fluorescence correlation spectroscopy (FCS).

### 1.5.1 Single-particle tracking (SPT)

In SPT (Figure 1.3A), time-series of microscopy images of diffusing particles are acquired at subdiffractional resolution. By connecting the position of the particle in each image, single-particle trajectories are reconstructed. Curves of time dependence of the MSD are then calculated and, from their fitting with biophysical models corresponding to the expected diffusional process, diffusion coefficients are extrapolated (Manzo and Garcia-Parajo 2015; Kapanidis, Uphoff, and Stracy 2018).

### 1.5.2 Fluorescence recovery after photobleaching (FRAP)

With FRAP (Figure 1.3B), the fluorescent molecules in a region of the cell of interest are irreversibly photobleached by a short pulse of a high intensity laser. Due to the process of diffusion, unbleached fluorophores from the surrounding areas will diffuse into the bleached area, while bleached fluorophores will diffuse out. These processes will lead to the recovery of fluorescence in the bleached area, and the rate of recovery depends on the mobility of the diffusive molecules (Loren et al. 2015).

### 1.5.3 Fluorescence correlation spectroscopy (FCS)

With FCS (Figure 1.3C), the observation volume of a confocal microscope is positioned in the cell of interest and the intensity of fluorescence is measured over time. Due to the process of diffusion, the intensity of fluorescence will fluctuate over time. From the statistical analysis of the fluorescence intensity fluctuations, the average time required by the fluorescent molecule to cross the observation volume is extracted (Elson 2011; Ries and Schwille 2012).

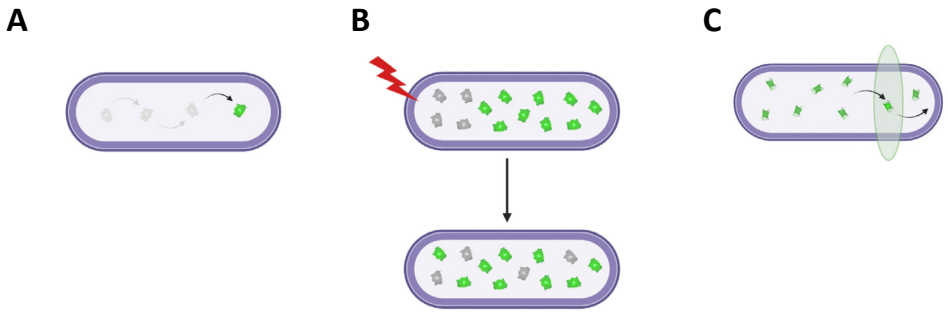


**Figure 1.3** Schematic representation of the principles that allow the measurement of fluorescent proteins diffusion with single-particle tracking (SPT; A), fluorescence recovery after photobleaching (FRAP; B), and fluorescence correlation spectroscopy (FCS; C).

### 1.5.4 Comparison between different techniques

These techniques are, to some extent, complementary (Figure 1.4). SPT, due to the uncertainty in localizing with high precision the fast-diffusive proteins, is primarily suited to measure the mobility of

membrane proteins or large cytoplasmic complexes. Nevertheless, recent advancements, such as single-molecule displacement/diffusivity mapping (SMdM), improved the sensitivity of SPT to the faster diffusive molecules (Xiang et al. 2020). While in the past two decades FRAP has been largely and successfully applied in bacteria, FCS is arguably the best suited technique for fast diffusive, cytoplasmic proteins. Moreover, while SPT requires dedicated, photoactivable, fluorophores (e.g. PA-mKate), FCS and FRAP reliably quantify protein mobility making use of ordinary GFP variants, provided they are monomeric and sufficiently brilliant. Both SPT and FCS operate best at low, and thus more physiological, expression level of the fluorescent protein and can more efficiently distinguish between Brownian and anomalous diffusion than FRAP. Additionally, SPT and FCS measure protein mobility locally within the cell, with FCS having also a significantly better temporal resolution than FRAP and SPT. On the contrary, FRAP is more sensitive to the large-scale mobility of freely-diffusive proteins.

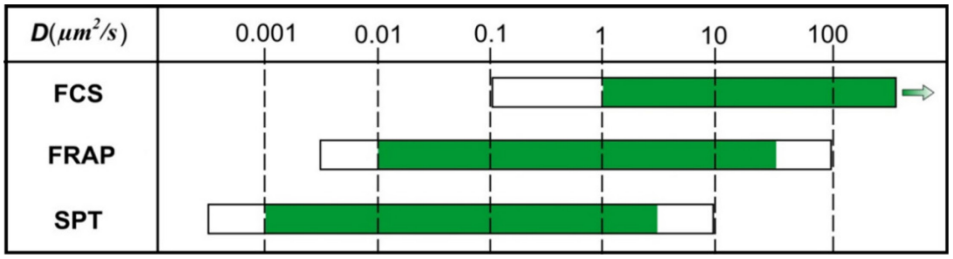


**Figure 1.4** Suitability of different light microscopy-based techniques to measure molecular diffusion in the indicated intervals of diffusion coefficient. The green part of the bars indicates the optimal range for each technique, the white part indicates the ranges of diffusion coefficients where the technique may be situationally useful. Figure adapted from (Loren et al., 2015).

## 1.6 Diffusion of fluorescent proteins in the bacterial cytoplasm

Fluorescent proteins like GFP, or its spectral variants, are often the probes of choice to study diffusion in bacteria because they lack interactions with other cellular components and can be expressed endogenously without introducing toxicity for the host cell. Different studies obtained a fairly wide range of estimates

on the diffusion coefficient of GFP in the cytoplasm of bacteria. The earliest studies based on FRAP provided values for the diffusion of GFP ranging from 3 to 9 $\mu m^2/s$ (Elowitz Michael et al. 1999; Konopka et al. 2006; Mullineaux et al. 2006; Kumar, Mommer, and Sourjik 2010; Mika et al. 2010; Nenninger, Mastroianni, and Mullineaux 2010), while a more recent one provided a faster diffusion coefficient, around 11 $\mu m^2/s$ (Schavemaker, Smigiel, and Poolman 2017). Measurements performed with FCS or SPT are in substantial agreement with the more recent FRAP measurements, providing estimates of the diffusion coefficient of GFP ranging from 8 to 18 $\mu m^2 s^{-1}$ (Meacci et al. 2006; English et al. 2011; Sanamrad et al. 2014; Rowland, Tuson, and Biteen 2016; Diepold et al. 2017; Rocha et al. 2019; Śmigiel et al.). The diffusion of GFP in the cytoplasm of bacteria is seven to ten times slower than in buffer (Terry, Matthews, and Haseloff 1995; Swaminathan, Hoang, and Verkman 1997), a clear indication of its high crowding and inhomogeneity.

## 1.7 Dependence of protein diffusion on protein size and charge, environmental conditions, antibiotics treatment, and cellular metabolism

Previous studies demonstrated that in bacterial cells the translational diffusion of cytoplasmic particles is influenced by properties of the proteins themselves, such as their mass, surface charge and protein-protein interactions, by properties of the cytoplasmic environment, such as the level of macromolecular crowding and cytosolic viscosity, and is affected by treatments with antibiotics and the overall cellular metabolism.

### 1.7.1 Size dependence of protein diffusion in the bacterial cytoplasm

As described in section 1.1, according to the Stokes-Einstein equation, the diffusion coefficient of a molecule is inversely proportional to its radius *R*. For globular proteins, *R* is accurately predicted by the radius of gyration (Tyn and Gusek 1990), which is the average distance of any point in a protein from its

center of mass. The radius of gyration depends on the molecular mass ($MM$) as $R \propto MM^{\beta}$. The exponent $\beta$ would be 0.33 for perfectly compact spherical particles. Evidences from experiments of small-angle X-ray scattering (SAXS) with globular proteins (Smilgies and Folta-Stogniew 2015) and theorical simulations (Enright and Leitner 2005), agree that $\beta$ is in practice within the range 0.35-0.43 for typical globular proteins. Such higher values, that reflect the fractal nature of the spatial distribution of protein mass, suggest that the size dependence of protein diffusion in solution is already steeper than what predicted by the Stokes-Einstein equation. In the highly crowded, inhomogeneous and confined environment of the bacterial cytoplasm, the Stokes-Einstein relation may then not be valid at all. One of the earliest studies of diffusion in bacteria already showed that the GFP fusion of the endogenous protein CheY displays a diffusion coefficient slower than free GFP (Cluzel, Surette, and Leibler 2000). Since then, several studies explicitly aimed at quantifying the size dependence of protein diffusion in bacterial cytoplasm (Figure 1.5). These studies yielded fairly different results, ranging from values consistent with the Stokes-Einstein relation for perfectly compacted spherical particles (~0.33 (Nenninger, Mastroianni, and Mullineaux 2010)), to values steeper than predicted by the Stokes-Einstein relation, even when considering imperfect protein globularity (~ 2 (Kumar, Mommer, and Sourjik 2010), ~ 0.7 (Mika et al. 2010; Stracy et al. 2021), and ~ 0.54(Śmigiel et al. 2022)). The same value of $\beta \sim 0.7$ was extrapolated from the pooled data from multiple studies (Kalwarczyk, Tabaka, and Holyst 2012).

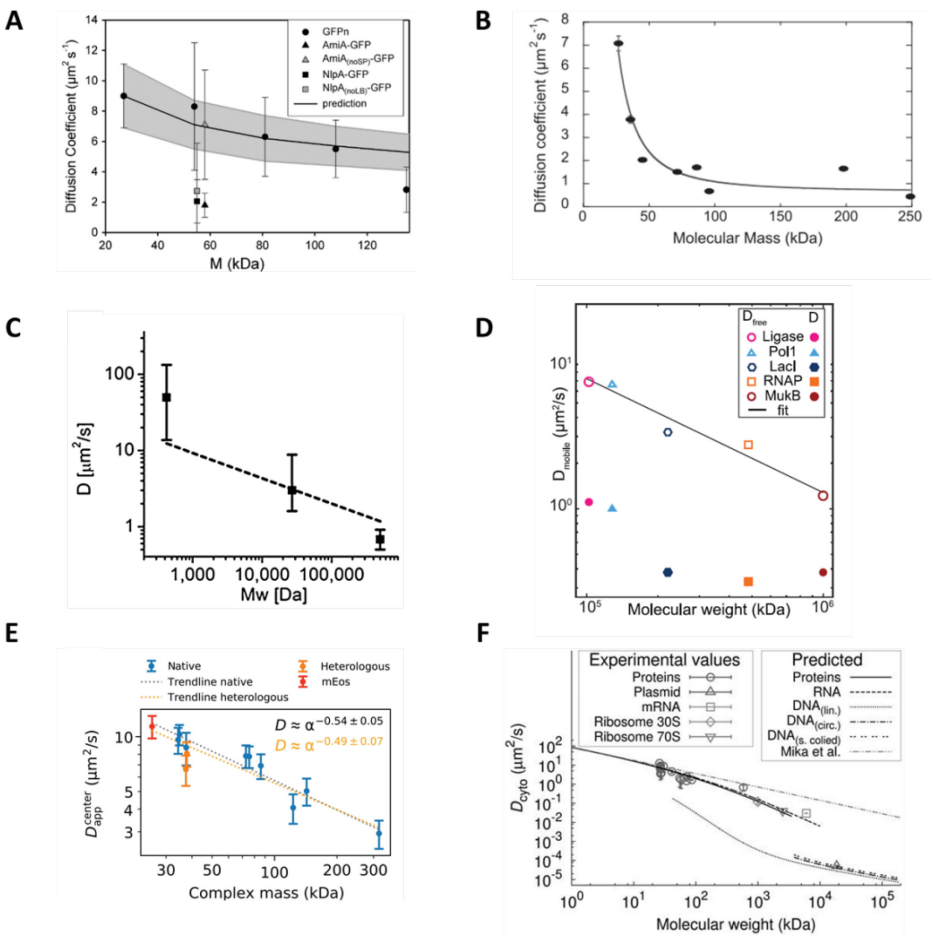


**Figure 1.5** Size dependence of protein diffusion in *E. coli* cytoplasm as quantified from different, independent studies. A taken from (Nenninger, Mastroianni, and Mullineaux 2010), B from (Kumar, Mommer, and Sourjik 2010), C from (Mika et al. 2010), D from (Stracy et al. 2021), E from (Śmigiel et al. 2022), and F from (Kalwarczyk, Tabaka, and Holyst 2012).

The conclusions from these studies are partially limited by the small number of proteins each of them investigated, and the apparently large discrepancies in the estimated size dependence may thus simply reflect the peculiar properties of the chosen protein probes. Nevertheless, the results from most of these studies, highlighted a pronounced non-globularity of the investigated cytoplasmic probes (*i.e.* $\beta > 0.4$), a conclusion consistent with the typical shape of the fluorescent constructs, where two or more proteins are connected by flexible linkers. For such multidomain proteins, shape fluctuations and hydrodynamic

interactions between the different domains can have a sizeable effect on the effective diffusion coefficient of the whole protein (Agudo-Canalejo and Golestanian 2020), and they might thus be important to consider when interpreting deviations from the Stokes-Einstein relation.

### 1.7.2 Effect of surface properties on protein mobility

Different studies experimentally investigated the role of a protein's surface in determining its diffusional properties. In a first study (Schavemaker, Smigiel, and Poolman 2017), the diffusion of a set of GFP mutants with a net surface charge ranging from – 30 to + 25 was measured by FRAP in *E. coli*. The mean diffusion coefficient of the negatively charged mutants was found the same as that of neutral GFP, ~11 $\mu m^2/s$. As the charge increases, the diffusion coefficient decreases down to 0.14 $\mu m^2/s$ for + 25 GFP. Further evidences from *in vivo* and *in vitro* experiments, suggested that the slower diffusion of positively charged mutants is caused by interactions with mRNA-ribosome complexes. This finding lead to speculate that the bacterial proteome evolved to minimize the presence of positively charged amino acids on the surface of proteins that do not require to interact with nucleic acids. In a more general framework, the existence of an organism-dependent physicochemical code of surface charge and hydrophobicity was postulated. The adherence to this code would minimize non-specific, short-living, "quinary" protein-protein interactions (McConkey 1982). The existence of such code would explain the reduced mobility, due to their increased stickiness, of heterologous human proteins (Mu et al. 2017) in *E. coli* cytoplasm compared with their endogenous counterparts.

### 1.7.3 Dependence of protein mobility on environmental osmolarity and temperature

Environmental perturbations that alter the macromolecular crowding and viscosity of the cytoplasm, have been shown to also affect the mobility of cytoplasmic probes.

A great effort was put by different groups into characterizing the effects of osmotic upshift on the bacterial cytoplasm. As *E. coli* cells are exposed to higher osmolarity, cytoplasmic water is extruded, the

macromolecular crowding increases and the mobility of cytoplasmic probes decreases (Konopka et al. 2006; Wlodarski et al. 2020). At the highest values of osmolarity, the nucleoid creates physical barriers to free diffusion (Mika et al. 2010). *E. coli* can counteract the osmotic effect, and partially restore faster protein mobility, in the short term by taking up potassium ions from the medium, and in the long term by synthetizing specific osmoprotectants molecules (Konopka et al. 2009; Liu et al. 2019). Importantly, such effect of osmotic upshift on cytoplasmic dynamics was quantified using either free GFP (Konopka et al. 2006; Konopka et al. 2009; Liu et al. 2019), or large protein complexes (Mika et al. 2010) and exogenous multiprotein particles (Wlodarski et al. 2020).

The effect of environmental temperature on protein mobility has been so far only marginally investigated. According to the Stokes-Einstein relation, reported in 1.1, the diffusion of a molecule depends directly on the system's temperature in Kelvin and inversely on the viscosity of the fluid, which itself changes with temperature. In the biologically relevant range, the sensitivity of diffusion to temperature is primarily determined by the temperature dependence of water viscosity. Consistently, diffusion of GFP in the cytoplasm of the bacterium *Listeria monocytogenes* was recently reported to increase with the environmental temperature in the range 7 - 48°C (Tran et al. 2021) to an extent larger than what expected from the Stokes-Einstein relation. Paradoxically, if the cultures are grown at temperatures >30°C and then diffusion is measured at the same temperature, diffusion appears to rather decrease as the environmental temperature increases, possibly due to peculiar adaptations in the proteome composition of cells grown at high temperatures. Similarly, it has been recently demonstrated that the budding yeast *Saccharomyces cerevisiae* synthesizes carbohydrates (glycogen and trehalose) to adapt the viscosity of its cytoplasm to the environmental temperature and to thus keep a constant rate of cytoplasmic diffusion (Persson, Ambati, and Brandman 2020). It remains to be investigated if *E. coli* possess similar growth-temperature adaptations of cytoplasmic structure.

### 1.7.4 Effects of antibiotics treatment on protein diffusion

Antibiotics exert their antimicrobial activity by interacting with specific and well characterized cellular targets and inhibiting vital cellular processes. They have also been shown to have more profound effects on the structure of the cytoplasm, in particular on the conformation of the nucleoid. The treatment of *E. coli* cells with chloramphenicol, an inhibitor of the peptidyl transferase activity of the ribosome, leads to the condensation of the nucleoid (Chai et al. 2014; Bakshi et al. 2014), while the treatment with rifampicin, an inhibitor of the β subunit of the RNA polymerase, leads to nucleoid expansion (Cabrera Julio et al. 2009; Bakshi et al. 2014). In more recent years, the impact of antibiotics treatment on cytoplasmic diffusion has been investigated. In particular, the treatment with rifampicin has been observed to increase the mobility of large endogenous particles in *Bacillus subtilis* (Rotter et al. 2021), and of large multiprotein particles in *E. coli* (Wlodarski et al. 2020). Instead, no effect of chloramphenicol was observed on the mobility of large multiprotein particles (Wlodarski et al. 2020). The increased mobility after rifampicin treatment may depend on a reduced confinement of the investigated particles at the cell poles (Rotter et al. 2021) or on the more general reduction in macromolecular crowding after RNA knockdown (Wlodarski et al. 2020). Importantly, the conservation of the rifampicin effect for small proteins, or a possible size-specific effect of chloramphenicol, has not yet been investigated.

### 1.7.5 Effects of metabolism and energy state on protein diffusion

A number of studies focused on the effect of metabolism on cytoplasmic diffusion. When the synthesis of ATP is blocked, the cytoplasm of *E. coli* turns from a fluid to a glass-like state where the mobility of large particles, both endogenous and exogenous, is strongly impaired (Parry et al. 2014). Importantly, a similar decrease in cytoplasmic mobility is observed also in yeast cells after energy depletion (Munder et al. 2016) or glucose starvation (Joyner et al. 2016). The observation that a similar reduction in mobility is not observed for GFP (Montero Llopis et al. 2012), suggests that the size of the probe is a crucial parameter

to consider when investigating the effect of physicochemical perturbations on the cytoplasm viscosity. Moreover, despite these findings, the exploration of possible interplays between cellular metabolism, biosynthetic activity and cell growth in the regulation of cytoplasmic fluidity and diffusion at the level of single proteins is still lacking.

## 1.8 Enhanced protein diffusion

Growing evidence gathered in the last decade, showed that the diffusion coefficients of enzymes from different classes (such as catalase, urease, alkaline phosphatase, aldolase) increases in presence of their substrate, and that this increase directly depends on their catalytical activity (Muddana et al. 2010; Riedel et al. 2015; Xu et al. 2019). Importantly, even the diffusion of inert tracers increases when they are dispersed in active enzyme solutions (Zhao et al. 2017). Several interpretations, based on both experimental results and theoretical simulations, have been proposed to explain these observations: chemoacustic effect, where the heat released during the catalysis generates a pressure wave that propels the enzyme (Riedel et al. 2015), phoretic effect along self-generated concentration gradients (Colberg and Kapral 2014), collective hydrodynamic effects (Mikhailov and Kapral 2015) and conformational fluctuations of dumbbell-shaped enzymes (Illien et al. 2017), only to mention some. In presence of a gradient of substrate, such enhanced enzyme diffusion can lead to the chemotaxis of the enzyme along the gradient (Yu et al. 2009; Sengupta et al. 2013; Sengupta et al. 2014; Dey et al. 2014; Zhao et al. 2018). All the experimental evidences of enhanced enzyme diffusion and chemotaxis were provided by experiments with FCS or SPT, performed, however, uniquely *in vitro*. While for some endogenous enzymes it might be possible to observe reduced diffusion by knocking out their substrate's biosynthetic pathway, the fine-tuning of substrate concentrations that is necessary to effectively demonstrate real enhanced enzyme diffusion remains challenging inside a living cell.

# 2. Aim

Protein diffusion is a fundamental phenomenon in all living cells since it allows the relocation of (macro)molecules to the cellular district where their function is required and it limits the rates of biochemical reactions. While extensive work has been carried out in the past years to elucidate the spatiotemporal dynamics of protein diffusion in bacterial cells, a number of questions still remain open. This work aimed to answer some of them. At first, we aimed to clarify whether protein diffusion in the bacterial cytoplasm is Brownian or anomalous, by combining experiments with simulations and mathematical models. We then aimed to develop a biophysical model that would accurately represent the observed size dependence of protein diffusion in bacterial cytoplasm. Next, we investigated how the size dependence of protein diffusion is influenced by different physicochemical perturbations and by the cellular state. Lastly, we aimed to prove that enhanced diffusion of enzymes could be observed in living systems.

# 3. Results

## 3.1 Construction of a sfGFP-tagged library of proteins endogenous of *E. coli*

One of the main drawbacks of previous studies on the size dependence of protein diffusion in *E. coli* cytoplasm was the limited sample size that was investigated. Therefore, we generated a plasmid-encoded library of 31 cytoplasmic proteins (Table 1) of *E. coli* fused to superfolder GFP (sfGFP). We followed several criteria in selecting the proteins to be included in the library. While the fusion to GFP normally does not compromise protein functionality, the association of subunits in homomultimers is at times reported to be affected by fusion to GFP (Montecinos-Franjola et al. 2020). To prevent uncertainties on the oligomeric state, and thus on the size, of the GFP constructs, we considered only monomeric proteins. DNA-binding proteins are known to display complex diffusional behavior, due to the combination of 3D diffusion in the cytoplasm, binding and 1D sliding along DNA (Stracy et al. 2021). We therefore selected only proteins that are not known to bind DNA, although we did not exclude *a priori* proteins that interact with other proteins. The structure of all selected proteins is known and roughly globular, avoiding effects of the irregular protein shape on mobility. The proteins we ultimately included in the library belong to different cellular pathways and perform different enzymatic activities (Table 1).

**Table 1.** Molecular mass, biological function and diffusional parameters for all the sfGFP-constructs measured in this study. The number of cells measured with each technique is also indicated.

| Protein name | Molecular mass of sfGFP-construct | Biological function | IPTG concentration for FCS (for FRAP) | Number of cells (FCS) | $\tau_D$ (µs; avg. ± SE) | α (Avg. ± SE) | Diffusion coefficient, FCS (µm²/s, Avg. ± SE) | Number of cells (FRAP) | Diffusion coefficient, FRAP (µm²/s, Avg. ± SE) |
|---|---|---|---|---|---|---|---|---|---|
| *sfGFP* | 26.9 | - | 5 µM (15 µM) | 52 | 561 ± 14 | 0.86 ± 0.01 | 14.7 ± 0.3 | 11 | 11.3 ± 1.3 |
| *YggX* | 39.2 | Probable Fe (2+)-trafficking protein | 5 µM (5 µM) | 8 | 611 ± 19 | 0.85 ± 0.01 | 12.9 ± 0.4 | 10 | 9.4 ± 1.6 |
| *ClpS* | 39.2 | ATP-dependent Clp protease adapter protein | 0 µM | 11 | 1054 ± 33 | 0.75 ± 0.01 | | | |
| *FolK* | 45.1 | 2-amino-4-hydroxy-6-hydroxymethyldihydropteridine pyrophosphokinase | 0 µM | 8 | 734 ± 24 | 0.87 ± 0.01 | 11.6 ± 0.4 | | |
| *Crr* | 45.2 | Component of glucose-specific phosphotransferase enzyme IIA | 0 µM | 14 | 1065 ± 36 | 0.87 ± 0.01 | | | |
| *UbiC* | 45.7 | Chorismate pyruvate-lyase | 15 µM | 14 | 1140 ± 58 | 0.87 ± 0.01 | | | |
| *ThpR* | 46.9 | RNA 2',3'-cyclic phosphodiesterase | Discarded due to instability of sfGFP-construct | | | | | | |
| *CoaE* | 49.6 | Dephospho-CoA kinase | 0 µM | 11 | 854 ± 47 | 0.87 ± 0.01 | 9.8 ± 0.6 | | |
| *Adk* | 50.6 | Adenylate kinase | 5 µM (15 µM) | 23 | 802 ± 26 | 0.88 ± 0.00 | 10.6 ± 0.4 | 16 | 9.8 ± 1.5 |
| *Cmk* | 51.7 | Cytidylate kinase | 5 µM | 16 | 1163 ± 58 | 0.87 ± 0.01 | | | |
| *NagD* | 54.1 | Ribonucleotide monophosphatase | Discarded due to non-uniform protein localization | | | | | | |
| *KdsB* | 54.6 | 3-deoxy-manno-octulosonate cytidylyltransferase | 0 µM | 11 | 1659 ± 70 | 0.84 ± 0.01 | | | |
| *Map* | 56.3 | Methionine aminopeptidase | 0 µM | 20 | 1830 ± 78 | 0.81 ± 0.01 | | | |
| *MmuM* | 60.4 | Homocysteine S-methyltransferase | 5 µM | 14 | 2241 ± 138 | 0.73 ± 0.01 | | | |
| *RihA* | 60.8 | Pyrimidine-specific ribonucleoside hydrolase | Discarded due to non-uniform protein localization | | | | | | |
| *PanE* | 60.8 | 2-dehydropantoate 2-reductase | 0 µM (5 µM) | 18 | 1059 ± 26 | 0.85 ± 0.01 | 7.8 ± 0.2 | 11 | 5.2 ± 0.6 |
| *SolA* | 67.9 | N-methyl-L-tryptophan oxidase | 0 µM | 7 | 795 ± 31 | 0.82 ± 0.01 | 9.9 ± 0.5 | | |
| *Pgk* | 68.1 | Phosphoglycerate kinase | 0 µM | 16 | 991 ± 41 | 0.90 ± 0.01 | 8.6 ± .0.3 | | |
| *EntC* | 69.9 | Isochorismate synthase | 15 µM | 15 | 1777 ± 119 | 0.82 ± 0.01 | | | |
| *AroA* | 73.1 | 3-phosphoshikimate 1-carboxyvinyltransferase | 5 µM | 9 | 995 ± 69 | 0.86 ± 0.01 | 8.7 ± 0.7 | | |
| *ThrC* | 74.1 | Threonine synthase | 0 µM | 14 | 908 ± 28 | 0.87 ± 0.01 | 9.1 ± 0.3 | | |
| *MurF* | 74.4 | UDP-N-acetylmuramoyl-tripeptide--D-alanyl-D-alanine ligase | 0 µM | 7 | 1008 ± 76 | 0.85 ± 0.02 | 8.3 ± 0.7 | | |
| *DsdA* | 74.9 | D-serine dehydratase | 0 µM | 14 | 1017 ± 53 | 0.89 ± 0.01 | 8.4 ± 0.4 | 10 | 7.8 ± 0.7 |
| *HemN* | 79.7 | Oxygen-independent coproporphyrinogen III oxidase | 0 µM | 13 | 1262 ± 54 | 0.86 ± 0.01 | 6.7 ± 0.4 | | |
| *PrpD* | 80.9 | 2-methylcitrate dehydratase | 0 µM | 12 | 1866 ± 140 | 0.84 ± 0.01 | | | |
| *DnaK* | 96.0 | Molecular chaperone | 5 µM | 10 | 2296 ± 78 | 0.76 ± 0.01 | | | |
| *MalZ* | 96.0 | Maltodextrin glucosidase | 0 µM | 9 | 3725 ± 229 | 0.77 ± 0.01 | | | |
| *GlcB* | 107.5 | Malate synthase G | 5 µM (15 µM) | 16 | 1315 ± 45 | 0.86 ± 0.01 | 6.4 ± 0.2 | 10 | 6.7 ± 1.1 |
| *MetE* | 111.7 | 5-methyltetrahydropteroyltriglutamate--homocysteine methyltransferase | 5 µM | 8 | 1137 ± 53 | 0.87 ± 0.01 | 7.4 ± 0.3 | | |
| *LeuS* | 124.2 | Leucine--tRNA ligase | 0 µM | 14 | 1637 ± 75 | 0.86 ± 0.01 | 5.1 ± 0.2 | | |
| *AcnA* | 124.7 | Aconitate hydratase A | 5 µM (15 µM) | 19 | 1415 ± 56 | 0.86 ± 0.01 | 6.1 ± 0.2 | 10 | 4.3 ± 0.4 |
| *MetH* | 163.0 | Methionine synthase | 0 µM (5 µM) | 9 | 1402 ± 45 | 0.81± 0.01 | 5.8 ± 0.1 | 15 | 4.0 ± 0.5 |

The library was built by cloning with Gibson assembly (Gibson et al. 2009) the genes encoding the selected proteins (Figure 3.1) in the expression vector pTrc99A (Amann, Ochs, and Abel 1988), under the control of the *trc* promoter, inducible by isopropyl β-D-1-thiogalactopyranoside (IPTG), and *in frame* at their C-terminus to the gene encoding sfGFP. The two genes are separated by the sequence encoding a short, flexible linker (Gly-Gly-Gly-Gly-Ser, GGGGS) (Chen, Zaro, and Shen 2013). sfGFP was chosen as a fluorescent tag because it is a brighter, more robustly and rapidly folded variant of EGFP (Pédelacq et al. 2006). Compared with the reference sequence, our sfGFP carries an additional mutation where the valine residue 206 was mutated to arginine (V206R): the mutation of alanine to a positive amino acid was shown to be sufficient for the true monomerization of fluorescent proteins (von Stetten et al. 2012; Guerra et al. 2022). In parallel, we generated a collection of two to four covalently-linked sfGFP oligomers (Nenninger, Mastroianni, and Mullineaux 2010; Vámosi et al. 2016). Each monomer was connected to the next via the same GGGGS linker used for the endogenous proteins' library. The diffusion of these oligomers would be affected only by their mass, since they lack interactions with cytoplasmic components. The codon usage was optimized to prevent homologous recombination and the genes were synthesized by Integrated DNA Technologies (IDT) and sub-cloned into pTrc99A.

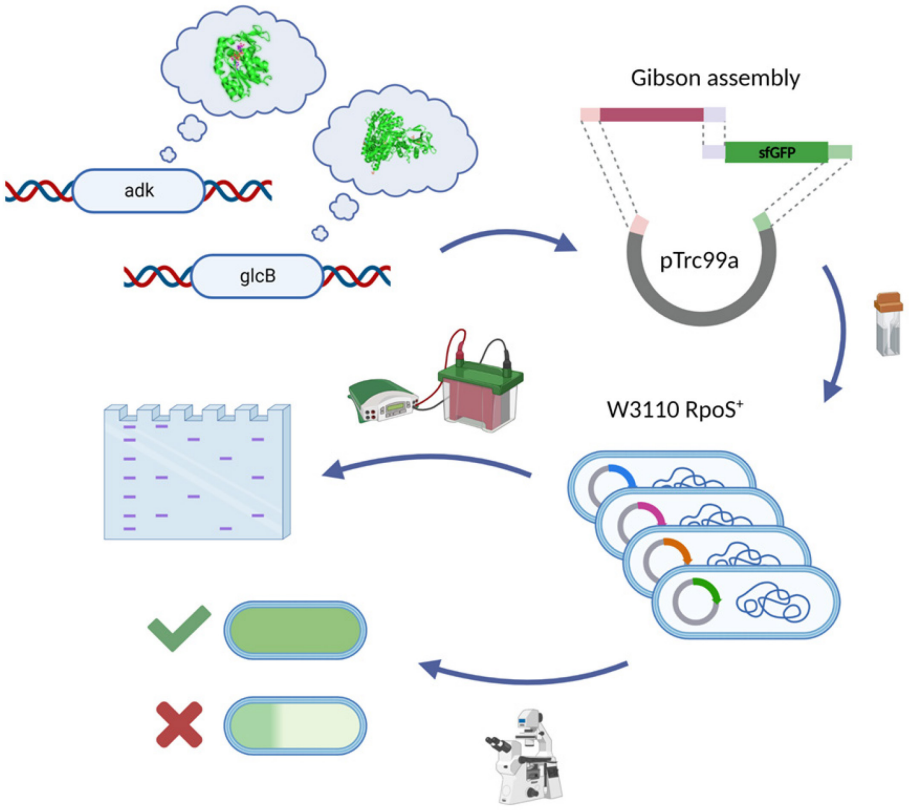


**Figure 3.1** Workflow of the construction of the sfGFP-tagged library of cytoplasmic *E. coli* proteins. Genes encoding globular, monomeric proteins were cloned by Gibson assembly into pTrc99A expression vector, fused at their C-terminus to sfGFP. Such generated constructs were transformed into a W3110 *E. coli* strain and their stability and homogeneous cellular localization were validated, respectively, by western blot and microscopy. Constructs that did not pass pass such screening were excluded from subsequent experiments.

The expected size and stability of each construct was verified by sodium dodecyl sulphate-poly-acrylamide gel electrophoresis (SDS-PAGE) and immunoblotting with an antibody anti-GFP (Figure 3.2A). The first batch of constructs that were generated showed relatively pronounced degradation to free sfGFP (~ 10 - 50%). After the deletion of the ATG start codon of sfGFP such degradation was markedly reduced (~ 0 - 5%). All the subsequent constructs were routinely generated deleting the start codon from sfGFP. After this step of optimization, only one of the constructs, ThpR-sfGFP, showed >20% degradation

to free sfGFP, and it was therefore excluded from further analyses. Of note, this was also the sole construct with an atypically high isoelectric point (pI), and all remaining constructs have pI ranging from 5.1 to 6.2, as common for cytoplasmic proteins (Schwartz, Ting, and King 2001). For all the constructs, the apparent mass observed in the immunoblot was matching that expected based on the amino acid sequence. On the contrary, the immunoblot of the sfGFP covalently-linked oligomers showed all the constructs being highly unstable (Figure 3.2B). Since the number of bands for each construct corresponded to the number of internal methionines, we speculated that such a high number of clearly defined bands may arise from alternative translation from the internal methionines. However, mutating the four methionine residues in the first subunit of the tetrameric construct to residues that have been previously confirmed to not affect sfGFP folding or fluorescence (Soundrarajan et al. 2012), was not sufficient to improve the protein stability. We thus focused only on the endogenous constructs for the subsequent analyses.

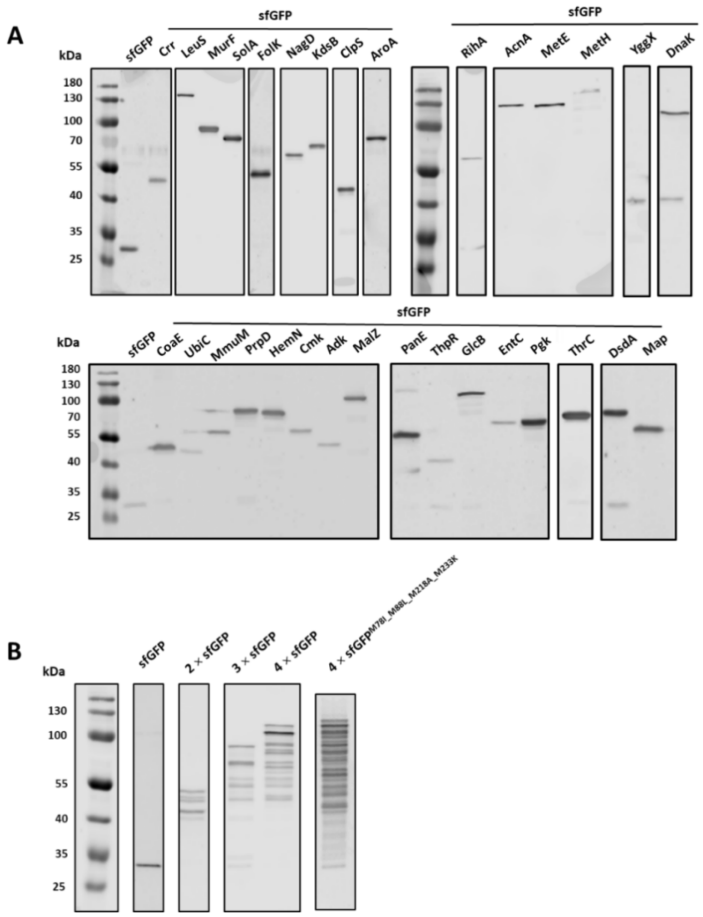


**Figure 3.2** Expression analyses by SDS-PAGE (10% gel concentration) and immunoblotting, using a primary antibody specific for GFP, for all sfGFP-constructs of endogenous proteins (A) and sfGFP-covalently linked oligomers (B).

We further performed microscopy experiments to verify the homogeneous distribution of the fusion proteins in the cytoplasm and to choose the more suitable IPTG concentration for the subsequent FCS and FRAP experiments (Table 1). The absolute majority of constructs showed a uniform localization in the cytoplasm (Figure 3.3A). Only the constructs RihA-sfGFP and NagD-sfGFP showed inhomogeneous cytoplasmic localization and were, for this reason, excluded from subsequent experiments (Figure 3.3B). The peculiar localization of NagD-sfGFP lead us to speculate that this protein may have a previously unknown localization to the nucleoid. However, in a strain where the chromosome was tagged with mCherry fused to the nucleoid-associated protein HUα, NagD clusters showed a clear filament-like

structure that does not co-localize with the nucleoids and it was rather pushed towards the cell periphery (Figure 3.3C).

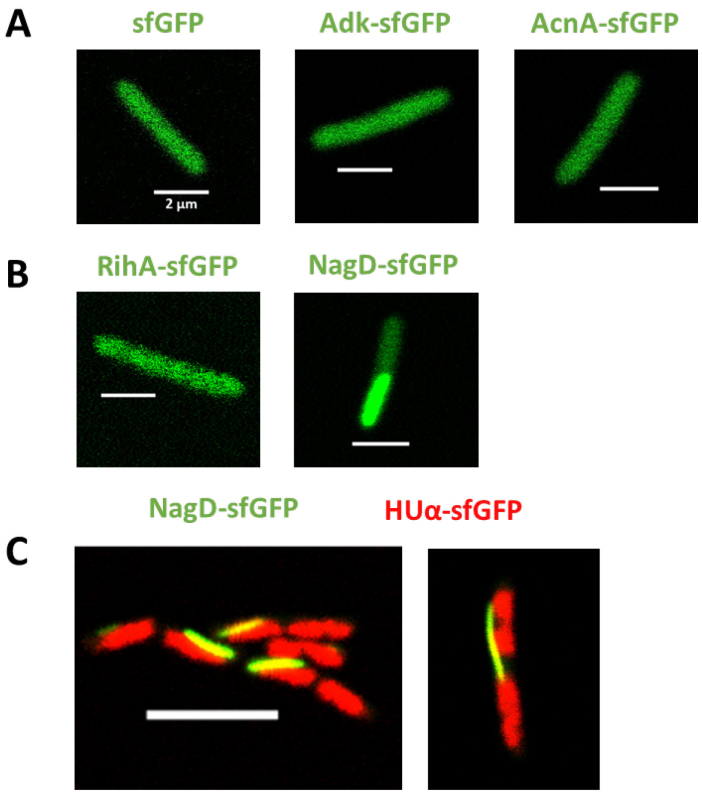


**Figure 3.3** Fluorescence microscopy of different strains constructed for this study. Examples of strains expressing sfGFP or the indicated sfGFP-tagged cytoplasmic protein displaying homogeneous (A) or inhomogeneous (B) cytoplasmic localization. Scale bar is 2 µm. (C) Examples of cells coexpressing NagD-sfGFP (green) and HUα-mCherry (red). Scale bar is 5 µm.

We then measured the growth curves of the strains expressing free sfGFP and the remaining 28 fusion proteins, compared with the reference strain carrying the empty vector. We observed that the expression of most fusion proteins had little effect on *E. coli* growth (Figure 3.4), and even for several proteins that delayed the onset of the exponential growth, the growth rate around the mid-log phase ($OD_{600}$ ~ 0.5-0.8), when cultures were harvested for measurements of protein diffusion, was similar.

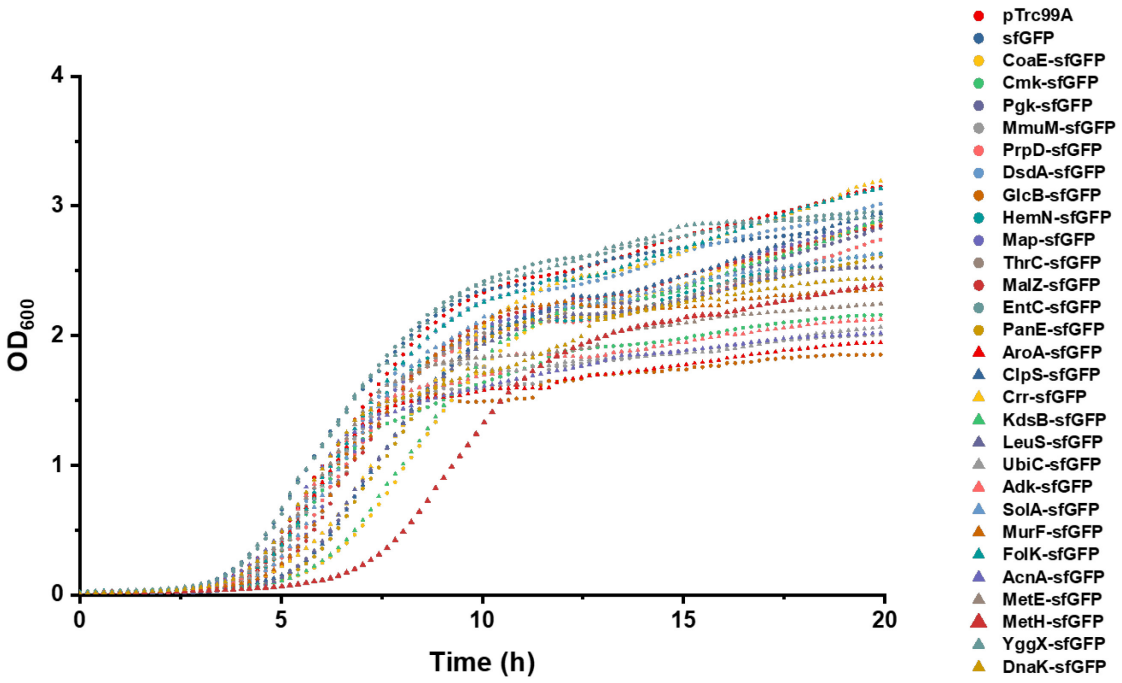


**Figure 3.4** Growth curves for the *E. coli* strains carrying the pTrc99A empty vector or the indicated pTrc99A-encoded sfGFP-tagged protein. Growth curves were measured at 37°C, in the same M9 medium and at the same protein expression level used for diffusion experiments. The optical density of cultures was monitored at 600 nm ($OD_{600}$) and the measured values were normalized for an optical path of 1 cm.

## 3.2 Optimization of a workflow for FCS experiments in bacteria

Since FCS has been applied to the measurement of diffusion in bacteria in a much smaller number of studies than FRAP and SPT (see section 1.5 for a general overview of the three techniques), we optimized a protocol to obtain robust and reliable FCS data. In order to reduce the impact of photobleaching on FCS measurements, a typical problem for bacteria due to their small size, cell length was moderately (approximately twofold) increased by treatment with the cell-division inhibitor cephalexin for 45 min, yielding an average cell length of ~5 μm. The resulting larger cell volume indeed reduced the rate of photobleaching. During each FCS measurement, the laser focus of the confocal microscope was positioned

in the cytoplasm close to the polar region, in order to keep the confocal volume possibly away from both the cell membrane and the nucleoid, and the fluorescence intensity in the confocal volume was measured over time (Figure 3.5). For each individual cell, six subsequent acquisitions of 20 seconds each were performed at the same position (technical replicates). The intensity of fluorescence fluctuates over time due to the diffusion-driven change in the number of fluorescent molecules in the confocal volume. The autocorrelation function (ACF), that is the temporal self-similarity of the fluorescence intensity fluctuations after progressively longer lag times ($\tau$), was independently calculated for each technical replicate and fitted to extract the mobility parameters of the fluorescent proteins.

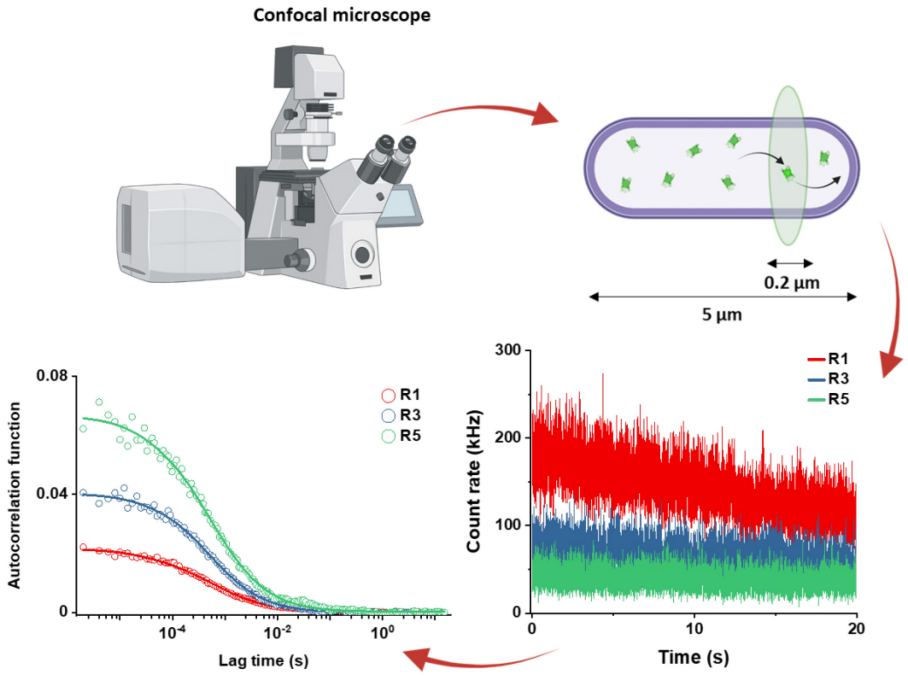

**Figure 3.5** Workflow of a typical FCS experiment for a cell expressing sfGFP. For clarity, only the traces and the autocorrelation functions for the first, third and fifth acquisitions are shown (*i.e.* R1, R3, R5; different colors). See text for more details.

Again due to the limited size of bacterial cells, FCS measurements require precise positioning of the confocal volume in the bacterial cytoplasm for the entire duration of the FCS experiment. The focal stability of the sample was increased by thermal equilibration on the microscope stage before measurements. Nevertheless, before fitting an autocorrelation function, we verified the stability of the lateral (*xy*) positioning of the observation volume by visually analyzing for lateral drifts in the confocal images routinely acquired immediately before and after the FCS acquisition. Measurements showing *xy* drift were excluded from the analysis (Figure 3.6).

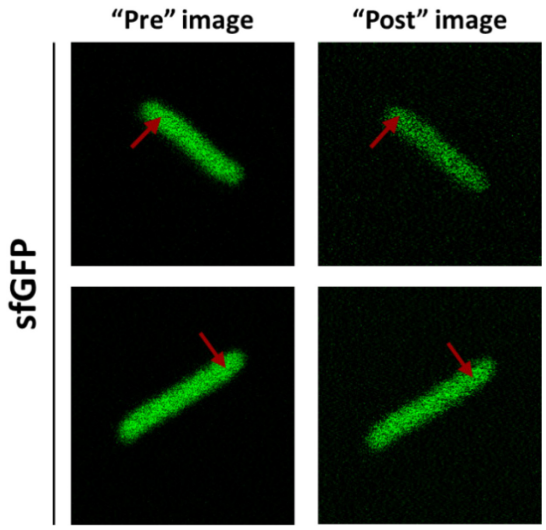


**Figure 3.6** Typical examples of presence (upper row) or absence (lower row) of lateral focal drift during FCS measurements. The *xy* position of the confocal volume (red arrows) was annotated in the pre-acquisition image and it was verified that such positioning did not change in the post-acquisition image after 120 seconds. Substantial lateral drift could be observed for <10% of experiments, whereas most measurement showed no perceptible lateral drift.

The long-term photobleaching due to the progressive decrease of the total number of fluorescent proteins during FCS experiments (Figure 3.7) is unavoidable due to the small volume of *E. coli* cells, and it requires correction to avoid artifacts.

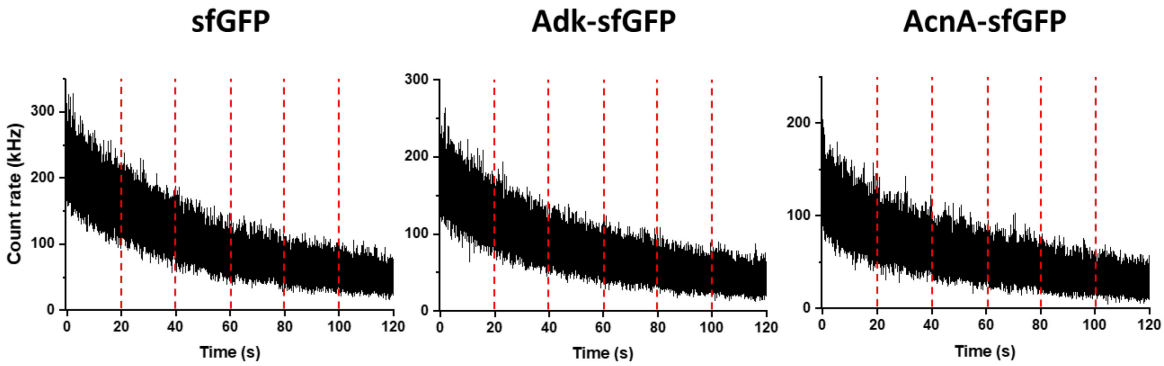


**Figure 3.7** Typical traces of fluorescence intensity during FCS measurements. The vertical red dashed lines separate sequential fluorescence intensity acquisitions on the same cell.

We observed that almost identical ACFs were obtained when correcting for the photobleaching using either multi-segment detrending (Jay Unruh, Stowers Institute for Medical Research, USA) or a local averaging approach (Wachsmuth et al. 2015) (Figure 3.8 and section 5.8.4 in Materials and methods for further details).

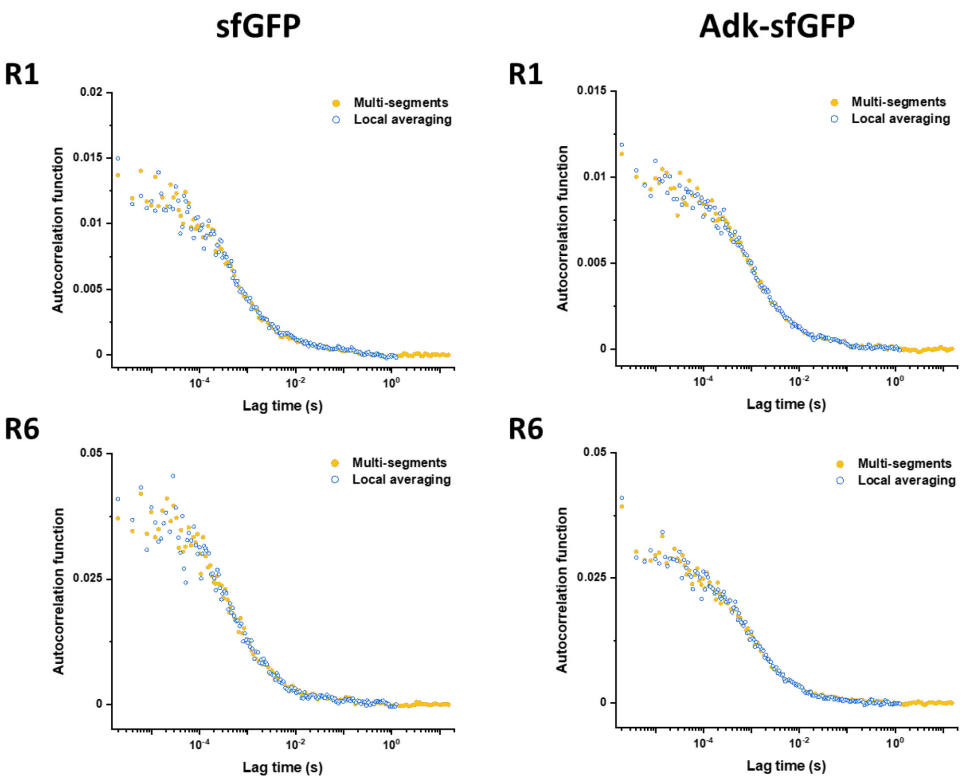


**Figure 3.8** Comparison of experimental ACFs corrected for photobleaching performing detrending with multi-segments (yellow dots) and local averaging (blue dots) approaches for sfGFP and Adk-sfGFP and different data acquisition segments (R1 vs R6). See section 5.8.4 in materials and methods for further details.

An additional process that could potentially affect autocorrelation functions is the short-term photobleaching of the fluorophore in the confocal volume, also known as cryptic photobleaching, which can artificially accelerate the decrease of the autocorrelation function and lead to an underestimation of the protein residence time (Macháň, Foo, and Wohland 2016). This process is different from long-term photobleaching, which is caused by the continuous illumination in the entire illumination light cone. However, the effect of cryptic photobleaching was shown to be typically <5%, even for proteins that diffuse 10 to 100 times slower and have higher bleaching rates than our constructs (Stasevich et al. 2010; Wachsmuth et al. 2015).

## 3.3 FCS data analysis

Each calculated ACF was then fitted with a biophysical model, representative of the diffusional process expected in the investigated system, to extrapolate the mobility of the fluorescent molecule. We initially considered the model of Brownian diffusion that quantifies the mobility of the fluorescent molecule with its diffusion (or residence) time ($\tau_D$) in the confocal volume (See also figures 1.3C and 3.5). Mathematically, $\tau_D$ is the value of the lag time at the inflection point of the ACF. The diffusion coefficient can then be calculated as $D = k\ {}^{1}/_{\tau_D}$ , where $k$ describes the geometry of the confocal volume (see section 5.8.3 in materials and methods for further details). Such a model of pure Brownian diffusion proved however unsatisfactory to accurately fit the experimental data, especially at long time scales (Figure 3.9). Therefore, we went on considering the model of anomalous diffusion (see section 1.1), that introduces the anomalous diffusion exponent ($\alpha$), that mathematically is the slope of the fitting function at the inflection point, to adjust for the skewed diffusion at longer time scales. As described in section 1.4, the anomalous diffusion exponent quantifies the anomaly of diffusion due to phenomena like macromolecular crowding, confinement, or protein-protein interactions. The anomalous diffusion model proved to be considerably better than the purely Brownian diffusion model to fit the experimental data (Figure 3.9). However, calculating a diffusion coefficient from ACFs fitted with the anomalous diffusion model is not straightforward and therefore for the purpose of this thesis, the results will be presented with both parameters of $\tau_D$ and $\alpha$.

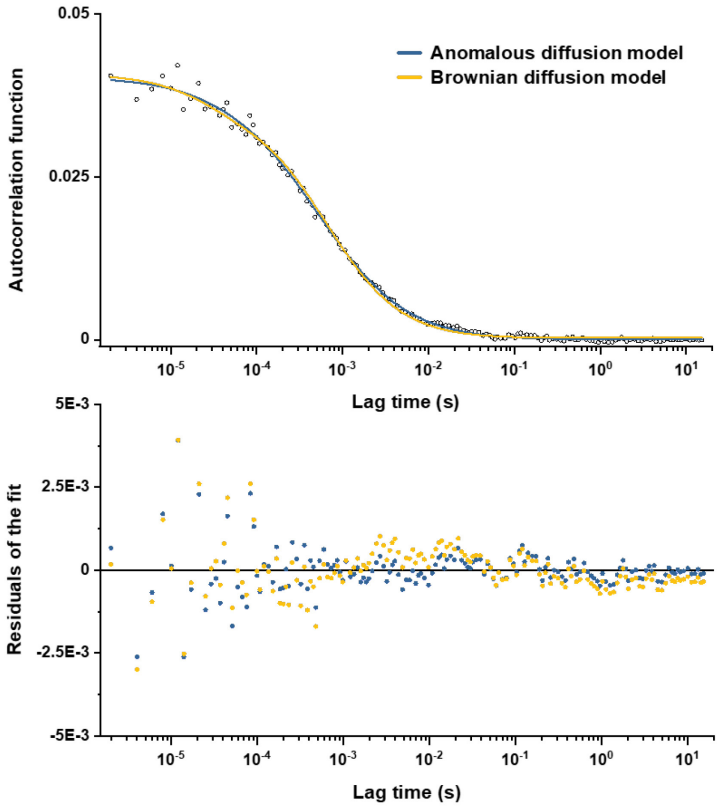


**Figure 3.9** Comparison between the fits of a representative experimental ACF with Brownian and anomalous diffusion models, as indicated by different colors (upper panel), with the corresponding values of residuals (lower panel).

Although, as mentioned above, all finally used protein constructs showed no or little degradation, we tested a possible impact of the fraction of free sfGFP for the construct that displayed the strongest (~15%) degradation, DsdA-sfGFP (Figure 3.2A). To this end, we fitted the FCS data using a model of two-components anomalous diffusion (Figure 3.10), where the weight of the fast component (*i.e.* the free sfGFP) was fixed to 15% and its values of $\tau_D$ and $\alpha$ to the average values obtained for sfGFP (Table 1). The average value of $\tau_D$ for the slow component (*i.e.* the full-length DsdA-sfGFP construct) was only ~7% lower compared to the regular fit using the one-component model, and the value of $\alpha$ remained unchanged,

suggesting that the impact of an even smaller fraction of free sfGFP for other constructs could also be neglected.

A

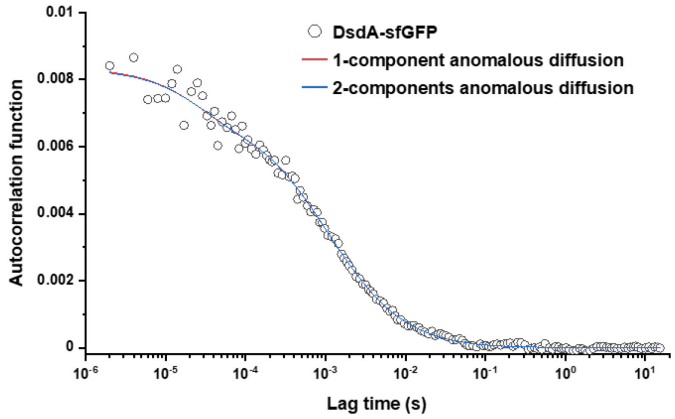


B

| Model | $\tau_D$ (µs; avg. ± SE) | α (avg. ± SE) |
|---|---|---|
| 1-component | 1017 ± 53 | 0.89 ± 0.01 |
| 2-components | 1092 ± 62 | 0.88 ± 0.02 |

**Figure 3.10** (A) Fitting of a representative ACF for DsdA-sfGFP with a two-component model for anomalous diffusion where the fast component corresponding to free sfGFP was fixed to 15% (corresponding to the degree of degradation of the fusion protein estimated from the immunoblot) and with $\tau_D$ = 561 µs and $\alpha$ = 0.86 (the average values obtained for sfGFP). For comparison, standard fitting with a one-component anomalous diffusion model is also shown. (B) Average values of $\tau_D$ and $\alpha$ obtained with the two-component and one-component model.

## 3.4 Size dependence of cytoplasmic protein mobility measured by FCS

The anomalous diffusion model was then used to determine the diffusion time and the anomalous diffusion exponent for all the ACFs (Figure 3.11).

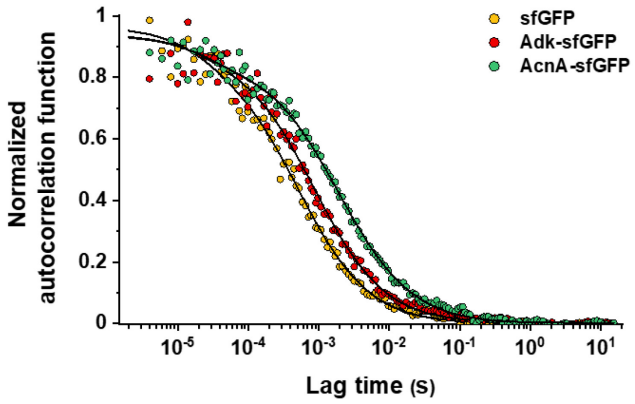


**Figure 3.11** Representative ACFs measured by FCS for the indicated protein constructs and fitted with the anomalous diffusion model (solid lines). All ACF curves were normalized to their respective maximal values to facilitate comparison.

Since the values of $\tau_D$ and $\alpha$ for each bacterial cell are calculated as the average of the six sequential technical replicates (Figure 3.5), we confirmed that there was no systematic trend in the fitted values of $\tau_D$ and $\alpha$ with the time of the fluorescence trace acquisition (Figure 3.12).

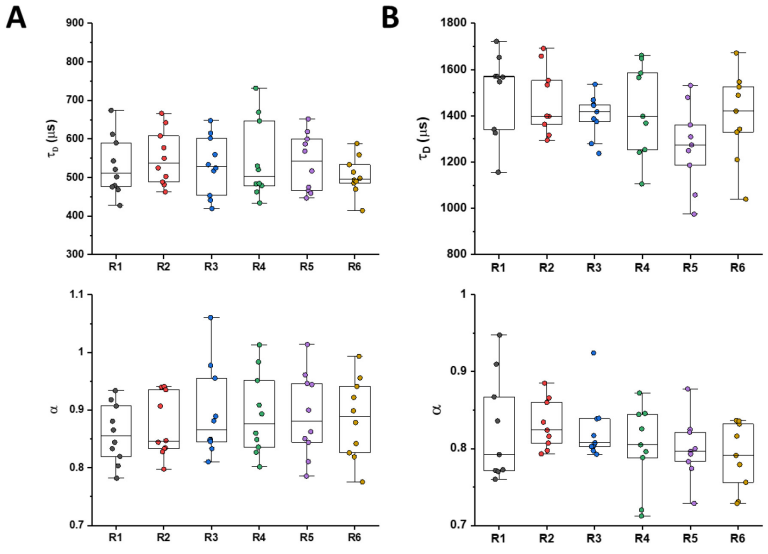


**Figure 3.12** Values of $\tau_D$ and $\alpha$ determined by fitting the anomalous diffusion model to experimental ACFs for the six sequential technical replicates per individual cell expressing sfGFP (A) or MetH-sfGFP (B).

The recorded fluorescence images (Figure 3.3) evidenced that the expression of the fluorescent proteins, and even the leaky, basal expression in absence of IPTG, varies quite substantially between different constructs. We thus verified that the expression level does not affect the measured values of $\tau_D$ or $\alpha$. We grew in parallel different *E. coli* cultures and induced the expression of sfGFP with different concentrations of IPTG, ranging from 5 to 100 μM. The mobility of sfGFP was then measured in a number of individual cells from each culture. No significant difference was observed in either $\tau_D$ or $\alpha$ (Figure 3.13).

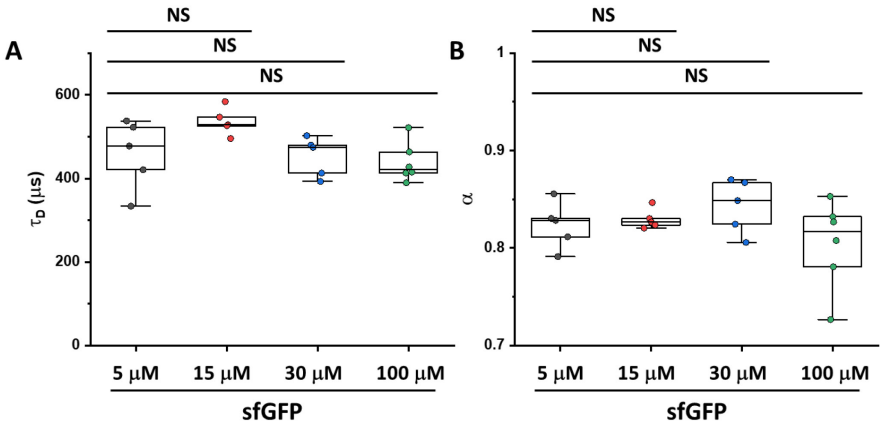


**Figure 3.13** Values of $\tau_D$ (A) and $\alpha$ (B) for sfGFP in individual cells at different protein expression level. NS: no statistically significant difference in a two-tailed heteroscedastistic *t*-test.

We then measured the diffusion of sfGFP and of all sfGFP-constructs in several individual cells (biological replicates) by FCS (Figure 3.14). The measurements were acquired during at least two independent experiments. The average values of $\tau_D$ and $\alpha$ for each individual cell were calculated as the average of the six technical replicates for that cell.

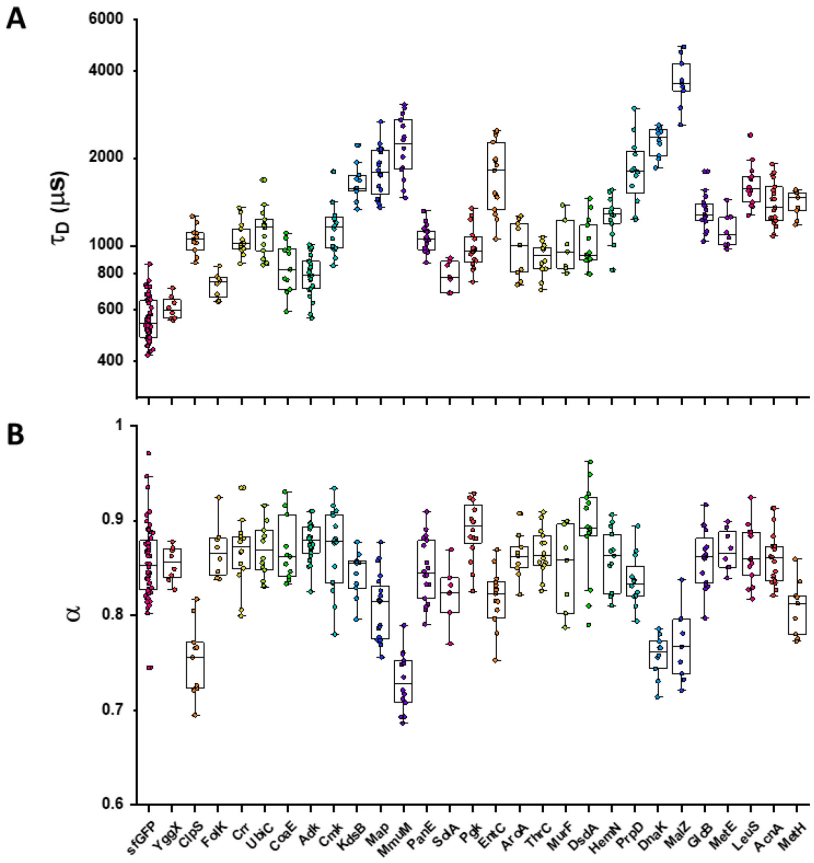


**Figure 3.14** Individual measurements of $\tau_D$ and $\alpha$ for all *E. coli* protein constructs included in the analysis of mass dependence. Each dot in the box plot represents the values of $\tau_D$ (A) and $\alpha$ (B) for one individual cell.

We next plotted the mean value of $1/\tau_D$, which reflect protein mobility, against the molecular mass of the respective protein constructs (Figure 3.15A). This dependence revealed a clear trend, where the mobility of more than half of the constructs decreased uniformly with their molecular mass, thus constituting a group that could be qualitatively described as "fast-diffusive" proteins. A subset of constructs instead exhibited a mobility much lower than other constructs of similar mass, and could be qualitatively described as "slow-diffusive" constructs. In contrast, the anomaly of diffusion $\alpha$ showed no apparent dependence on the protein size, ranging from 0.8 to 0.86 for most of the constructs (Figure 3.15B). Notably, the few

protein constructs with $\alpha$ of ~ 0.8 or lower were also among the ones with low mobility. These constructs are fusions of sfGFP to ClpS, Map, MmuM, DnaK and MalZ.

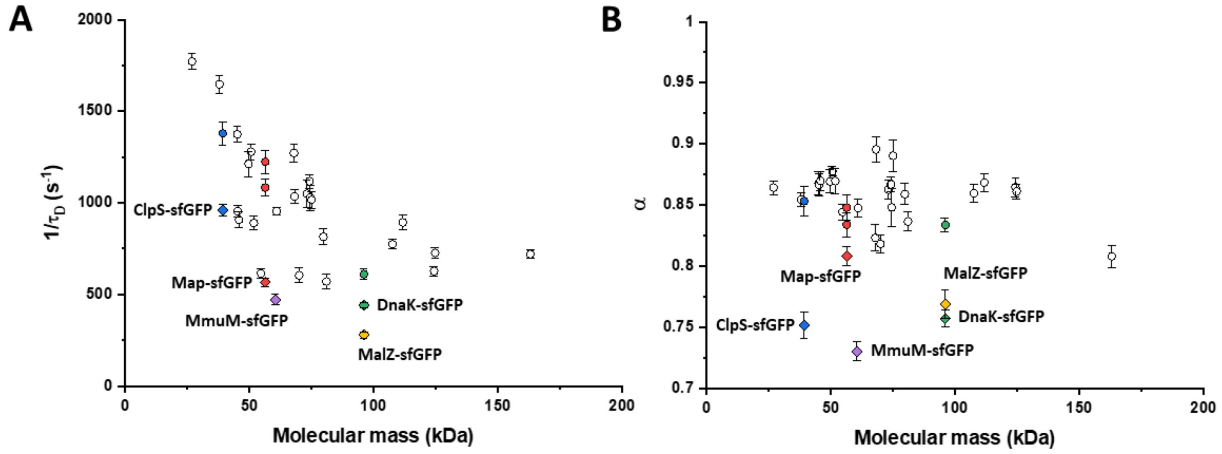


**Figure 3.15** Dependence of protein mobility ($1/\tau_D$; A) and apparent anomaly of diffusion ($\alpha$; B) on molecular mass. Each symbol represents the average value for all individual cells that have been measured for that particular construct (see Figure 3.14) and the error bars represent the standard error of the mean. Protein constructs with low mobility for which the effects of specific interactions were further investigated (see below) are highlighted in color and labeled. The values of $1/\tau_D$ and $\alpha$ for both the original constructs (diamonds) and the constructs where mutations were introduced to disrupt interactions (circles) are shown. For Map, two alternative amino acid substitutions that disrupt its interactions with the ribosome are reported.

To verify that the dimensions of the bacterial cells do not correlate with the measured protein mobility, the values of $1/\tau_D$ or $\alpha$ for all the measured cells expressing sfGFP were plotted against the length or the width of the correspondent cell and regression analysis was performed (Figure 3.16). Weak trends were observed where $1/\tau_D$ decreases as cell length or cell width increases. Instead, $\alpha$ increases as cell length or cell width increases. However, no trend appeared to be significant.

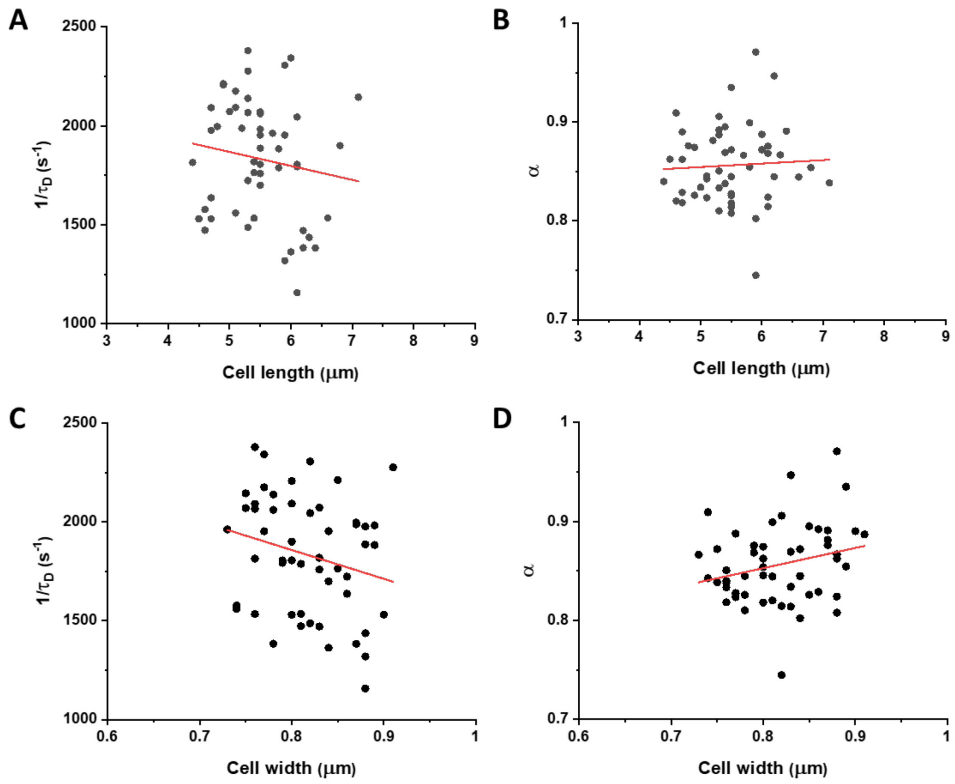


**Figure 3.17** Mobility ($1/\tau_D$; A, C) and anomaly of diffusion ($\alpha$; B, D) of sfGFP plotted against the width and length of the cells where they were measured. Solid red line represents the regression analysis for each plot. (A) p = 0.30, (B) p = 0.70, (C) p = 0.09 (D) p = 0.07.

Despite targeting an extracytoplasmatic protein (penicillin-binding protein) and being commonly used in the studies of cytoplasmic protein diffusion to achieve a larger cell size (Nenninger, Mastroianni, and Mullineaux 2010; Rowland, Tuson, and Biteen 2016), the antibiotic cephalexin could still be affecting protein mobility, since there are reports of its possible effects on cellular respiration rates (Lobritz et al. 2015). We thus directly compared sfGFP diffusion in control cells and in cells treated with cephalexin (Figure 3.18). To rule out the, even mild, effect of cell length on protein mobility, cells of similar size were measured in both conditions (~ 4-5 μm). No significant effect of the cephalexin treatment on protein mobility or anomaly of diffusion was observed.

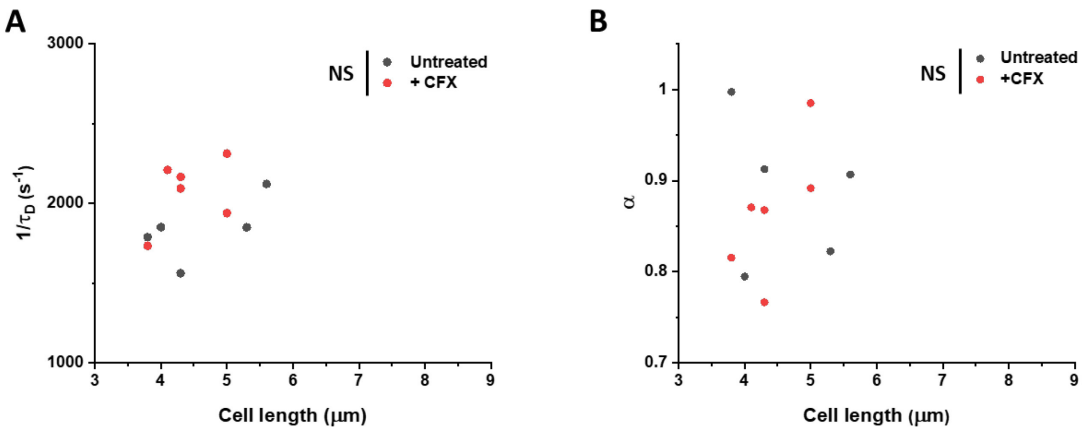


**Figure 3.19** Comparison of sfGFP mobility ($1/\tau_D$; A) and anomaly of diffusion ($\alpha$; B) in cephalexin-treated and untreated control *E. coli* cells. NS: no statistically significant difference in $1/\tau_D$ or $\alpha$ in a two-tailed heteroscedastistic *t*-test.

## 3.5 Macromolecular interactions reduce protein mobility

We reasoned that the main group of constructs that exhibited mobility close to the apparent mass-dependent upper limit (Figure 3.15) represents proteins whose diffusion is only limited by macromolecular crowding, and that the lower $1/\tau_D$ and $\alpha$ of other constructs might be due to their specific interactions with other cellular proteins or protein complexes. Indeed, for three of these proteins (ClpS, Map, DnaK) such interactions are well characterized and can be specifically disrupted.

ClpS (Figure 3.20A) is the regulatory subunit that delivers substrates tagged with the N-degron degradation sequence to the protease ClpAP (Roman-Hernandez et al. 2011). The substrate-binding site of ClpS is constituted by three amino acid residues (D35, D36, H66) that interact with the N-degron. If these residues are mutated into alanine, substrate binding *in vitro* is substantially reduced (Roman-Hernandez et al. 2011; Humbard et al. 2013). ClpS then docks to the hexameric ClpA through its long C-terminal tail. While it would be possible to prevent the docking through the deletion of the tail (Hou, Sauer, and Baker 2008), in this way ClpS mass would also be affected. We instead generated a *ΔclpA*

strain, since such gene knockout was reported to have normal growth and protein turnover (Katayama et al. 1988). Consistently with our hypothesis, we observed that the mobility of the mutant construct $ClpS^{D35A\_D36A\_H66A}$-sfGFP in the *ΔclpA* strain became significantly higher (Figure 3.20D) and less anomalous (Figure 3.20E), with both $1/\tau_D$ and $\alpha$ reaching levels similar to those of other proteins of similar mass.

Similar results were obtained for the other two constructs. Map is the methionine aminopeptidase that cleaves the N-terminal methionine from nascent polypeptide chains (Solbiati et al. 1999). Map performs its activity by docking to the negatively charged backbone of actively translating ribosomes through four positively charged lysine residues (K211, 218, 224, 226) located in a loop (Figure 3.20B). We thus hypothesized that such interaction is responsible for the reduced mobility and increased anomaly of diffusion of Map compared with constructs of similar size. If these residues are mutated into alanine, the *in vitro* affinity of Map for the ribosomes is reduced (Sandikci et al. 2013). Consistently, both the mobility increased (Figure 3.20D) and the anomaly of diffusion decreased (Figure 3.20E) significantly by alanine substitutions at all four lysine sites of Map-sfGFP. Interestingly, charge inversion of lysines to glutamic acid did not further increase Map-sfGFP mobility as was expected based on *in vitro* experiments (Sandikci et al. 2013).

DnaK is the major bacterial chaperone that binds to the short hydrophobic polypeptide sequences that become exposed during protein synthesis, membrane translocation or protein unfolding (Genevaux, Georgopoulos, and Kelley 2007). DnaK accommodates its substrate peptides inside a hydrophobic pocket (Figure 3.20C). By analogy with the previous results, we speculated that such interactions with client proteins may reduce DnaK measured mobility. *In vitro* experiments showed that the substitution of the valine residue 436 with bulkier phenylalanine creates steric hindrance that markedly decreases substrate binding to DnaK (Mayer, Rüdiger, and Bukau 2000). As such, both the $1/\tau_D$ and $\alpha$ of the $DnaK^{V436F}$-sfGFP

were significantly higher than for the correspondent wild-type construct (Figure 3.20D, E). Nevertheless, in this case the $1/\tau_D$ did not reach the levels of other proteins of similar molecular mass (Figure 3.15A), which is likely explained by the multiple interactions of DnaK with other components of the cellular protein quality control machinery besides its binding to substrates (Kumar and Sourjik 2012).

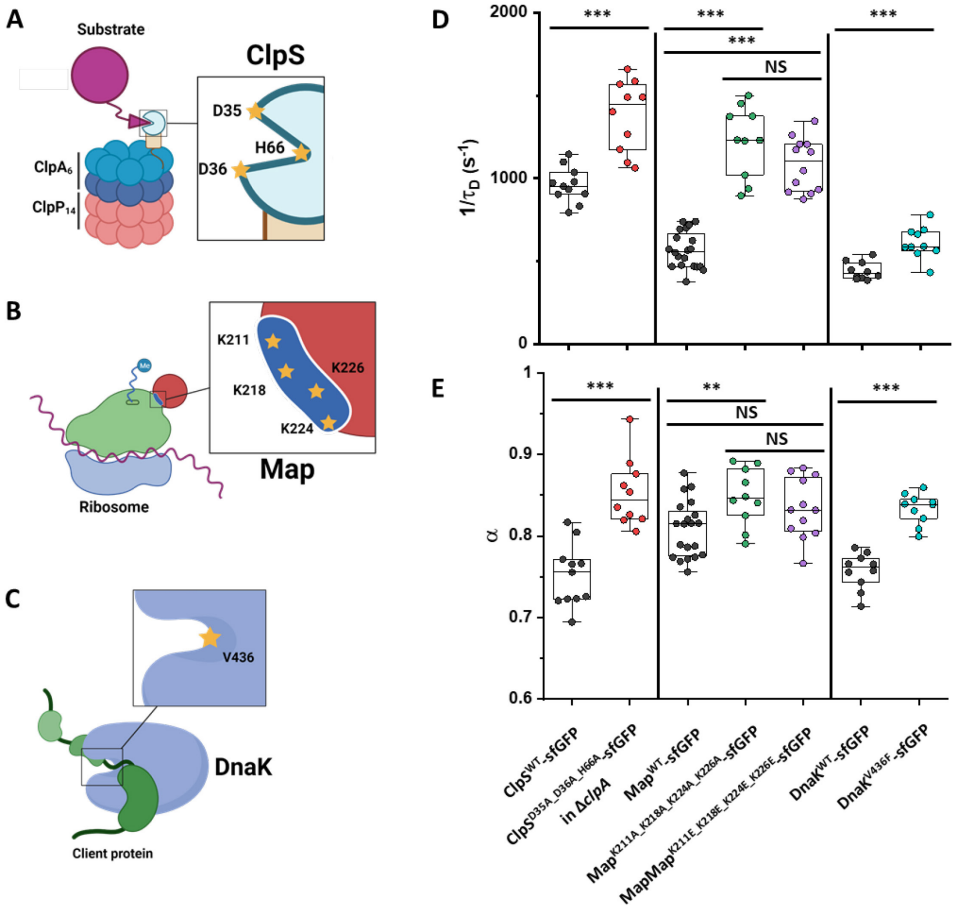


**Figure 3.20** Cartoons illustrating the cellular interactions that could affect mobility of ClpS (A), Map (B), and DnaK (C). Mobility ($1/\tau_D$; D) and anomaly of diffusion ($\alpha$; E) of ClpS, Map and DnaK and of indicated mutants with disrupted protein interactions. ***p<0.0001; **p<0.001; NS: no statistically significant difference in a two-tailed heteroscedastistic *t*-test.

Importantly, none of the aforementioned effects on diffusion depend on a substantially smaller size or a reduced stability of the mutant proteins compared with its wild-type form, as indicated by immunoblot analysis (Figure 3.21).

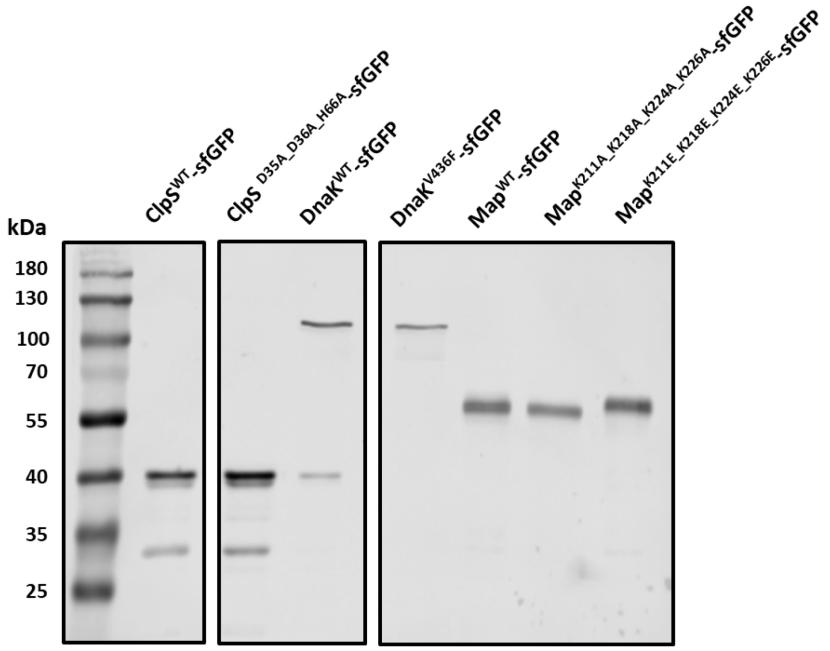


**Figure 3.21** The expression of indicated point mutants of ClpS, DnaK and Map was analyzed by SDS-PAGE (10% gel concentration) and immunoblotting using a primary antibody specific for GFP. All mutants displayed a dominant band corresponding to the expected molecular mass of the full-length fusion, and comparable to that of the wild-type counterpart. ClpS$^{D35A_D36A_H66A}$-sfGFP was measured in the same *ΔclpA* background used for the FCS experiments.

## 3.6 Apparent anomaly of diffusion could be largely explained by confinement

When FCS measurements are performed in a confined space with dimensions comparable to those of the confocal volume, such confinement may affect the apparent mobility of fluorescent molecules (Gennerich and Schild 2000; Jiang et al. 2020). To investigate the effect of confinement on our FCS measurements, Dr. Remy Colin from our department performed Brownian dynamics simulations of FCS experiments

with particles undergoing three-dimensional, purely Brownian diffusion inside a bacterial cell-like volume (Figure 3.22A, *inset*). The simulations were performed for a wide range of reported values of *E. coli* cell width, from 0.7 to 1 μm (Grossman, Ron, and Woldringh 1982), and for several different values of the ansatz diffusion coefficient. The ACFs calculated from the simulated FCS experiments were then fitted with models of Brownian and anomalous diffusion (Figure 3.22A). In agreement with what observed for the experimental autocorrelation functions (Figure 3.9), the Brownian diffusion model did not accurately fit the simulated data, particularly at longer time scales. Instead, for the values of cell diameter commonly observed under our growth conditions, 0.8-0.9 μm (Figure 3.17), and over a wide range of particle diffusion coefficients, the simulated autocorrelation functions could be satisfactorily fitted with the anomalous diffusion model (Figure 3.22B), yielding an anomalous diffusion exponent of around 0.8-0.9 (Figure 3.22C). This made us hypothesize that the relatively small apparent deviation from Brownian diffusion in the fit, with $\alpha$ above 0.8 common to most constructs, may primarily reflect a confinement-induced effect rather than proper sub-diffusion.

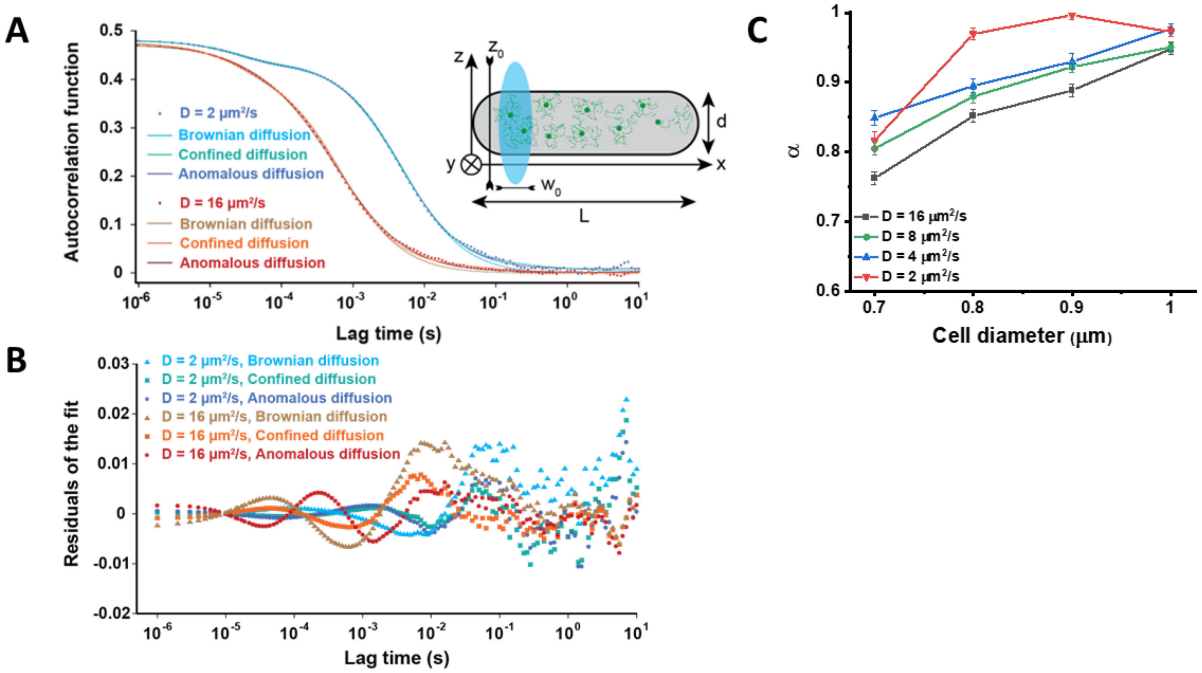

**Figure 3.22** Representative ACFs (A) and residuals of the fit (B) from simulated fluorescence intensity fluctuations. Simulations were performed in the confined geometry of a cell with indicated length *L* and diameter *d*, and dimensions of the measurement volume $\omega_0$ and $z_0$, representing an experimental FCS measurement (*Inset*; see section 5.8.3 in materials and methods), for two different values of the ansatz diffusion coefficient. Solid lines are fits by the models of unconfined Brownian diffusion, anomalous diffusion and by the Ornstein-Uhlenbeck (OU) model of Brownian diffusion under confinement (see below), as indicated. (C) Exponent $\alpha$ extracted from the fit with the anomalous diffusion model of the ACFs simulated for different values of the cell diameter.

We thus speculated that reduced anomaly of diffusion (i.e. $\alpha$ closer to 1) should be observed if the confinement is reduced by experimentally increasing the cell diameter or if the FCS experiments are performed further away from the cell membranes. Increase in *E. coli* cell diameter can be achieved by treatment with the inhibitor of bacterial cell wall biosynthesis A22 (Ouzounov et al. 2016) (Figure 3.23A). In agreement with the simulation results, after the treatment with A22, in addition to the standard cephalexin-induced elongation, the anomalous diffusion exponent of sfGFP increased significantly (Figure 3.23B). A small, but significant increase in sfGFP mobility is also observed (Figure 3.23C).

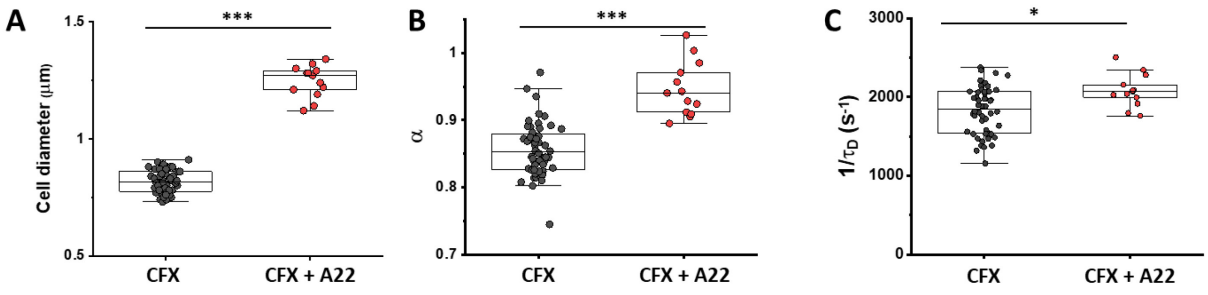


**Figure 3.23** Effects of the combined treatment with cephalexin (CFX) and A22 on *E. coli* cells width (A), and on sfGFP anomaly of diffusion (B) and mobility (C). *** $p<0.0001$; * $p<0.05$ in a two-tailed heteroscedastistic *t*-test.

It was recently reported that treatment with A22, in addition to cell elongation by expression of the SulA protein, reduces the dry mass density of *E. coli* cells (Oldewurtel Enno, Kitahara, and van Teeffelen 2021). As described in section 1.4, macromolecular crowding, that is linked to the cellular dry mass, has been observed to correlate with the anomaly of diffusion *in vitro*. To verify if a dry mass density reduction is present in our growth conditions and could thus be (partially) responsible for the observed reduction in the anomaly of diffusion, we performed a cell sedimentation assay (Figure 3.24). In presence of such reduction in cell dry mass density, we expected to observe an increase in the buoyancy of cells. To test this, cells treated with cephalexin or with cephalexin and A22 were loaded inside a microfluidic chamber suspended in motility buffer (MB) containing 20% iodixanol to match the density of the control untreated cells (Figure 3.24A), and Z-stack images of the whole microfluidic channel were acquired. The sedimentation was then quantified from the exponential decay of the cell fraction in the entire Z-stack (Figure 3.24A-G), that allows to calculate the cellular density mismatch (Figure 3.24H) (see section 5.11 in materials and methods for further details). To facilitate the cell count, these experiments were performed with a non-motile (*ΔfliC*) and non-aggregating, (*Δflu*) variant of the same *E. coli* strain W3110 $RpoS^{+}$ strain used in the other experiments. While the treatment with cephalexin slightly (by <0.1%) decreased the density of *E. coli* cells in this assay (Figure 3.24B, H), the additional treatment with A22, in our growth conditions, had only minor and not significant impact once the effect on sedimentation of the volume increase was accounted for (Figure 3.24C, H). We thus concluded that the influence of A22 on the anomaly of protein diffusion is most likely due to its effect on cell width and not on the cytoplasmic density.

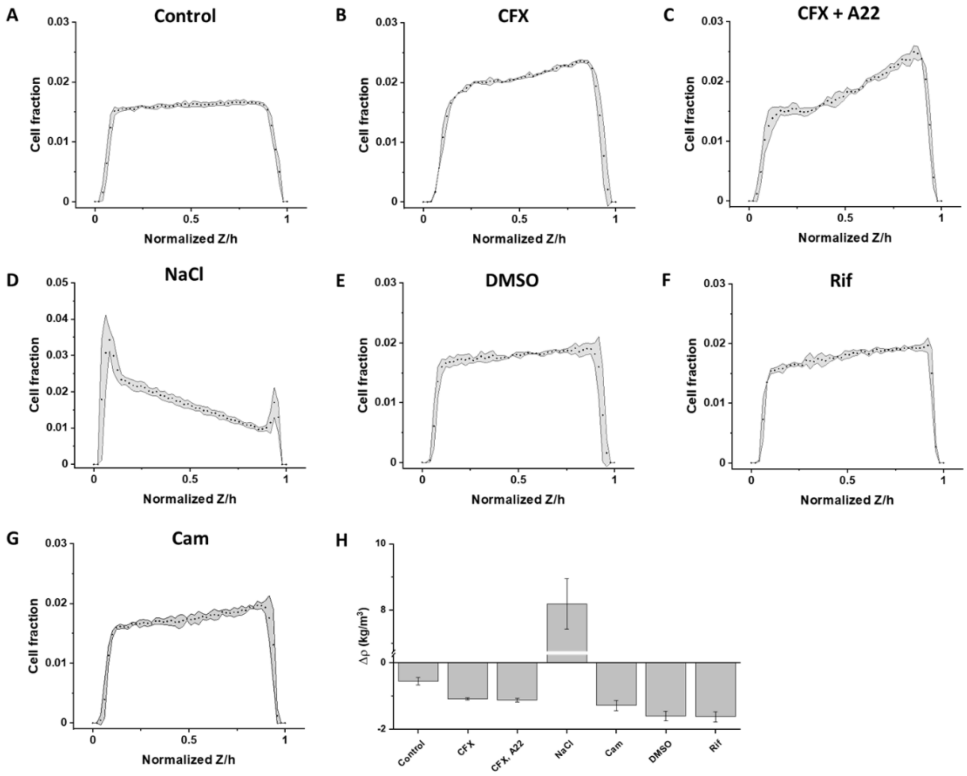


**Figure 3.24** Sedimentation assay of cellular density for control cells (A), or for cells after the indicated treatments (B – G). Dots represent the cell fraction at each given Z position normalized on the total height of the microfluidic channel (50 μm). The grey shadings indicate the standard deviation of the three technical replicates. Results presented in panels D – G are discussed in section 3.10. (H) Calculated values of cellular density mismatch ($\Delta\rho$) from MB with 20% iodixanol. Error bars represent the standard error of the mean. Calculations were performed as described in Materials and methods section 5.11.

Reduced anomaly of diffusion could also be observed by limiting the analysis to fluorophores diffusing at a distance from the cell boundary. We thus performed FCS measurements for sfGFP and AcnA-sfGFP with a smaller confocal volume, by reducing the pinhole size to a less optimal but smaller value of 0.66 Airy units. Consistently with our prediction, the value of $\alpha$ derived from these measurements was significantly higher for both proteins, >0.9 (Figure 3.25A). As expected, the residence time ($\tau_D$) of proteins in such a smaller confocal volume was also smaller, although the effect was more pronounced for AcnA-sfGFP than for sfGFP alone (Figure 3.25B).

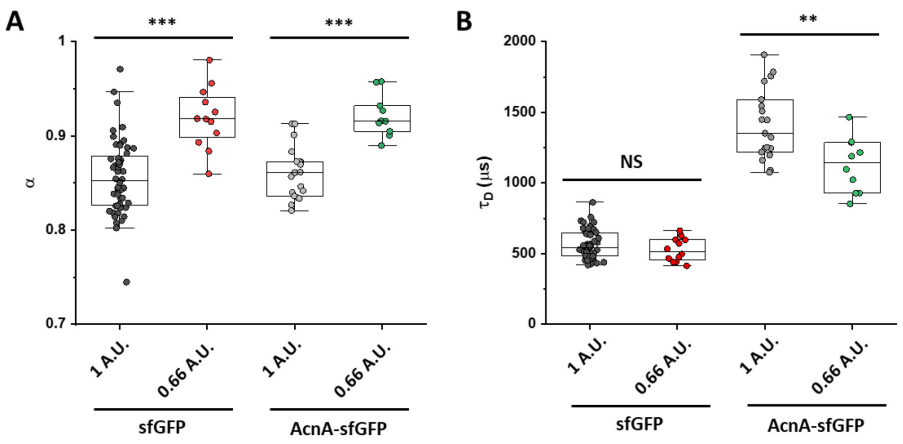


**Figure 3.25** Apparent anomaly of diffusion ($\alpha$, A) and residence time ($\tau_D$, B) for different protein constructs measured at different pinhole sizes (A.U. = Airy units). Smaller pinhole sizes are less optimal due to the reduced signal-to-noise ratio of the measurements.

## 3.7 Protein diffusion in bacterial cytoplasm corrected for confinement

Diffusion in the confined environment close to the pole of a bacterial cell can be simplified and mathematically described as an Ornstein-Uhlenbeck (OU) process where the Brownian motion of diffusing particles is confined by a harmonic trap (Figure 3.26).

**Figure 3.26** Cartoon representing an Ornstein-Uhlenbeck process where the Brownian diffusion of hypothetic GFP molecules is confined inside a harmonic trap of dimensions comparable to the width of a bacterial cell.

Our collaborators Dr. Jaime Agudo-Canalejo and Prof. Ramin Golestanian from the Max Planck Institute for Dynamics and Self-Organization in Göttingen, derived an OU model for fitting FCS data that includes the confinement of Brownian diffusing fluorescent particles within the width of the cell as trapping in a harmonic potential of the same width. The two models fit the ACF of the Brownian dynamic simulations comparably well, particularly at the long timescales where the anomalous diffusion model was improving over the purely Brownian diffusion model (Figure 3.22A, B), with the OU model having one less free parameter than the anomalous diffusion model. In the Brownian dynamic simulations, the OU model estimates the ansatz diffusion coefficient significantly better than the anomalous diffusion model (Figure 3.27A) and within ± 5% accuracy for the typical cell widths observed in our experiments (Figure 3.27B).

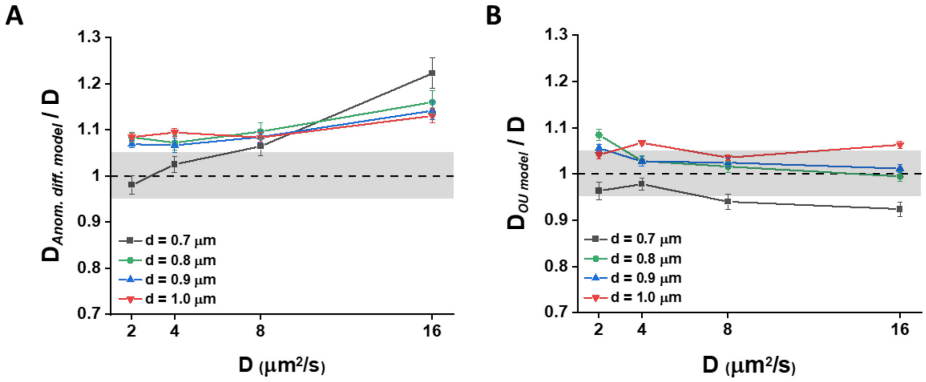


**Figure 3.27** Diffusion coefficients computed ($D=\omega_0^2/4\tau_D$) from the diffusion times extracted from the fit of the Brownian simulation data with (A) the anomalous diffusion model or (B) the Ornstein-Uhlenbeck (OU) model of Brownian diffusion under confinement at various value of the ansatz $D$ and of the cell diameter $d$, normalized by the ansatz $D$. The grey areas represent ± 5% accuracy.

The OU model proved also accurate in fitting the experimental data, comparably to the anomalous diffusion model (Figure 3.28).

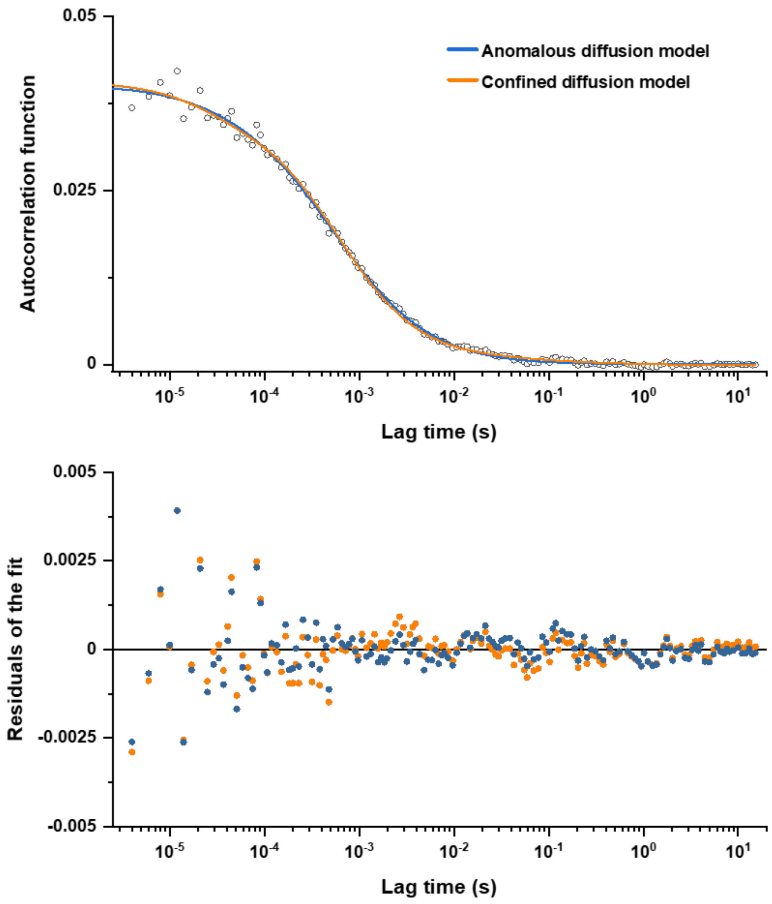


**Figure 3.28** Comparison between the fits of a representative experimental ACF with anomalous diffusion and confined diffusion models, as indicated by different colors (upper panel), with the corresponding values of residuals of the fit (lower panel).

We thus used the confined diffusion model to re-fit the ACF data for all constructs close to the apparent mass-dependent upper limit and to calculate their Brownian diffusion coefficients (Figure 3.29A), using the equation described in section 3.3. The dependence of *D* on molecular mass (see section 1.7.1 for a detailed introduction) for this set of constructs was scaling as $(MM)^{-\beta}$ with $\beta = 0.56 \pm 0.05$ (*i.e.* inverse-power law; Figure 3.29B, solid blue line), in great agreement with a recent report (Śmigiel et al. 2022), less steep compared to some of the previous estimates (Kumar, Mommer, and Sourjik 2010; Mika et al.

2010; Stracy et al. 2021) but still steeper than expected from the Stokes-Einstein relation (Nenninger, Mastroianni, and Mullineaux 2010), even when assuming $\beta$ = 0.4 for not perfectly globular proteins (Figure 3.29B, black dashed line) (Enright and Leitner 2005; Smilgies and Folta-Stogniew 2015). The shape of the fusions between an endogenous protein and sfGFP through a short linker, substantially deviate from that of a sphere, and can rather be approximated to that of a dumbbell. The more degrees of freedom of a dumbbell compared to a sphere, substantially affects its hydrodynamics and diffusional properties (Agudo-Canalejo and Golestanian 2020). Our collaborators Dr. Jaime Agudo-Canalejo and Prof. Ramin Golestanian adapted their previously derived model (Agudo-Canalejo and Golestanian 2020) to model the size dependence of the diffusion of two imperfectly-globular, covalently-linked proteins, one with mass equivalent to that of sfGFP and the other with the mass of the protein attached to it. The dependence of *D* on molecular mass predicted by this linked-protein model seems indeed to better recapitulate our experimental data, particularly for the smaller protein fusions (Figure 3.29B, solid yellow line), although it moderately overestimate *D* for several of the largest protein fusions (>100 kDa). Thus, we concluded that the size dependence of diffusion for the majority of cytoplasmic proteins follows the Stokes-Einstein relation, once the shape of the sfGFP-tagged protein constructs is taken into account.

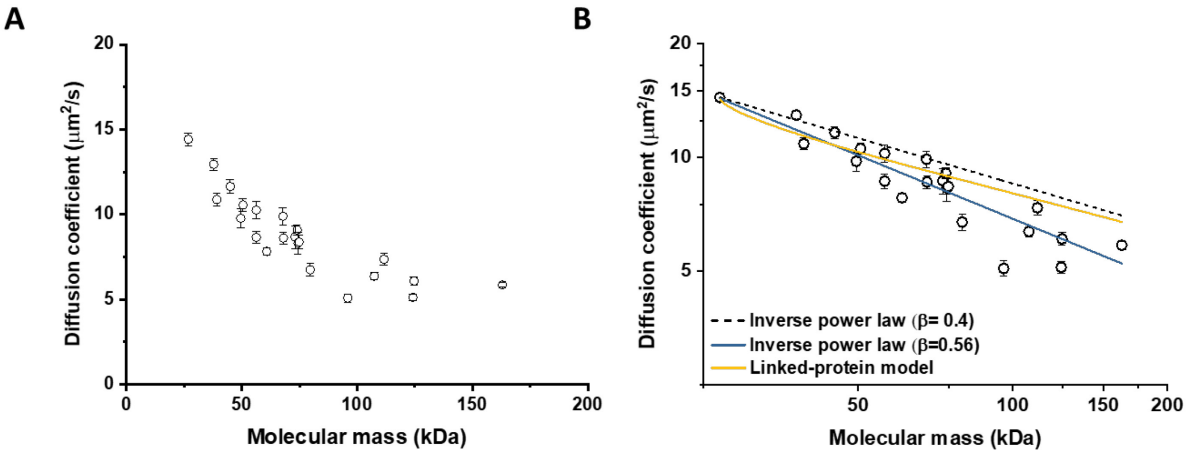

**Figure 3.29** (A) Dependence of the diffusion coefficient calculated from fitting the experimental ACFs with the OU model of confined diffusion. Only the subset of apparently freely diffusing constructs from Figure 3.15 has been analyzed with the OU model (see also Table 1). Each circle represents the average value for all individual cells that have been measured for that particular construct, and the error bars represent the standard error of the mean. Error bars that are not visible are smaller than the symbol size. (B) Fit of the mass dependence with an inverse power law (solid blue line, exponent $\beta = 0.56 \pm 0.05$), and predictions of the Stokes-Einstein relation (black dashed line) and of the model describing diffusion of two linked globular proteins (solid yellow line), both with exponent $\beta = 0.4$.

## 3.8 Protein diffusion coefficients measured using FRAP or FCS are consistent

Many previous measurements of protein diffusion in bacteria were performed using FRAP and typically provided estimates of protein diffusion coefficients smaller than those obtained in other studies by FCS (see section 1.6 for more details). We thus aimed to directly compare FRAP and FCS measurements for a set of constructs of different mass using the same cell growth conditions and microscopy sample preparation protocols. Due to the higher sensitivity of FCS at low fluorophore concentrations, however, several fusion constructs required higher induction by IPTG (Table 1) to obtain a fluorescence intensity suitable for FRAP. The cells were photobleached with a high intensity laser for 48 ms in a region close to the pole, similar to the position that was used for the FCS experiment. The recovery of fluorescence in the bleached area by diffusion from the unbleached areas was then followed for 11 s with the time resolution of 18 ms (Figure 3.30). Such time resolution was significantly higher than that of most earlier studies of FRAP in bacteria (Elowitz Michael et al. 1999; Kumar, Mommer, and Sourjik 2010; Nenninger, Mastroianni, and Mullineaux 2010), and comparable to that of more recent studies (Schavemaker, Smigiel, and Poolman 2017). A high time resolution is critical for an accurate comparison of FRAP measurements with the much more time-resolved FCS measurements.

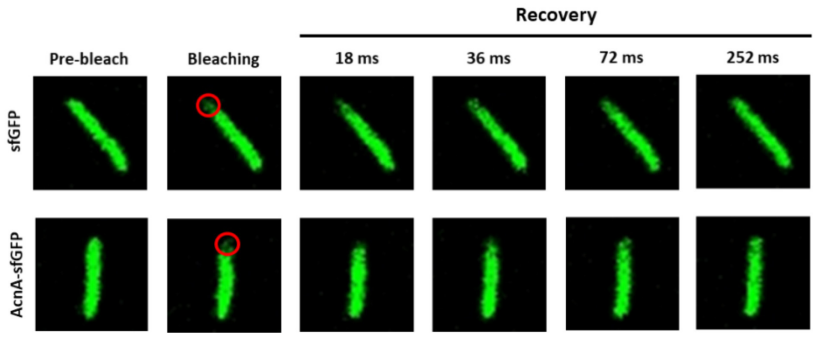


**Figure 3.30.** Examples of FRAP measurements for two different constructs, sfGFP and AcnA-sfGFP. A 3x3 pixels area close to one cell pole (red circle) was photobleached with a high intensity laser for 48 ms and the recovery of fluorescence in the bleached area was monitored for 11 s with the time resolution of 18 ms.

As a first approach to quantify protein mobility, we extrapolated the half-time of the fluorescence recovery ($t_{half}$) from the exponential fitting of the time course of fluorescence recovery in the photobleached spot (Figure 3.31A) for all the individual cells measured for each construct (Figure 3.31B). The mobile fraction, that quantifies the fraction of molecules that are mobile and free to diffuse, was always found higher than 0.8, and for several constructs also higher than 0.9 (Figure 3.31C), confirming that the investigated proteins are largely free-diffusive.

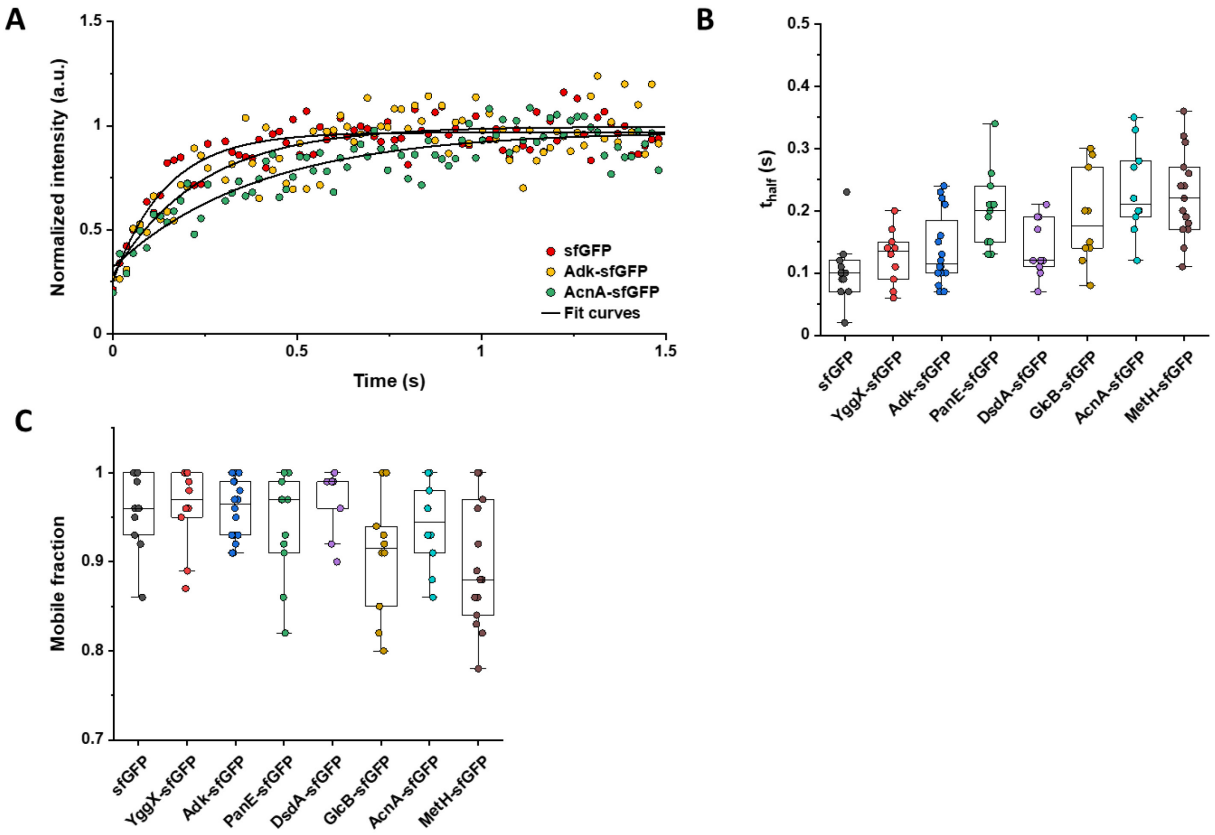


**Figure 3.31** (A) Representative curves of fluorescence recovery in FRAP experiments for the indicated protein constructs and their exponential fitting. (B) Individual measurements of $t_{half}$ from the exponential fit of the fluorescence recovery curves for the indicated *E. coli* protein constructs. Each dot in the box plot represents the values of $t_{half}$ for one individual cell. More details on the extrapolation of $t_{half}$ are reported in section 5.8.5. (C) Mobile fraction (calculated as the ratio between the intensity of fluorescence in the bleached spot after recovery and before photobleaching; more details in section 5.8.5) from each individual cell for all the constructs measured with FRAP.

Estimating a diffusion coefficient from the $t_{half}$ requires the precise characterization of the bleaching spot (Axelrod et al. 1976) and the analytical modelling of the cell geometry (Hallen and Layton 2010; Kang et al. 2012), that is particularly crucial in the small bacterial cells. Recently developed approaches based on the numerical simulation of the diffusional process, instead, automatically account for the cell geometry and the localization, shape, and non-negligible size of the diffraction-limited photobleached spot (Montero

Llopis et al. 2012). We thus computed the diffusion coefficients directly from the time courses of recovery (Figure 3.32A) using simFRAP (Blumenthal et al. 2015). simFRAP is a plugin for ImageJ based on an algorithm that simulates two-dimensional random walks in each pixel, using the first image acquired after bleaching to define initial and boundary conditions, and it resolves numerically the diffusion equation by iterative simulation. We observed very good correlation between such diffusion coefficients and the correspondent ones calculated from the fitting of FCS measurements with the confined diffusion model, although for most of the constructs the diffusion coefficients determined by FRAP were 5 to 30% lower than those obtained from the FCS data (Figure 3.32B and Table 1).

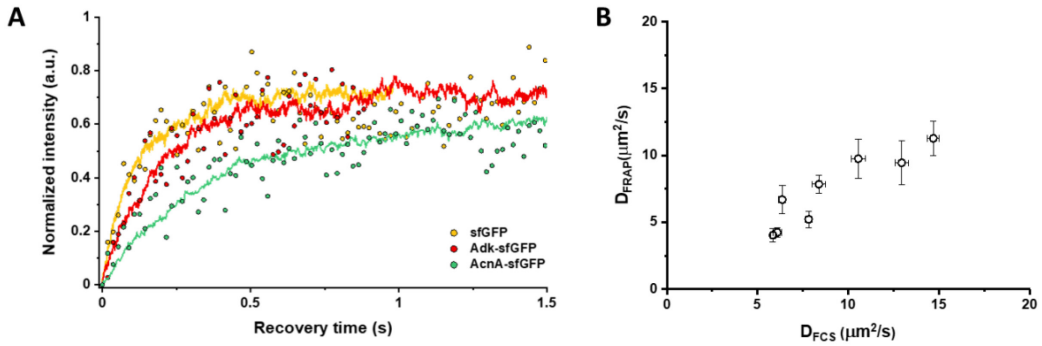


**Figure 3.32** (A) Representative curves of fluorescence recovery in FRAP experiments for the indicated protein construct and their fitting using simFRAP. The simulation performed by simFRAP proceeds until the recovery curve reaches a plateau, therefore it is interrupted at a different time for each curve. (B) Correlation between the diffusion coefficients measured in FCS experiments ($D_{FCS}$, fitting with the OU model; data from Figure 3.29) and in FRAP experiment ($D_{FRAP}$, fitting with simFRAP). Error bars represent the standard error of the mean. Error bars that are not visible are smaller than the symbol size.

## 3.9 Diffusive properties of cytoplasmic proteins are largely conserved between bacterial species

We then investigated whether sfGFP fusions to non-native proteins, originating from other bacteria, may show different diffusive properties in *E. coli* cytoplasm than their native counterparts, as expected from

the recently postulated existence of an organism-dependent "quinary" code of unspecific, short living interactions (Mu et al. 2017). Thus, we generated another plasmid-encoded collection of sfGFP-tagged proteins from other Gram-negative proteobacteria *Yersinia enterocolitica*, *Vibrio cholerae*, *Caulobacter crescentus* and *Myxococcus xanthus* and from the Gram-positive bacterium *Bacillus subtilis* that are homologous to several analyzed freely-diffusing *E. coli* protein constructs (respectively, Adk, Pgk and AcnA). We transformed *E. coli* with such constructs and we measured their diffusional properties with FCS. Within this set of constructs, we observed no significant differences of their $1/\tau_D$ values from *E. coli* homologues. An exception was AcnA from *M. xanthus* (Figure 3.33A), whose lower mobility might be a sign of its multimerization, although the cellular distribution of this construct was uniform. In contrast, all constructs showed slightly but mostly significantly increased anomaly of diffusion compared to *E. coli* proteins (Figure 3.33B), which might reflect the weakly increased propensity of non-native proteins to engage in unspecific interactions in *E. coli* cytoplasm. Consequently, with the aforementioned exception of AcnA-sfGFP from *M. xanthus*, the size dependence of protein mobility for such homologous follows that of their *E. coli* counterparts (Figure 3.33C), while no size dependence is observed in their anomaly of diffusion (Figure 3.33D).

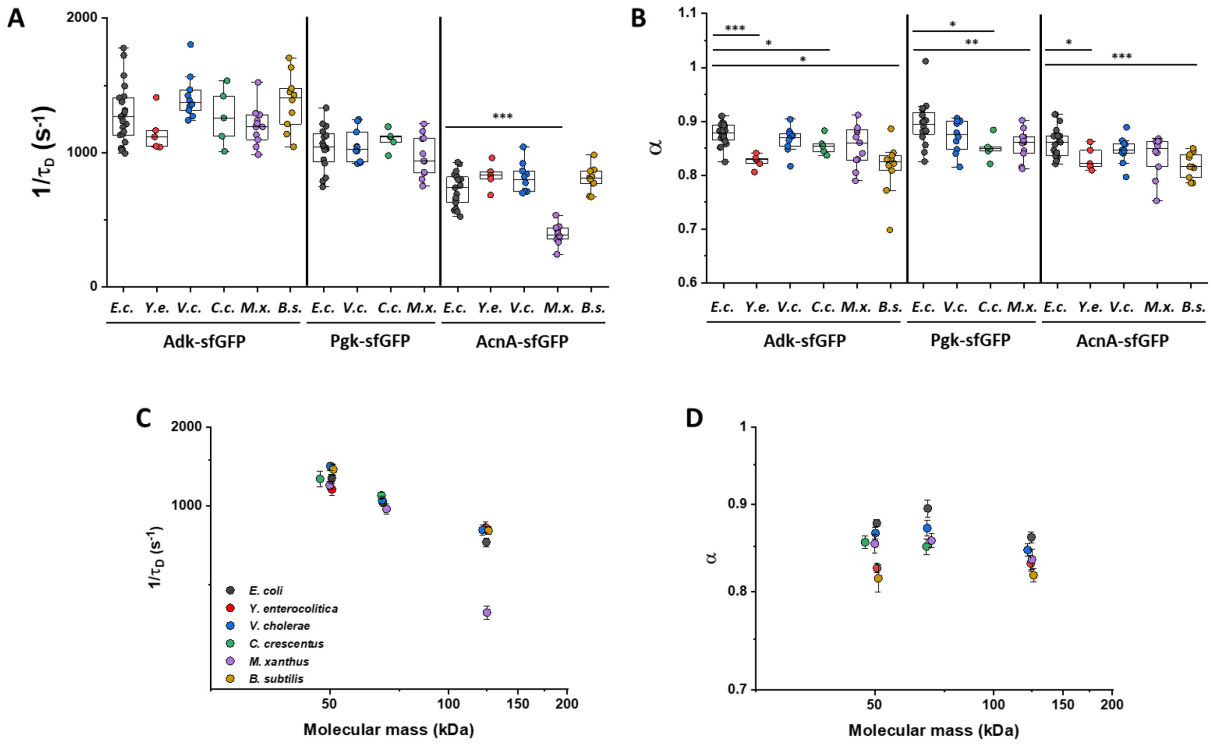


**Figure 3.33** Mobility ($1/\tau_D$; A) and anomaly of diffusion ($\alpha$; B) of homologous proteins from other bacterial species in *E. coli*. Dots represents the measurements from individual cells expressing the indicated sfGFP construct from different bacterial species (*E.c. = Escherichia coli; Y.e. = Yersinia enterocolitica; V.c. = Vibrio cholerae; C.c. = Caulobacter crescentus; M.x. = Myxococcus xanthus; B.s. = Bacillus subtilis*). *** p<0.0001; **p<0.001; * p<0.05 in a two-tailed heteroscedastistic t-test. When not indicated, no statistically significant difference was observed. Size dependence of protein mobility ($1/\tau_D$; C) and anomaly of diffusion ($\alpha$; D) of sfGFP fusions to the homologous of Adk, Pgk and AcnA from the indicated bacterial species. Each dot represents the average values calculated from the individual measurements shown in A and B, respectively, and the error bars represent the standard error of the mean. Error bars that are not visible are smaller than the symbol size.

## 3.10 Effects of physicochemical perturbations and cellular state on protein diffusion

Selected "fast-diffusive" constructs of different sizes were then used as probes to characterize the impact of different environmental and cellular perturbations on the cytoplasmic diffusion. The effect of several

of these conditions were previously explored using free GFP or large cytoplasmic particles, while the, possibly peculiar, effect on proteins with intermediate size is still uncharacterized.

### 3.10.1 Ionic strength

We started with the previously characterized decrease in mobility of GFP and large protein complexes or aggregates upon osmotic upshift (Konopka et al. 2006; Konopka et al. 2009; Mika et al. 2010; Liu et al. 2019; Wlodarski et al. 2020). *E. coli* cells exposed to increased ionic strength by addition of 100 mM NaCl showed a decrease in cell length and width (Figure 3.34A, B) and an increase in cell density in the sedimentation assay (Figure 3.24D), compared with control conditions. Such effect is consistent with the notion that higher osmolarity induces volume contraction and thus an increase in the cytoplasmic density (Wlodarski et al. 2020). The mobility of sfGFP decreases progressively and significantly as the ionic strength of the external medium increases from 105 to 505 mM (Figure 3.34C, D), comparably to previously measured values (Konopka et al. 2009). At the highest ionic strength, the formation of plasmolysis spaces was observed, therefore only the intermediate ionic strength of 305 mM was further investigated with other protein constructs. Importantly, the mobility of all other tested constructs decreased proportionally (Figure 3.34C), meaning that – in this range of molecular sizes – the effect of a moderate osmotic upshift can be interpreted as a simple increase in cytoplasmic viscosity due to higher molecular crowding, which is in contrast to the different effects of high osmolarity on small molecules and on GFP (Mika et al. 2010). Notably, no effect is observed on the anomaly of diffusion for any protein construct (Figure 3.34E).

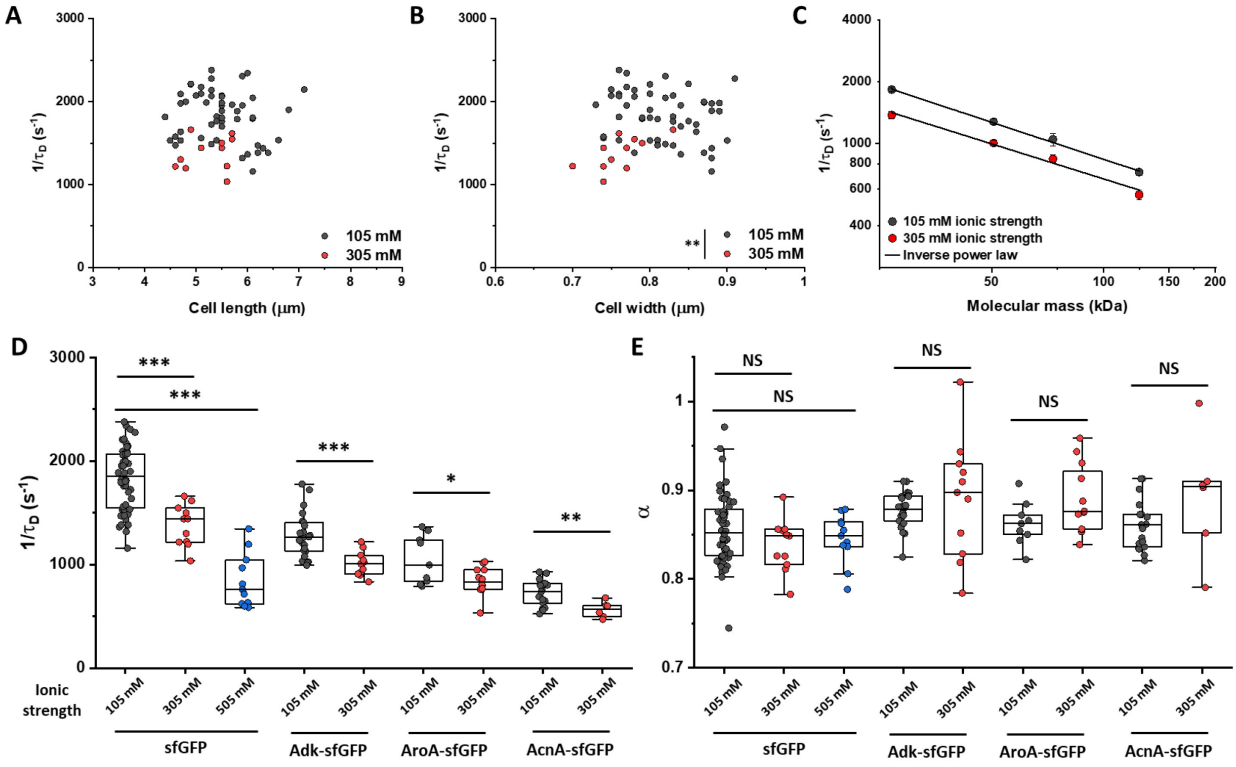


**Figure 3.34** Mobility ($1/\tau_D$) of sfGFP in individual bacterial cells at the indicated ionic strength plotted as function of the respective cell length (A) and width (B). Significance analysis was performed for the respective cell dimension. **p<0.001 in a two-tailed heteroscedastistic *t*-test. (C) Effect of ionic strength on the size dependence of cytoplasmic protein mobility ($1/\tau_D$). Protein mobility was measured in cells that were resuspended in either tethering buffer (total ionic strength of 105 mM) or in the same buffer supplemented with additional 100 mM NaCl (total ionic strength 305 mM). Each dot represents the average value of protein mobility of all the cells measured for the construct of the indicated molecular mass in the indicated condition of ionic strength. Error bars represent the standard error. Error bars that are not visible are smaller than the symbol size. The solid black lines are the fit with an inverse power law to extract the size dependence of protein mobility (105 mM ionic strength, $\beta = 0.60 \pm 0.01$; 305 mM ionic strength, $\beta = 0.57 \pm 0.05$) (D). Individual values of protein mobility ($1/\tau_D$; D) and anomaly of diffusion ($\alpha$; E) from single cells expressing the indicated protein constructs at the indicated condition of ionic strength. sfGFP was also measured in tethering buffer supplemented with 200 mM NaCl (total ionic strength 505 mM). *** p<0.0001; **p<0.001; * p<0.05; NS: no statistically significant difference in a two-tailed heteroscedastistic *t*-test.

### 3.10.2 Environmental and growth temperature

Next, we studied the effect of environmental temperature on cytoplasmic protein mobility. According to the Stokes-Einstein equation, the diffusion of a particle depends on the system's temperature in Kelvin and on the viscosity of the fluid, which itself changes with temperature (see also section 1.7.3). In the biologically relevant range, the temperature sensitivity of diffusion is primarily determined by the temperature dependence of water viscosity. We thus compared the diffusion of sfGFP and of two fast-diffusive constructs at the environmental (imaging) temperatures of 25°C and 35°C. Expectedly, the effect of imaging temperature was not linked to any changes of the cell size (Figure 3.35A, B). The measured increase in mobility between 25°C and 35°C affects the three proteins proportionally by approximately 20-25% (Figure 3.35C, D). Importantly, this effect is consistent with the expected temperature-dependent decrease in water viscosity over 10°C (~2% per degree Celsius) (Huber et al. 2009). A weak, but consistent, increase in the anomaly of protein diffusion is also observed at higher environmental temperature (Figure 3.35E).

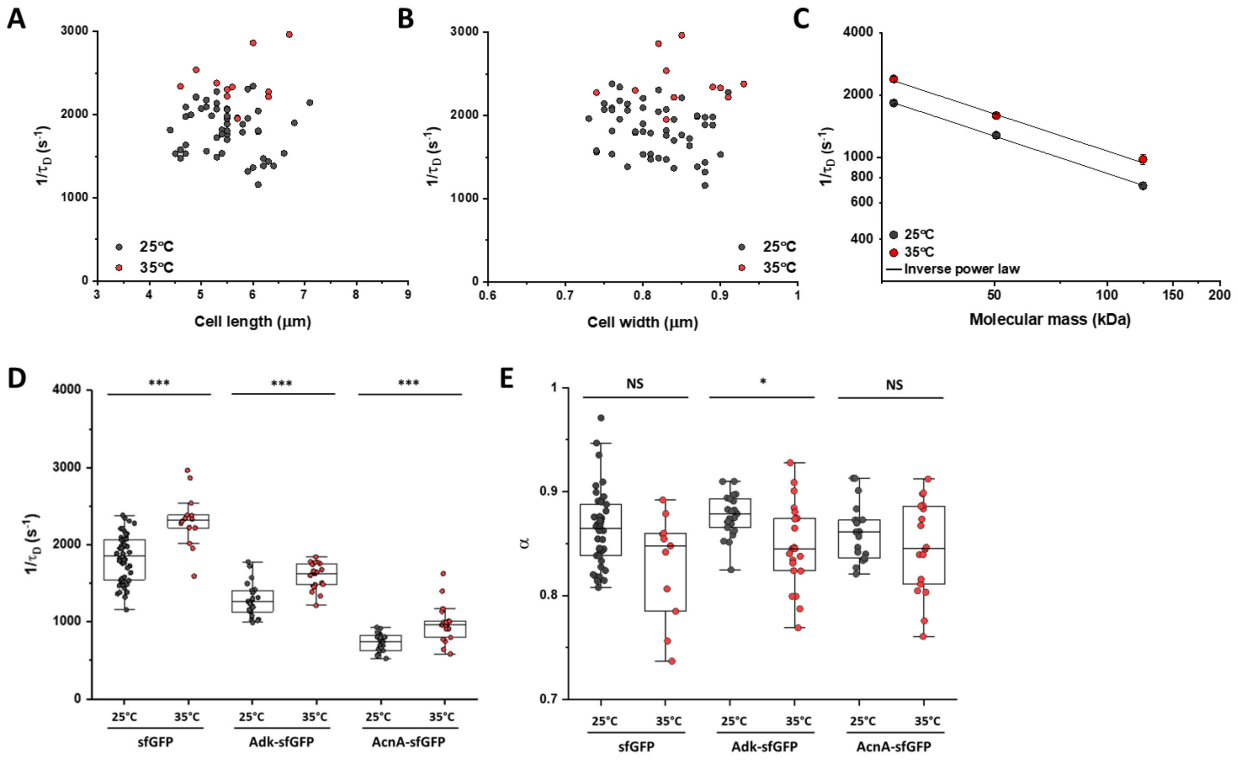


**Figure 3.35.** Mobility ($1/\tau_D$) of sfGFP in individual bacterial cells at the indicated environmental temperature plotted as function of the respective cell length (A) and width (B). (C) Effect of environmental temperature on the size dependence of cytoplasmic protein mobility ($1/\tau_D$). As for the other experiments, cultures were grown at 37°C and during the experiments bacterial cells were incubated at 25°C or 35°C. Each dot represents the average value of protein mobility of all the cells measured for the construct of the indicated molecular mass at the indicated environmental temperature. Error bars represent the standard error of the mean. Error bars that are not visible are smaller than the symbol size. The solid black lines are the fit with an inverse power law to extract the size dependence of protein mobility (25°C, $\beta = 0.60 \pm 0.01$; 35°C, $\beta = 0.60 \pm 0.05$). Individual values of protein mobility ($1/\tau_D$; D) and anomaly of diffusion ($\alpha$; E) measured in single cells expressing the indicated protein constructs at the indicated temperature. *** $p<0.0001$; * $p<0.05$; NS: no statistically significant difference in a two-tailed heteroscedastistic *t*-test.

We then tested if the viscosity of the *E. coli* cytoplasm adapts to the growth temperature in order to maintain constant diffusion rates of macromolecules, as recently observed in budding yeast (Persson,

Ambati, and Brandman 2020) and, in a possibly more complex fashion, in *Listeria* (Tran et al. 2021). We thus compared the mobility of sfGFP at the imaging temperatures of 25°C and 35°C in cells grown at 25°C or 37°C. Contrary to what observed in yeast and *Listeria*, no growth temperature-specific effect was observed in the mobility or the anomaly of diffusion (Figure 3.36) of sfGFP, suggesting that – at least in the tested temperature range – *E. coli* lacks a growth temperature-dependent regulation of cytoplasmic viscosity.

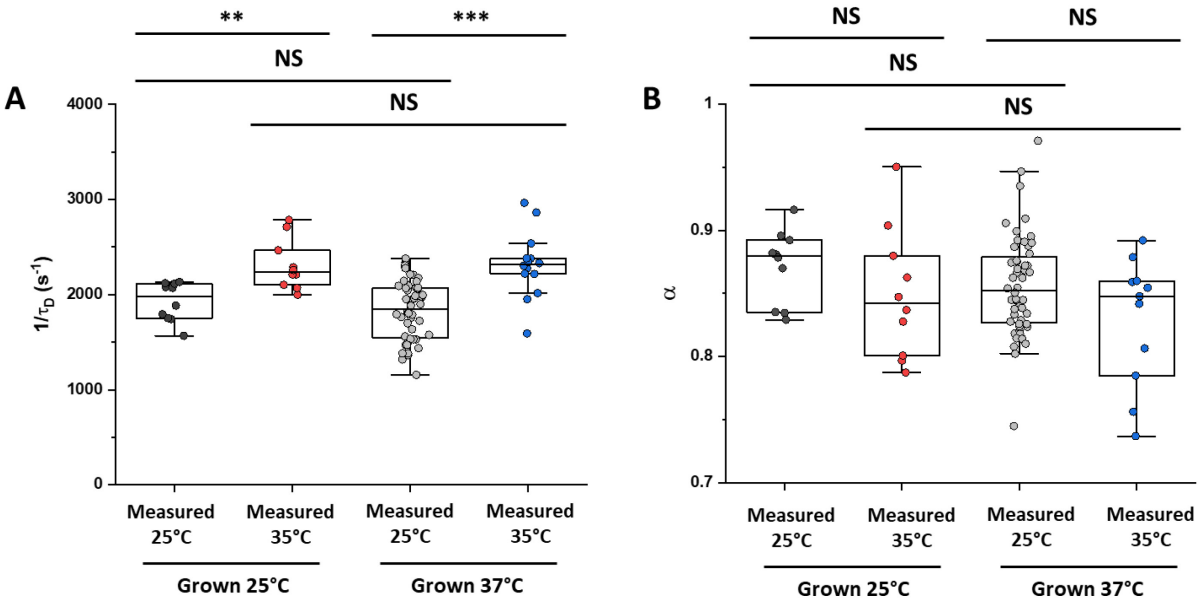


**Figure 3.36** Mobility ($1/\tau_D$; A) and anomaly of diffusion ($\alpha$; B) for sfGFP in cells grown either at 25°C or at 37°C and measured either at 25°C or at 35°C. *** $p<0.0001$; ** $p<0.001$; NS: no statistically significant difference in a two-tailed heteroscedastistic *t*-test.

### 3.10.3 Antibiotics treatment

The mobility of chromosomal loci and of large cytoplasmic aggregates was recently shown to be affected by several antibiotics, in apparent correlation with changes in the cytoplasmic density (Wlodarski et al. 2020). We first tested rifampicin, an antibiotic that blocks RNA transcription by inhibiting the β subunit

of the bacterial RNA polymerase and that was reported to increase the mobility of cytoplasmic particles (Rotter et al. 2021; Wlodarski et al. 2020). The cell dimensions are not significantly affected by rifampicin treatment (Figure 3.37A, B) and only a minor decrease in cell density was observed in our sedimentation assays (Figure 3.24E, F, H) beyond the effect of the DMSO that was used as a solvent for rifampicin. Conversely, rifampicin treatment led to a marked increase in protein mobility (Figure 3.37C, D). Such higher protein mobility is consistent with the previously observed rifampicin-induced reduction of macromolecular crowding in the bacterial cytoplasm (Wlodarski et al. 2020). We subsequently tested the effect of chloramphenicol, an antibiotic that blocks protein translation by inhibiting the peptidyl transferase activity of the ribosomes. The treatment with chloramphenicol caused a minor increase in cell width (Figure 3.37B) and a decrease in cell density (Figure 3.24G, H). However, protein mobility rather decreased in chloramphenicol-treated cells, opposite to what could be expected based alone on the chloramphenicol-induced reduction of cell density. Similar to the effects of osmolarity and temperature, the increase in protein mobility caused by the rifampicin treatment, and its decrease induced by chloramphenicol were similar for all tested proteins (Figure 3.37C), except for the AcnA-sfGFP construct that was disproportionally affected by chloramphenicol in both mobility and anomaly of diffusion, that is otherwise unaffected by the tested antibiotic treatments (Figure 3.37E).

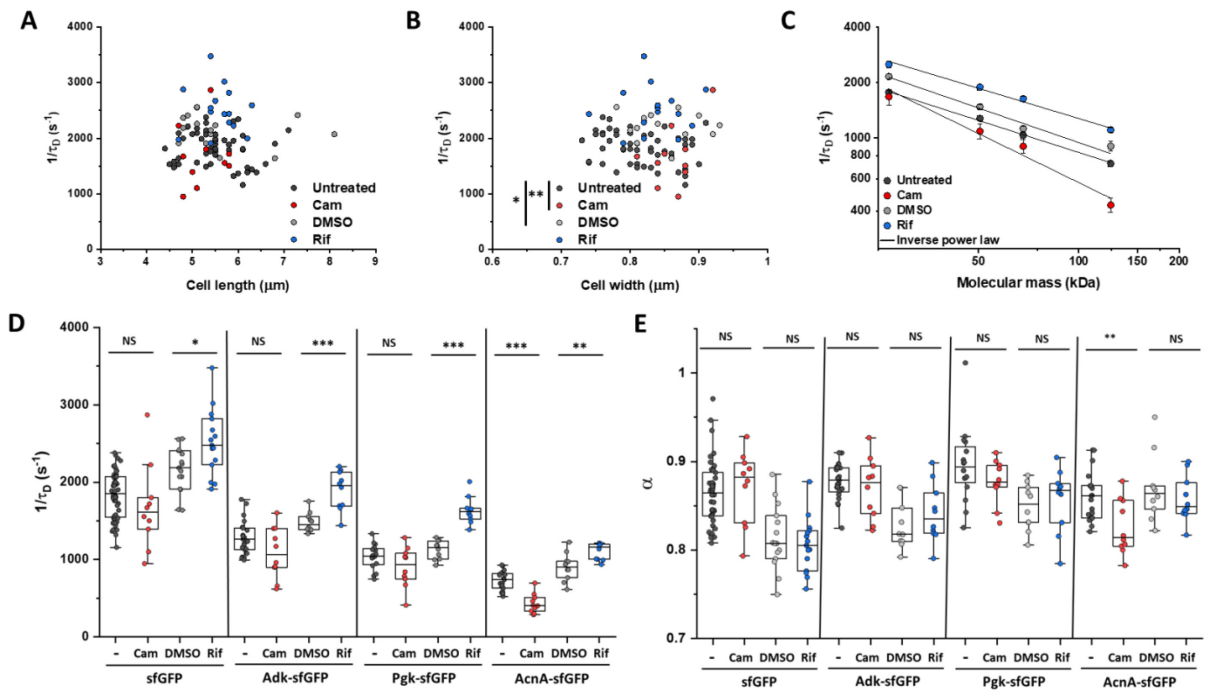


**Figure 3.37** Mobility ($1/\tau_D$) of sfGFP in individual bacterial cells after treatment with chloramphenicol (Cam; 200 µg/ml), rifampicin (Rif; 200 µg/ml in 0.1% v/v DMSO) or DMSO control (0.1% v/v) plotted as function of the respective cell length (A) and width (B). Significance analysis was performed for the respective cell dimension. **p<0.001; * p<0.05 in a two-tailed heteroscedastistic *t*-test. Antibiotics were added to growing *E. coli* cultures 60 minutes prior to harvesting. (C) Size dependence of cytoplasmic protein mobility ($1/\tau_D$) after treatment with the indicated antibiotics. Each dot represents the average value of protein mobility of all the cells measured for the construct of the indicated molecular mass after the indicated treatment. Error bars represent the standard error. Error bars that are not visible are smaller than the symbol size. The solid black lines are the fit with an inverse power law to extract the size dependence of protein mobility (Untreated, $\beta = 0.58 \pm 0.02$; Cam, $\beta = 0.88 \pm 0.11$; Rif, $\beta = 0.54 \pm 0.04$; DMSO, $\beta = 0.62 \pm 0.07$). Individual values of protein mobility ($1/\tau_D$; D) and anomaly of diffusion ($\alpha$; E) from single cells expressing the indicated protein constructs after the indicated treatment. *** p<0.0001; **p<0.001; * p<0.05; NS: no statistically significant difference in a two-tailed heteroscedastistic *t*-test.

It is well known that the treatment of *E. coli* cells with chloramphenicol leads to the compaction of the nucleoid (Bakshi et al. 2014). The high spatial resolution provided by FCS, allowed us to compare the

diffusion of sfGFP and of a larger construct inside and outside of such compacted nucleoid, visualized by staining with the DNA-binding molecule SYTOX Orange (Figure 3.38A). We observed that the reduced protein mobility after chloramphenicol treatment could not be simply explained by the compaction of the nucleoid, since it was only marginally lower inside than outside of the nucleoid (Figure 3.38B). This effect may be consistent with the minor contribution of DNA to the cellular macromolecular crowding (van den Berg, Boersma, and Poolman 2017). It should be noted that no significant difference in the anomaly of diffusion was observed inside or outside of the nucleoid (figure 3.38C).

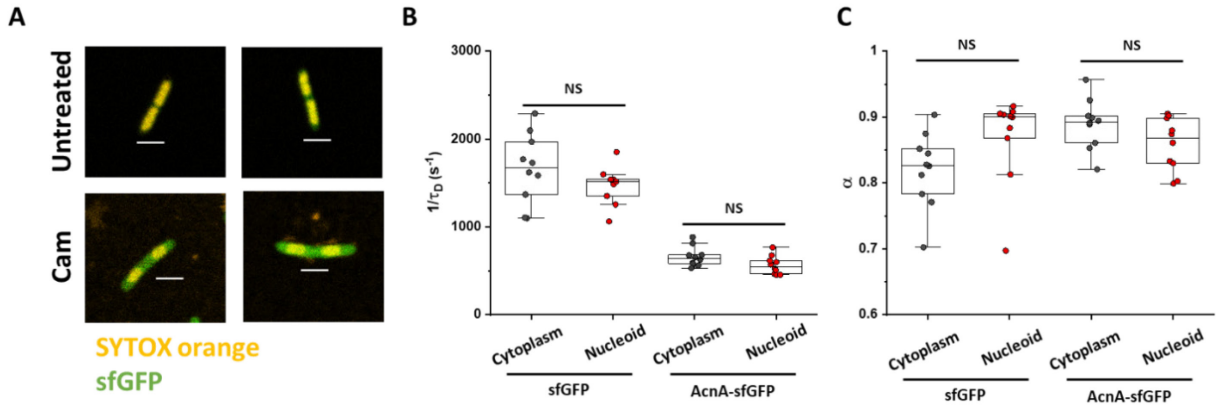


**Figure 3.38** (A) Representative microscopy images of control *E. coli* cells (upper row) and cells treated with chloramphenicol (Cam; lower row), after staining with the DNA-binding dye SYTOX Orange (300 nM). Scale bar is 2 µm. Mobility ($1/\tau_D$; B) and anomaly of diffusion ($\alpha$; C) of sfGFP and of one larger construct (AcnA-sfGFP) was measured in both the cytoplasm and in the nucleoid of chloramphenicol treated cells. NS: no statistically significant difference in a two-tailed heteroscedastistic *t*-test.

### 3.10.4 Cell growth, biosynthetic activities and metabolism

Previous researches on protein diffusion intentionally avoided measuring diffusion in bacterial cells that were growing or diving. Therefore, the effect of cell growth on protein diffusion has likely been overlooked. We thus performed FCS experiments in cells incubated at 35°C on agarose pads prepared in

M9 salts or M9 salts plus glucose and casamino acids. These conditions had only minor impact on the cell shape (Figure 3.39A, B). Although at this high temperature residual growth was observed also for cells on M9 salts pads, cell growth in presence of nutrients was expectedly much more pronounced. The measured protein mobility was also much higher in the presence of nutrients, and this increase was again similar for the four tested differently-sized constructs (Figure 3.39C, D), while no consistent trend was observed in the anomaly of protein diffusion across these conditions (Figure 3.39E).

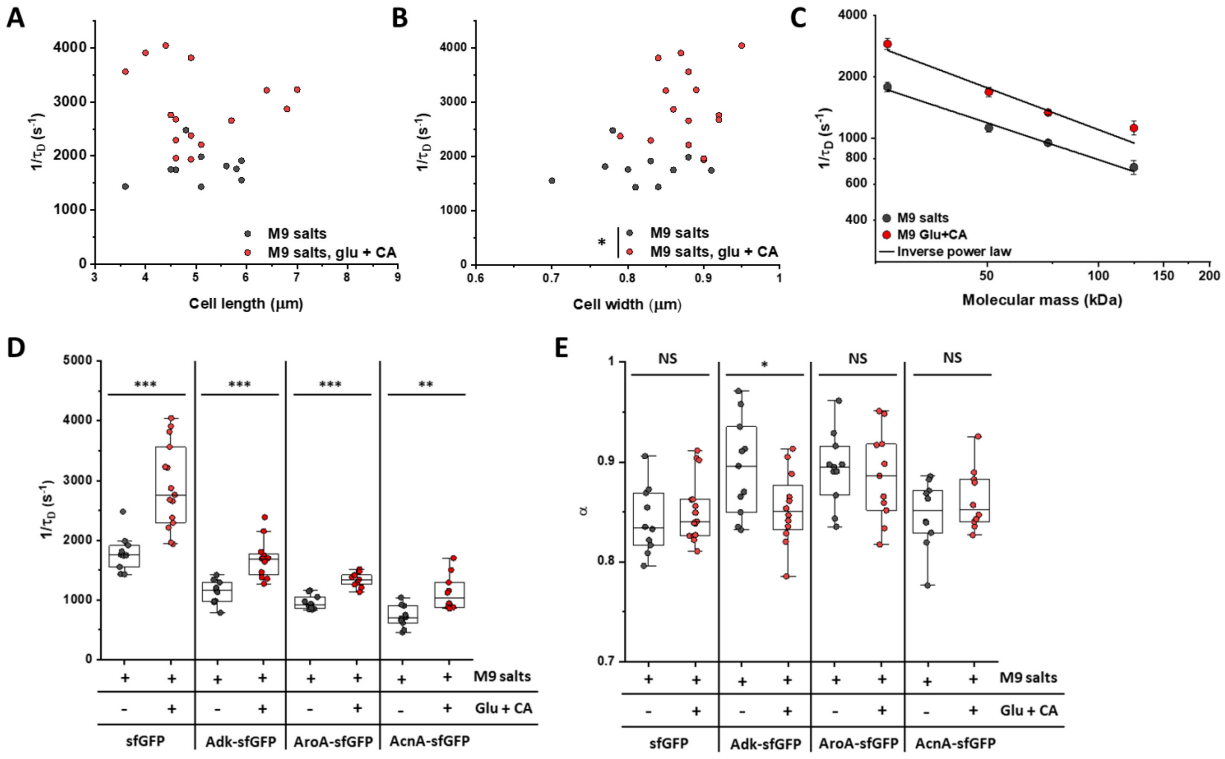


**Figure 3.39** Mobility ($1/\tau_D$) of sfGFP in individual bacterial cells incubated at 35°C on agarose pads containing either only M9 salts or M9 salts supplemented with 20 mM glucose and 0.2% casamino acids (Glu + CA) plotted as function of the respective cell length (A) and width (B). Significance analysis was performed for the respective cell dimension. * $p<0.05$ in a two-tailed heteroscedastistic *t*-test. (C) Size dependence of cytoplasmic protein mobility ($1/\tau_D$) at the indicated nutrients conditions. Each dot represents the average value of protein mobility of all the cells measured for the construct of the indicated molecular mass in the indicated condition. Error bars represent the standard error. Error bars that are not visible are smaller than the symbol size. The solid black lines are the fit with an inverse power law to extract the size dependence of protein mobility (M9 salts, $\beta$

= 0.60 ± 0.05; M9 glu + CA, $\beta$ = 0.68 ± 0.10). Individual values of protein mobility ($1/\tau_D$; D) and anomaly of diffusion ($\alpha$; E) from single cells expressing the indicated protein constructs at the indicated nutrients conditions. *** p<0.0001; **p<0.001; * p<0.05; NS: no statistically significant difference in a two-tailed heteroscedastistic *t*-test.

To further distinguish the respective contributions of metabolic activity, biosynthesis, and the resulting cell growth on protein diffusion, we incubated bacterial cells in presence of both nutrients and chloramphenicol on the agarose pad (Figure 3.40). Chloramphenicol is a bacteriostatic antibiotic, and arrests bacterial growth by blocking the translation of new proteins. Similar to our previous experiments where chloramphenicol was added to the batch culture, its addition had no or little effect on the mobility of sfGFP or the AcnA-sfGFP construct in absence of nutrients. In contrast, protein mobility in presence of nutrients was strongly affected by chloramphenicol treatment. Thus, the previously observed enhanced protein mobility in presence of nutrients appears to be primarily due to active protein production and cell growth. Nevertheless, even chloramphenicol-treated cells exhibited a moderate increase in protein mobility in presence of nutrients, indicating that the metabolic activity contributes to the overall effect of growth on diffusion. It is possible that the contribution of the metabolic activity might be even larger than it appears in this experiment, since the inhibition of protein translation might reduce metabolic activity.

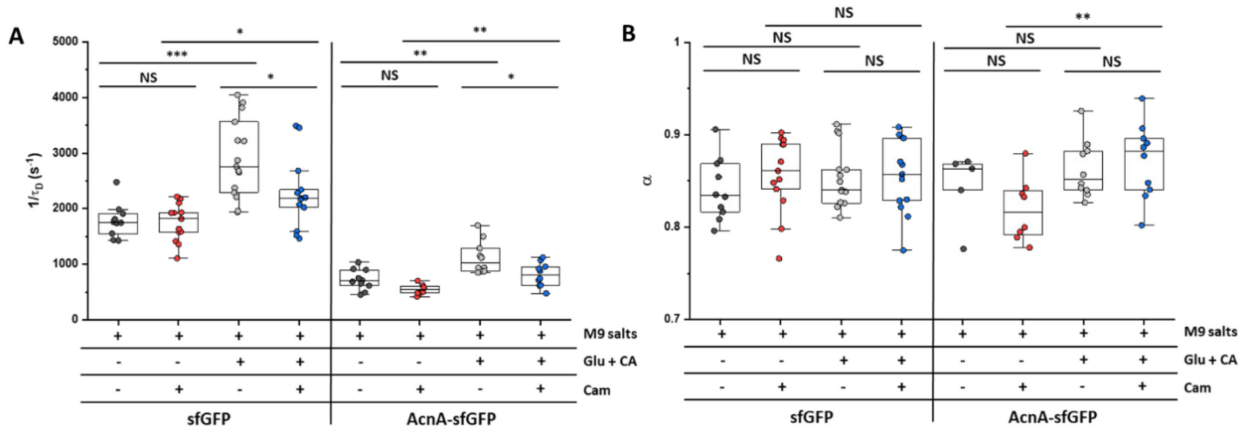

**Figure 3.40** Individual values of protein mobility ($1/\tau_D$; A) and anomaly of diffusion ($\alpha$; B) of the indicated protein constructs measured in cells incubated at 35°C on agarose pads containing either only M9 salts or M9 salts together with 20 mM glucose and 0.2% casamino acids (Glu + CA). Where indicated, chloramphenicol (Cam, 200 μg/ml) was also added to the agarose pads. *** p<0.0001; ** p<0.001; * p<0.05; NS: no statistically significant difference in a two-tailed heteroscedastistic *t*-test.

### 3.10.5 Growth phase

Bacterial cells in stationary phase, has largely stopped both the biosynthetic activity and the cell growth. We thus compared the mobility of "fast-diffusing" proteins of different mass between cells in exponential phase and in stationary phase, ~24 hours after the inoculation. For a more equal comparison with the much shorter cells in the stationary phase, the cultures in exponential phase were not treated with cephalexin (Figure 3.41A). Consistently with our hypothesis that protein mobility scales with cell growth, we observed that the mobility of all constructs was much lower in cells in stationary phase (Figure 3.41B), and such effect was roughly proportional for constructs of different mass. The anomaly of diffusion instead was not affected by the growth phase (Figure 3.41C).

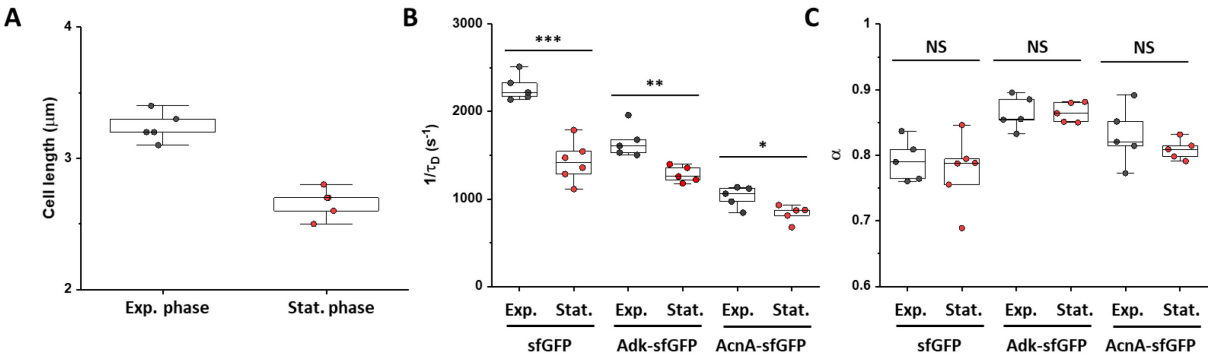


**Figure 3.41** (A) Comparison of cell length between cells in exponential and stationary phase. Cells in exponential phase were grown as usual, except that for this experiment were not treated with cephalexin. Cells in stationary phase were grown for ~ 24h after inoculation from the glycerol stock. Individual values of protein mobility ($1/\tau_D$; B) and anomaly of diffusion ($\alpha$; C)

of the indicated sfGFP construct in cells in exponential or stationary phase. *** p<0.0001; ** p<0.001; * p<0.05; NS: no statistically significant difference in a two-tailed heteroscedastistic *t*-test.

### 3.10.6 Cellular energy state

Several studies in bacteria and budding yeast have shown that in presence of the inhibitor of respiration-dependent ATP synthesis dinitrophenol (DNP), the mobility of large multiprotein complexes is drastically reduced (Munder et al. 2016; Parry et al. 2014). To test if a similar effect is conserved also for single proteins, we compared the mobility of sfGFP and of two constructs with larger mass in control cells and in cells incubated on the agarose pad in presence of DNP. No general effect of DNP on protein mobility or anomaly of diffusion was observed in these conditions (Figure 3.42), at either 25°C or 35°C thus suggesting that the impact of growth on the diffusion of individual proteins cannot be simply explained by the energy state of the cell. An interesting exception was the mobility of Adk-sfGFP, which was indeed reduced by the DNP treatment at high temperature. This might be a specific effect related to the enzymatic activity or conformation of Adk that binds ATP as a substrate. We thus decided to further investigate the effect of ATP on protein diffusion by taking a different approach.

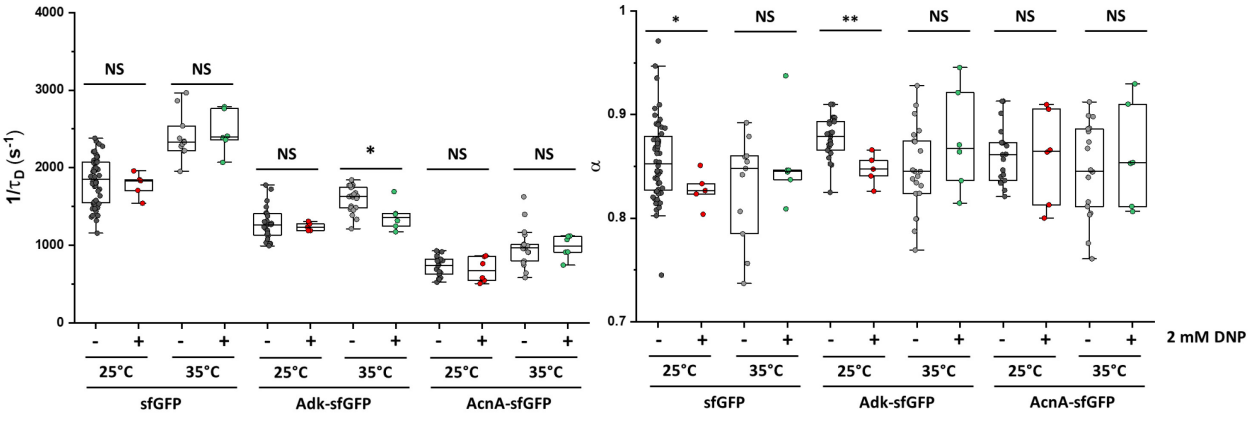


**Figure 3.42** Individual values of protein mobility ($1/\tau_D$; A) and anomaly of diffusion ($\alpha$; B) of sfGFP and of two constructs with higher molecular mass measured in bacterial cells treated in batch for 60 minutes with 2 mM DNP and compared with the

respective untreated control. Measurements were performed on 1% agarose pads prepared in tethering buffer and supplemented with 2 mM DNP at the indicated incubation temperature. ** $p<0.001$; * $p<0.05$; NS: no statistically significant difference in a two-tailed heteroscedastistic *t*-test.

## 3.11 *In situ* evidences of enhanced diffusion

Having observed a significant increase in protein mobility in presence of nutrients, possibly due to the cytoplasmic stirring promoted by the energy released through different enzymatic activities (Figure 3.39), we speculated that removing the nutrients from the cytoplasm would reduce such stirring. A consistent *corpus* of classic literature proved that after the permeabilization of the inner membrane of bacterial cells with toluene, small molecules can be efficiently eluted from the cytoplasm, while the macromolecules are largely retained (Jackson Robert and DeMoss 1965; Deutscher 1974; De Smet, Kingma, and Witholt 1978; McMurry, Hendricks, and Levy 1986). Although toluene-treated bacteria are not capable to grow, if the required substrates are provided exogenously, permeabilized cells are still capable of performing the synthesis and repair of DNA, the transcription of RNA and protein translation (Wickner and Hurwitz 1972; Ben-Hamida and Gros 1973; Deutscher 1974; Boye 1980; McMurry, Hendricks, and Levy 1986). We first investigated whether the permeabilization of the inner membrane of *E. coli* had measurable effects on cytoplasmic protein mobility. To prove that the cytoplasm of our toluene-treated cells was indeed in equilibrium with the surrounding buffer, and it was thus also likely depleted from the endogenous metabolites, we routinely performed the staining of the toluene-treated cells with the DNA-binding dye SYTOX Red at a concentration sufficiently low to only stain permeabilized cells (Figure 3.43A). Of note, SYTOX Red appeared to stain the cell cytoplasm rather homogeneously, possibly due to a toluene-induced expansion of the nucleoid. We then measured the diffusion of several sfGFP constructs in the cytoplasm of cells treated with toluene and fitted the ACFs with the anomalous diffusion model (Figure 3.43B). In

agreement with our expectations, we observed that the mobility (Figure 3.43C) of all the investigated protein constructs was significantly reduced after toluene treatment. Interestingly, we also observed that the anomaly of diffusion increases significantly for all the tested constructs (Figure 3.43D).

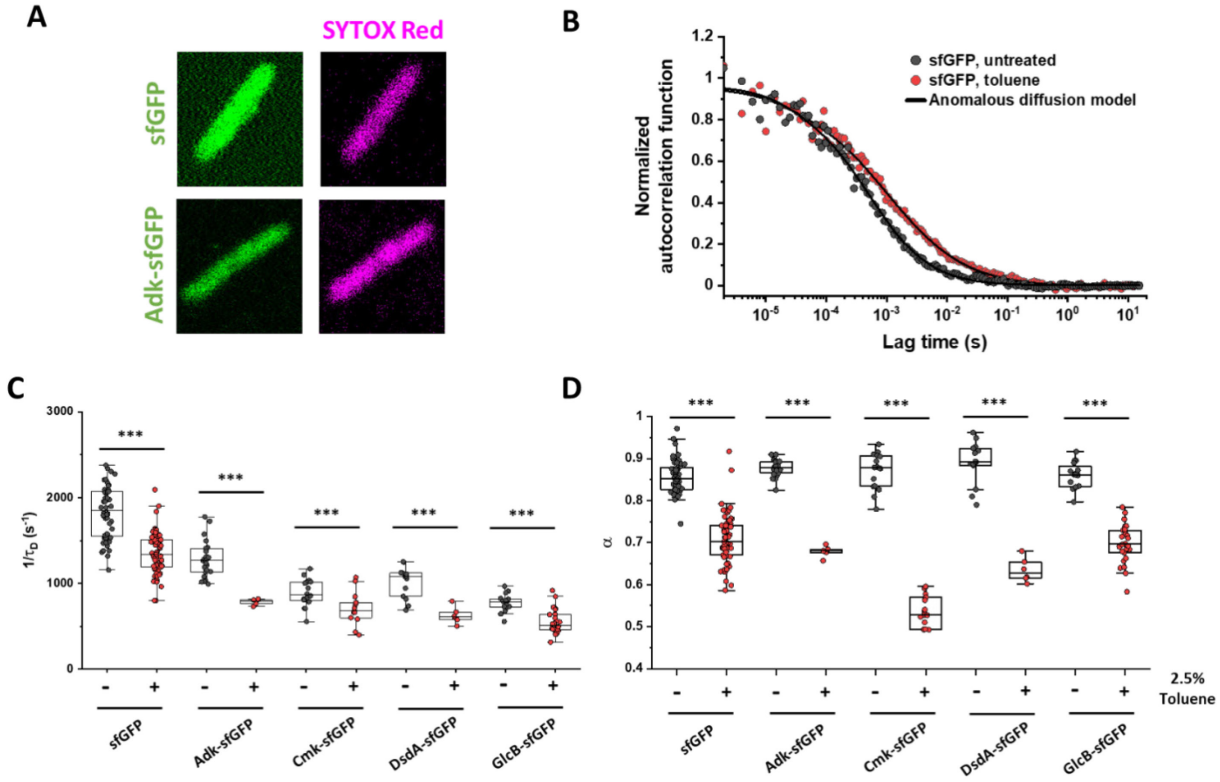


**Figure 3.43** (A) Representative microscopy images of *E. coli* cells expressing the indicated sfGFP construct after permeabilization with toluene and staining with of the DNA-binding dye SYTOX Red (15 nM). Cell permeabilization was performed by incubation with 2.5% toluene for 15 minutes in tethering buffer supplemented with 10 mM $MgCl_2$ to prevent considerable loss of cytoplasmic macromolecules (De Smet, Kingma, and Witholt 1978). (B) Representative autocorrelation functions (ACFs) for sfGFP in control untreated cells and in toluene-treated cells fitted with the anomalous diffusion model (solid lines). The ACF curves were normalized to their respective maximal values to facilitate comparison. Individual values of protein mobility ($1/\tau_D$; C) and anomaly of diffusion ($\alpha$; D) of the indicated protein construct measured in untreated control cells or in toluene-permeabilized cells. *** $p<0.0001$ in a two-tailed heteroscedastistic *t*-test.

We then reintroduced ATP back to permeabilized cells, to study its specific effect on protein diffusion inside a bacterial cell, albeit not alive (*i.e. in situ*). Interestingly, the mobility of sfGFP increases steadily with progressively higher concentrations of ATP (Figure 3.44A, B) and it appears to saturate at 5-10 mM of ATP. Of note, at concentrations of ATP in the range commonly measured in *E. coli* (~ 1-3 mM) (Buckstein Michael, He, and Rubin 2008; Bennett et al. 2009; Yaginuma et al. 2014), sfGFP mobility in toluene-treated cells becomes comparable to that of untreated cells. Importantly, such effect appears to depend largely, but not entirely, on the hydrolysis of ATP, since an equal concentration of the non-hydrolysable ATP analogue AMP-PNP, produces a smaller, but still significant increase in sfGFP mobility. No significant effect on the anomaly of diffusion is observed after reintroduction of ATP (Figure 3.44C).

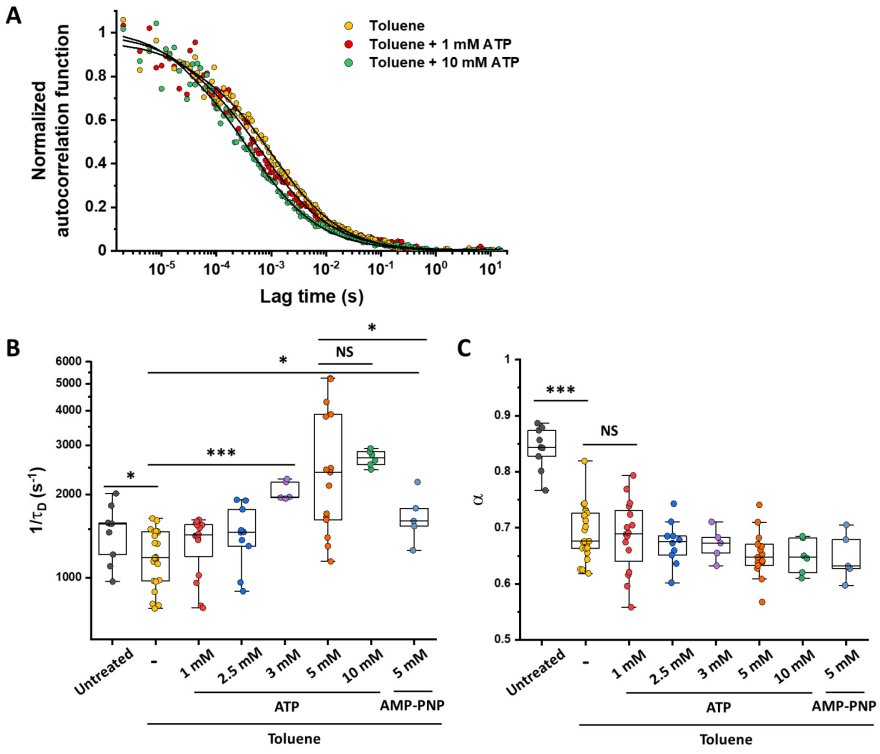

**Figure 3.44** (A) Representative autocorrelation functions (ACFs) fitted with the anomalous diffusion model (solid lines) for sfGFP in cells after treatment with toluene or cells from the same batch supplemented with the indicated concentration of ATP. The ACF curves were normalized to their respective maximal values to facilitate comparison. Individual values of sfGFP mobility ($1/\tau_D$; B) and anomaly of diffusion ($\alpha$; C) measured in toluene-permeabilized bacterial cells. For these experiments, bacterial cells were attached to the bottom of multi-well plates with poly-L-lysine and overlaid with tethering buffer supplemented with the indicated concentration of ATP or AMP-PNP. *** $p<0.0001$; **$p<0.001$; * $p<0.05$; NS: no statistically significant difference in a two-tailed heteroscedastistic *t*-test. When not indicated, no statistically significant difference was observed.

We then looked further into the previously observed specific reduction in mobility of the enzyme Adk at low levels of cellular ATP (Figure 3.42). Adk is the adenosine kinase, that catalyzes the ATP-dependent phosphorylation of AMP to ADP. We thus incubated toluene-permeabilized *E. coli* cells expressing Adk-sfGFP with different concentrations of ATP. As previously observed with the inert sfGFP, also the diffusion of Adk is increased by the presence of ATP (Figure 3.45A, B), and such an increase scales with the concentration of ATP. If cells are incubated with equimolar concentrations of both the substrates ATP and AMP, the increase in Adk-sfGFP mobility is larger than with ATP alone. Importantly, incubation with AMP, AMP-PNP or the combination of the two, have a much lower effect on Adk-sfGFP mobility than that of equimolar concentrations of ATP or ATP and AMP. We also tested another ATP-hydrolyzing enzyme, the cytidylate kinase Cmk that catalyzes the ATP-dependent phosphorylation of CMP to CDP. Consistently with the previous observations, its diffusion significantly increases when incubated with ATP (Figure 3.45C, D). However, the further addition of CMP, while increasing Cmk-sfGFP mobility compared with toluene-treated cells, did not further increase diffusion above that with ATP.

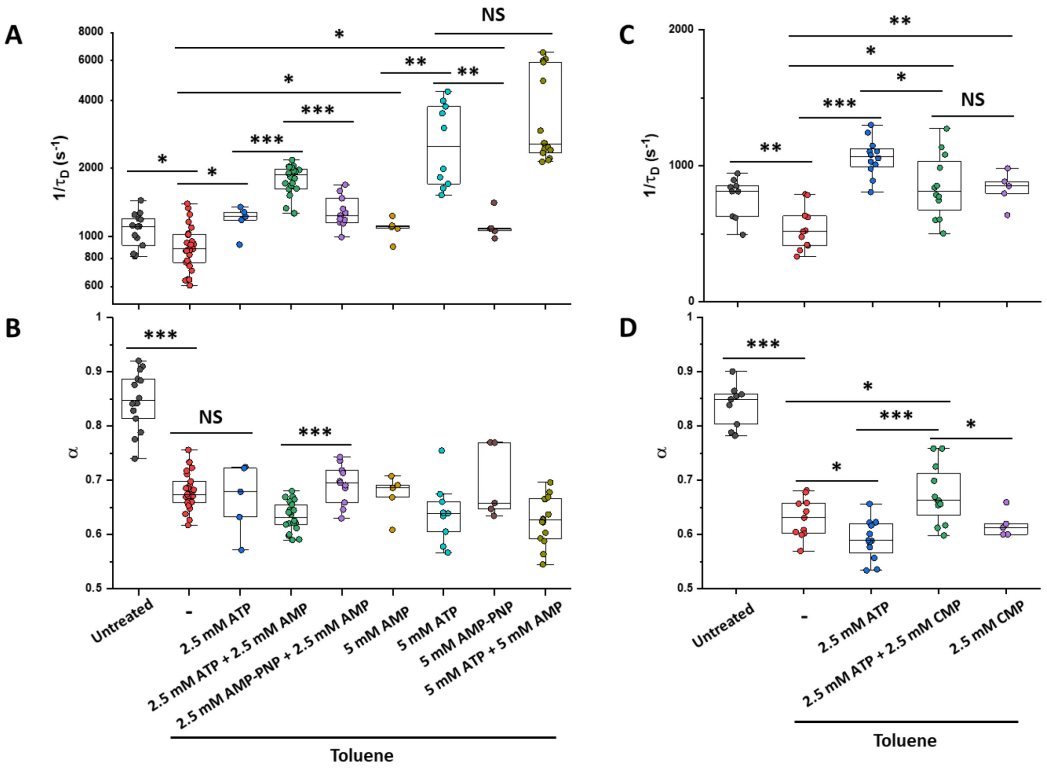


**Figure 3.45.** Individual values of Adk-sfGFP mobility ($1/\tau_D$; A) and anomaly of diffusion ($\alpha$; B) measured in toluene-permeabilized bacterial cells attached with poly-L-lysine to the bottom of multi-well plates and overlaid with tethering buffer supplemented with the indicated concentrations of ATP, AMP, and AMP-PNP. Individual values of Cmk-sfGFP mobility ($1/\tau_D$; A) and anomaly of diffusion ($\alpha$; B) measured in toluene-permeabilized bacterial cells attached to the bottom of multi-well plates with poly-L-lysine and overlaid with tethering buffer supplemented with the indicated concentrations of ATP and CMP. *** p<0.0001; **p<0.001; * p<0.05; NS: no statistically significant difference in a two-tailed heteroscedastistic *t*-test. When not indicated, no statistically significant difference was observed.

# 4. Discussion

Despite the substantial research effort produced in the past years, the dependence of protein diffusion on protein mass and shape, and the consequences of various physicochemical perturbations and of the cellular physiology on protein diffusion, remain still unclear. In this study, we addressed these questions, elucidating details on how protein diffusion rates are affected by properties typical of the single proteins, such as their mass, shape and protein-protein interactions, but also by the interplay between the external environment and the internal cellular physiology.

## 4.1 The diffusion of cytoplasmic proteins in bacterial cells is Brownian

To date, we performed the most extensive analysis of the size dependence of protein diffusion in bacterial cytoplasm by investigating the mobility of 28 sfGFP-tagged proteins endogenous of the cytoplasm of *E. coli* with fluorescence correlation spectroscopy. We observed that, based on their diffusional behavior, the constructs could be qualitatively sorted in a "fast-diffusive" or a "slow-diffusive" category. The 17 "fast diffusive" constructs showed a weak anomaly of diffusion, with an anomalous diffusion exponent that saturates at $\alpha = 0.8$ - 0.89, and a diffusion rate ($1/\tau_D$) that defines a clear upper bound to cytoplasmic protein mobility and decreases uniformly with the increase in the construct's molecular mass. This bound likely reflects the fundamental size-specific physical limit on protein diffusion in the crowded environment of the cytoplasm of *E. coli*. Results from our Brownian dynamics simulation suggested that the apparent weak anomaly of diffusion observed in our FCS data, that is consistent with previous reports

(Meacci et al. 2006), could be accounted for by confinement of the otherwise purely Brownian diffusing proteins in the small volume of a bacterial cell. Similar conclusions have been drawn by previous SPT studies for individual proteins (Bakshi, Bratton, and Weisshaar 2011; English et al. 2011). This interpretation is consistent with the observed decrease in the anomaly of diffusion in A22-treated *E. coli* with an increased cell diameter. The interpretation of these experiments might be complicated by the reduced cytoplasmic density of A22-treated bacteria (Oldewurtel Enno, Kitahara, and van Teeffelen 2021). Such reduced cytoplasmic density, and thus macromolecular crowding, may contribute to the observed reduced anomaly of diffusion. However, under our growth conditions the effect of A22 on cell density seemed to be rather negligible. The interpretation that weak anomaly depends on cell confinement is also supported by the FCS measurements using a smaller, albeit less optimal due to lower signal-to-noise ratio, confocal volume, which yielded higher value of $\alpha$, as could be expected from protein diffusion measured in a volume distant from the cell boundary.

### 4.2 Size dependence for the diffusion of dumbbell-shaped proteins *in vivo*

The protein constructs that showed fast-diffusion and weak, confinement-dependent, anomaly of diffusion, were then used as inert tracers to estimate an unbiased size dependence of protein diffusion. We fitted the autocorrelation functions of these constructs by using a model of purely Brownian diffusion under confinement elaborated by approximating particles diffusion in proximity to the cell pole to an Ornstein-Uhlenbeck process of Brownian diffusion confined by a harmonic potential. The overall dependence of diffusion coefficients on the molecular mass showed the exponent $\beta = 0.56$, steeper than what expected by the Stokes-Einstein relation for fully compact particles ($\beta = 0.33$), or the more realistic case of not entirely compact proteins ($\beta \sim 0.4$). The size dependence obtained from our large dataset, is

comparable to estimates of $\beta$ ranging from 0.54 to 0.75, obtained from previous, more limited, datasets (Mika et al. 2010; Stracy et al. 2021; Śmigiel et al. 2022). We speculated that such commonly observed reduced "compactness" may depend on the peculiar dumbbell shape of a typical globular protein tagged with GFP via a short linker. Indeed, a model that takes in consideration the specific shape of two, imperfectly globular, proteins connected via a short linker, predicts very well the size dependence of protein diffusion, in particular for sizes smaller than 75 kDa. Above this value, this model tends to overestimate protein mobility, possibly because larger proteins are formed by different domains whose additional degrees of freedom are not fully predicted by a model of two linked proteins, or because large proteins are more impacted by protein-protein interactions (von Bülow et al. 2019).

### 4.3 Protein diffusion is homogeneous over different spatiotemporal scales

Most of the previous studies about protein mobility were performed using FRAP. We thus directly compared the diffusion of a subset of "fast-diffusive" constructs, with different masses, measured with FRAP and FCS under the same growth and experimental conditions. As commonly observed in literature, the diffusion coefficients measured with FRAP are 5-30% lower than those measured with FCS. This underestimation is partially explained by technical reasons, since the fast-diffusive proteins already begin the recovery during the relatively long time necessary to perform the photobleaching. Nevertheless, considering that diffusion coefficients estimated in the more recent works (Schavemaker, Smigiel, and Poolman 2017) are comparable with the values obtained in our work, the significantly lower values from the earliest works may be the result of the much lower temporal resolution in older set-ups (Elowitz Michael et al. 1999; Kumar, Mommer, and Sourjik 2010; Nenninger, Mastroianni, and Mullineaux 2010). Moreover, discrepancies in the estimated diffusion coefficients of similar proteins in independent studies may also be caused by differences in cell growth (e.g. growth medium) or sample preparation (e.g.

environmental temperature or osmolarity). The size dependences obtained with FRAP and FCS are in very good agreement, thus suggesting that the cytoplasm exerts homogeneous hindrance to protein diffusion over the 0.2 - 1 μm length scale explored by the two techniques.

### 4.4 Strong anomaly of diffusion depends on macromolecular interactions

A smaller group of 11 "slow-diffusive" constructs showed a mobility lower than that expected from their size and in some cases also a pronounced anomaly of diffusion. At least three of them were known to have extensive interactions with other components of the cytoplasm: ClpS interacts with the ClpAP protease and with proteins to be degraded, DnaK interacts with co-chaperones and with client proteins to be folded, while Map interacts with ribosomes. Theoretical studies indeed suggest that binding of diffusing molecules to crowders can lead to anomalous diffusion (Guigas and Weiss 2008; Saxton 2007). When the formation of these complexes was inhibited, their mobility and anomaly of diffusion was restored to values comparable to those dictated by their molecular mass at the confinement exerted by the cell width. Strong anomaly of diffusion is also observed for MmuM and MalZ constructs. Only putative interactors could be identified in literature for these two proteins. MmuM (*alias* YagD) is involved in the S-methylmethionine metabolism and is expressed in the same transcriptional unit as MmuP (*alias* YkfD), reported as a putative S-methylmethionine permease (Thanbichler, Neuhierl, and Böck 1999). The diffusional properties of MmuM could then be indicative of interactions with MmuP. The eventual observation of higher mobility of MmuM in a *ΔmmuP* strain may confirm the physical interaction between the two proteins. MalZ is reported to be prone to aggregation *in vitro*, and the incubation with chaperonins GroEL and GroES improves its folding (Paul, Punam, and Chaudhuri 2007; Pastor et al. 2016). The reduced mobility of MalZ could thus be explained by the formation of small aggregates, not visible under the microscope. The higher mobility of MalZ in a strain where chaperonins are overexpressed (Goltermann, Sarusie, and Bentin 2015)

could confirm this hypothesis. Measuring the diffusion of a protein of interest by FCS in conditions where its putative interactions are abolished, could then be an unusual, but effective, strategy to test hypotheses on protein-protein interactions *in vivo*. Our data also suggest that the set of proteins used in studies that estimated an aberrantly steep size dependence of protein diffusion (Kumar, Mommer, and Sourjik 2010), may have been biased towards "slow-diffusive" proteins such as chaperones (DnaK and HtpG), that interact with client proteins, and chemotaxis proteins (CheW, CheR, CheA) that interact with each other and with membrane chemoreceptors.

### 4.5 *E. coli* cytoplasm offers only mild hindrance to the diffusion of non-native proteins

Interestingly, the anomaly of diffusion of many sfGFP fusions to proteins from other bacterial species is slightly, but consistently higher than that of their *E. coli* counterparts, possibly suggesting the presence of short-lived, unspecific interactions between such exogenous proteins and components of the *E. coli* cytoplasm. Instead, the diffusion rates of such proteins are comparable to those of their *E. coli* counterparts, as expected from their very similar molecular mass (± 3 kDa). Therefore, there appear to be only little adaptation of proteins to the specific cytoplasmic environment of the bacterial host, or, from another point of view, the cytoplasmic structure is conserved across bacterial species with similar lifestyles, a feature that might favor protein functioning after horizontal gene transfer. Possible exceptions may be bacteria that live in harsh environments, characterized by high salinity or extreme pHs (Schavemaker, Smigiel, and Poolman 2017).

The cumulative evidence from these experiments suggests that protein diffusion in bacterial cytoplasm is Brownian and that the apparent weak anomaly of diffusion is largely explained by the confinement within the small diameter of the bacterial cell. Larger than expected anomaly is primarily, but possibly not

uniquely, associated with the presence of protein-protein interactions. Our experiments do not completely clarify if the strong anomaly of diffusion depends on the interactions with largely immobile partners that would act as "traps" for molecules that otherwise perform Brownian diffusion, or, as observed in bacteria for large mRNA molecules (Lampo et al. 2017) and exogenous multi-protein complexes (Yu et al. 2018), it is an emergent property of diffusing particles above a mass threshold much higher than the mass range explored in this study. Being anomalous diffusion a phenomenological property, both hypotheses could be true in different cases.

## 4.6 Macromolecular crowding, cytosolic viscosity and metabolic stirring affect diffusion of differently-sized proteins in a proportional manner

We then selected several "fast-diffusive" constructs of different molecular mass as inert tracers to investigate the effects that different physicochemical perturbations, likely experienced by free-living cells, have on the structure and the viscosity of the cytoplasm and thus on protein mobility.

### 4.6.1 Ionic strength and rifampicin oppositely affect macromolecular crowding and protein diffusion

We observed that conditions that alter macromolecular crowding have strong effects on protein mobility. Increasing the osmolarity of the medium leads to a decrease in protein mobility. This effect is well known and it has been characterized in details in several previous studies (Konopka et al. 2006; Konopka et al. 2009; Mika et al. 2010; Liu et al. 2019; Wlodarski et al. 2020). However, such studies focused on the effect on either free fluorescent proteins or on large multi-protein complexes. By investigating proteins of different mass, we concluded that their mobility is proportionally (~20%) affected under conditions of mild osmotic upshift. Such effect is consistent with previous measurements where a similar shift in osmolarity was investigated with FRAP (Konopka et al. 2009), possibly suggesting that the increase in

crowding is homogeneous at different length scales. Experiments *in vitro* showed that the anomaly of diffusion of fluorescent probes scales with the crowding of the solution: in these experiments crowding is typically increased by adding polyethylene glycol (PEG) (Banks and Fradin 2005; Goins, Sanabria, and Waxham 2008; Balbo et al. 2013). Since we did not observe a significant effect on the anomaly of diffusion at increased macromolecular crowding *in vivo*, strong anomaly of diffusion may be a peculiar characteristic of highly concentrated PEG solutions, that thus would not accurately mimic the molecular crowding in the cytoplasm.

After the inhibition of RNA transcription with rifampicin, a mass-independent ~ 20% increase in protein mobility was observed. Such increase in protein mobility is consistent with the expected fraction of the bacterial cell dry weight constituted by RNAs (~25-30%) (Cayley et al. 1991; Zimmerman and Trach 1991). We then concluded that the observed increase in protein mobility depends on the reduction in the total macromolecular crowding inside the bacterial cell due to the knocking down of RNAs, in particular messenger RNAs, whose half-life is of the order of minutes (Selinger et al. 2003), but possibly also of ribosomal RNAs whose half-life is also reported to be comparable with the relatively long incubation of cells with rifampicin in our experiments (Fessler et al. 2020). Consistently with the minor contribution of DNA to the cytoplasmic macromolecular crowding (~3% of the bacterial cell dry weight (van den Berg, Boersma, and Poolman 2017)), we observed only a minor decrease of protein mobility inside the compacted nucleoid of cells treated with chloramphenicol, compared with cell areas free of nucleoid in the same sample.

### 4.6.2 Cytoplasmic viscosity affects protein diffusion and it is insensitive to the growth temperature and the cellular energy state

The temperature dependence of the cytoplasmic viscosity in the tested range was similar to that of water and consistent with the Stokes-Einstein relation, decreasing by 20-30%, in a size-independent manner, for

an environmental temperature increase of 10°C (Huber et al. 2009). Furthermore, the same temperature dependence of protein mobility was observed upon treatment with the protonophore DNP, that deenergizes cells by dissipating the proton gradient, arguing against a contribution of active (nonthermal) stirring of cytoplasm (Weber, Spakowitz, and Theriot 2012) when *E. coli* cells lack nutrients and are non-growing. While *E. coli* adapts its membrane fluidity (Sinensky 1974) and intracellular signaling (Almblad et al. 2021; Oleksiuk et al. 2011) to the growth temperature, we did not observe dependence of the effective cytoplasmic viscosity on the growth temperature. Since growth-temperature dependent adaptation of the cytosolic viscosity was recently reported for budding yeast *Saccharomyces cerevisiae* (Persson, Ambati, and Brandman 2020) and for *Listeria monocytogenes* (Tran et al. 2021), it is surprising that such compensation apparently does not exist in *E. coli*. One possible explanation for this difference might be the broader range of growth temperatures of these organisms compared to *E. coli*.

### 4.6.3 Cytoplasmic stirring might emerge from the collective contribution of metabolism, biosynthetic reactions, and cell growth

Finally, we observed that the cellular state strongly influences cytoplasmic protein mobility. In conditions of high environmental temperature and presence of nutrients, the diffusion rate of several investigated proteins increased proportionally to their mass (~30-40%). If biosynthesis and growth were blocked by inhibiting new protein translation upon chloramphenicol treatment, protein diffusion rates were reduced, but still significantly higher than in absence of nutrients. Thus, the metabolism of glucose and amino acids appears sufficient to increase the mobility of small proteins. Additional, and possibly stronger, contributions are given by biosynthetic reactions (protein translation in particular) and cell growth. Of note, the contribution of metabolic activity in presence of nutrients may have been actually underestimated since the inhibition of protein biosynthesis by chloramphenicol could possibly indirectly reduce metabolic activity. The observed phenomenon may be different from the previously characterized ATP-dependent

fluidization of the bacterial cytoplasm that enables the mobility of large multiprotein complexes but apparently does not affect free GFP (Montero Llopis et al. 2012; Parry et al. 2014) or other small proteins, as also confirmed by our experiments. The observed decrease in protein mobility upon entering in stationary phase is probably of complex interpretation. On one hand, biosynthesis and cell growth are less pronounced during stationary phase (Navarro Llorens, Tormo, and Martínez-García 2010). On the other hand, the cytoplasm of cells in stationary phase is more crowded, since these cells are smaller in length, but have a similar content of macromolecules than cells in exponential phase (Zimmerman and Trach 1991). While the interplay between energy-, metabolism- and growth-dependent effects on the diffusional properties of bacterial cytoplasm remains to be further investigated, our results suggest that the cumulative effect of the energy released by the enzymatic activities from metabolism, biosynthetic reactions, and cell growth may generate active stirring and cytoplasmic mixing that increase the diffusion of proteins.

In conclusion, the size dependence of protein mobility in the *E. coli* cytoplasm appears to be surprisingly robust, since it is largely conserved after exposing the bacteria to several different physicochemical perturbations known to alter the viscosity or the composition of the cytoplasm and even for proteins coming from bacterial species others than *E. coli*. We hypothesize that the biophysical properties of the bacterial cytoplasm have evolved so that the relative diffusion rate of proteins with different sizes remain constant under the various conditions that a bacterial cell may experience in the environment. An imbalance in the diffusion rate of proteins in a particular size range might in fact affect protein complexes formation and ultimately hamper cellular processes.

## 4.7 ATP hydrolysis is sufficient to restore cytoplasmic mixing and enhance diffusion of inert proteins

If the cytoplasmic membrane is permeabilized by toluene treatment and the metabolites are extracted from the cytoplasm, the diffusion rates of several proteins were drastically reduced, possibly due to a complete "freeze" of the metabolic and biosynthetic activities or to the previously observed condensation of the cytoplasm after damages to the inner membrane (Chongsiriwatana et al. 2017; Wong et al. 2021). Such condensation of the cytoplasm could also justify the observed increase in the anomaly of diffusion as an increase in the confinement perceived by the diffusing proteins. The reintroduction of 1-3 mM ATP, and thus the reactivation of the ATP-dependent enzymes, that alone account for ~10% of the proteome in *E. coli*, is sufficient to restore the diffusion rates of several proteins to values comparable to those in intact cells. Living cells maintain millimolar concentrations of ATP in their cytoplasm (Buckstein Michael, He, and Rubin 2008; Bennett et al. 2009; Yaginuma et al. 2014), values that are much higher than the $K_D$ of most ATP dependent enzymes. Such a paradox is justified from the notion that ATP acts as a biological hydrotope that promotes the solvation of macromolecules that would otherwise aggregate (Patel et al. 2017). The observed increase in diffusion in presence of ATP depends to a small extent also on such solvation: in permeabilized cells incubated with AMP-PNP, that cannot be hydrolyzed but can still act as an hydrotope, the protein diffusion rates increased, albeit not to the same level observed with an equal concentration of ATP. Taken together, our experiments suggest that protein diffusion rates are proportional to the "activity" in the cytoplasm. In cells metabolically inactive after toluene treatment, the cytoplasm as a whole freezes and even the diffusion of small proteins is reduced. The reactivation of a fraction of the enzymes appears sufficient to restore the cytoplasm mixing and increase the diffusion rates of inert proteins, as previously observed *in vitro* (Zhao et al. 2017). Restoring cytoplasm mixing would then facilitate the turnover of substrates at the active sites of the enzymes and thus begin a positive

feedback loop where more enzymatic activity promotes more diffusion through cytoplasmic mixing. Such positive feedback loop appears to saturate, in our experiments, at ~ 5-10 mM ATP, possibly as a consequence of the recently hypothesized thermodynamic limit to the amount of metabolic energy that a cell can dissipate without compromising its biomolecular functions (Losa et al. 2022). Notably, at concentrations of ATP ~ 5-10 mM ATP, the diffusion rate of sfGFP in permeabilized cells bacame comparable to that we previously measured in intact, growing cells. In agreement with this observation, recent measurements at the single-cell level proved that in growth conditions similar to ours, *E. coli* cells indeed reach concentrations of ATP ~ 5 mM (Lin and Jacobs-Wagner 2022).

## 4.8 ATP-dependent enzymes are capable of enhanced diffusion *in situ*

Experiments *in vitro* have shown that the mobility of several different types of enzymes is enhanced in presence of their substrates, a process thus named enhanced diffusion. For the first time, we observed this process inside a cell, although not alive (*i.e. in situ*). In permeabilized cells, the mobility of the ATP-dependent enzyme Adk, in presence of both its substrates ATP and AMP, increases to an extent larger than in presence of ATP alone. Experiments with the non-hydrolysable ATP analogue AMP-PNP, that can be bound, but not hydrolyzed by Adk, suggest that such effect depends on both the acquisition of a closed conformation upon substrate binding (Whitford et al. 2007) and, possibly to a larger extent, on the actual catalytic activity of Adk. The lacking of pronounced enhanced diffusion in the enzyme Cmk may suggests that the latter undergoes smaller conformational changes than Adk (Schultz et al. 1997), since the catalytic properties of the two enzymes are similar (Saint Girons et al. 1987; Bucurenci et al. 1996). A combination of theoretical modelling and simulations may help elucidating the molecular mechanism that underlies the apparent enhanced diffusion in Adk and the reason why such is not observed in Cmk. It

remains also to be determined if the enhanced diffusion we observe could also promote chemokinesis, the directed motion of enzymes along a gradient of their substrates.

## 4.9. Concluding remarks

Diffusion is the main process that allocates (macro)molecules, proteins in particular, to the intracellular district where their function is needed. The study and precise quantification of protein mobility is thus of fundamental importance for the understanding of biological systems. Despite several aspects of protein mobility in bacterial cytoplasm has been elucidated in the past, drawing general conclusions from different studies was hampered by differences in the bacterial strain investigated, on the growth and imaging conditions, on the technique employed and on the small number of proteins investigated.

The main goal of this project was therefore to produce a comprehensive study on cytoplasmic protein diffusion and answer several open questions. By measuring the diffusion of a large number of protein constructs and combining experiments with theoretical simulations and mathematical modelling, we concluded that, in absence of strong protein-protein interactions, the diffusion of free proteins in the confined volume of the bacterial cytoplasm is largely Brownian. We also concluded that the size dependence of protein mobility can be more accurately predicted by considering the peculiar dumbbell shape of the GFP-tagged proteins employed in our study. The comparable diffusion coefficients obtained from measurements with FCS and FRAP also indicate that protein diffusion is homogeneous over different spatiotemporal scales.

Furthermore, we observed that perturbations to the cytoplasmic protein mobility, due to the fluidizing effect of cell growth or alterations to the cytoplasmic crowding and viscosity, have proportional effects on differently-sized proteins. These results suggest that protein diffusion in the *E. coli* cytoplasm remains

Brownian under all tested conditions, including growing cells, and the effects of these perturbations on protein mobility can be simply accounted for by changes in the cytoplasmic viscosity. We hypothesize that such proportional changes in the diffusion of differently-sized proteins might be important to maintain balanced rates of diffusion-limited cellular processes under various environmental conditions.

Finally, we observed that the diffusion of inert sfGFP molecules, in otherwise metabolically inactive cells, can be significantly increased by reactivating the enzymatic activity of ATP-dependent enzymes, possibly through metabolism-induced cytoplasmic stirring. Intriguingly, we also provide the first evidence that enhanced enzyme diffusion, so far at most observed only *in vitro*, can be observed also *in situ*, after providing metabolically inactive cells with the opportune substrates.

# 5. Materials and methods

## 5.1 Reagents and kits used

### 5.1.1 List of reagents used in this study

| Chemical | Company |
|---|---|
| 80% iodixanol | Opti-Prep |
| A22 hydrochloride | Sigma-Aldrich |
| Acetic acid | Roth |
| Agarose NEEO ultra-quality | Roth |
| Ammonium chloride | Roth |
| Ammonium persulphate | Roth |
| Ampicillin | Applichem |
| Bacto tryptone | Roth |
| Bromophenol blue | Sigma-Aldrich |
| Calcium chloride | Sigma-Aldrich |
| Casamino acids | Sigma-Aldrich |
| Cephalexin hydrate | Sigma-Aldrich |
| Chloramphenicol | Applichem |
| D-glucose | Applichem |
| Dimethyl sulphoxide | Roth |
| Dinitrophenol | Merck |
| Disodium phosphate | Sigma-Aldrich |
| dNTPs mix (10 mM) | NEB |
| EDTA | Merck |
| Gibson assembly Master Mix | NEB |
| Glycerol | Gerbu |

| | |
|---|---|
| Isopropyl β-D-1-thiogalactopyranoside | Roth |
| Kanamycin sulphate | Sigma-Aldrich |
| L-glycine | Sigma-Aldrich |
| L-methionine | Roth |
| Magnesium sulphate | Sigma-Aldrich |
| PEG 4000 | Sigma-Aldrich |
| Poly-L-lysine | Sigma-Aldrich |
| Potassium chloride | Sigma-Aldrich |
| Potassium phosphate dibasic | Sigma-Aldrich |
| Potassium phosphate monobasic | Sigma-Aldrich |
| Rifampicin | Merck |
| Sodium chloride | Roth |
| Sodium dodecyl sulphate | Sigma-Aldrich |
| Sodium hydroxide | Sigma-Aldrich |
| Sodium lactate | Sigma-Aldrich |
| SYTOX Orange Nucleic acid stain | ThermoFischer |
| SYTOX Red Dead cell stain | ThermoFischer |
| TEMED | Applichem |
| Toluene | Sigma-Aldrich |
| Tris base | Sigma-Aldrich |
| Tween 20 | Roth |
| Tween 80 | Roth |
| Yeast extract | Applichem |
| β-mercaptoethanol | Roth |

All enzymes were purchased from New England Biosciences.

All primers were purchased from Eurofins Scientific.

### 5.1.2 Kits used in this study

The kits were used according to the instructions of the guidelines given by the manufacturers.

| Kit | Manufacturer |
|---|---|
| GeneJET Plasmid Purification Kit | ThermoFischer Scientific, Dreieich |
| GeneJET PCR Purification Kit | ThermoFischer Scientific, Dreieich |
| GeneJET Gel Extraction Kit | ThermoFischer Scientific, Dreieich |
| Q5 site-directed mutagenesis kit | New England BioLabs GmbH, Frankfurt a.M. |

### 5.1.3 Multi-well plates

| Plate | Company |
|---|---|
| 96-well plates glass bottom | Greiner Bio-one |
| 2-well plates glass bottom, #1.5H | Ibidi |
| 8-well plates glass bottom, #1.5H | Ibidi |

## 5.2 Media and buffer solutions

### 5.2.1 Media

***Lysogeny broth (LB)***

10 g/l Tryptone

5 g/l Yeast extract

5 g/l NaCl

Adjusted to pH 7. For preparing LB agar plates, 15 g of agar were added to 1 l of LB liquid medium.

***M9***

48 mM $Na_2HPO_4$

22 mM $KH_2PO_4$

8.4 mM NaCl

18.6 mM $NH_4Cl$

2 mM $MgSO_4$

0.1 mM $CaCl_2$

0.4% glucose

0.2% casamino acids

The salts were prepared as 5x, diluted and sterile filtered. Nutrients were mixed with the 1x M9 salts prior to culture inoculation.

### 5.2.2 Buffers

***Tethering buffer***

10 mM $K_2HPO_4$

10 mM $KH_2PO_4$

1 μM methionine

10 mM sodium lactate

buffered with NaOH to pH 7 and sterile filtered.

***Permeabilization buffer***

10 mM $K_2HPO_4$

10 mM $KH_2PO_4$

10 mM $MgCl_2$

Buffered with NaOH to pH 7.

***Phosphate-buffered saline (PBS)***

137 mM NaCl

2.7 mM KCl

8 mM $Na_2HPO_4$

1.8 mM $KH_2PO_4$

Buffered to pH 7.4

***Motility buffer***

10 mM KPO4

0.1 mM EDTA

67 mM NaCl

Dissolved in ddH2O and adjusted to pH 7. Sterile filtered.

***TAE buffer (Tris-Acetate-EDTA - 50 x)***

242 g Tris base

57.1 g Glacial acetic acid

100 ml 0.5 M EDTA, pH 8

ddH2O was added up to a total volume of 1 l.

***TSS (Transfer Storage Solution)***

200 ml LB

20 g PEG 4000

10 ml DMSO

2.46 g $MgCl_2$

Adjusted to pH 6.5.

***SDS-PAGE sample buffer (Laemmli), 4x***

0.25 M Tris base, pH 6.8

8% SDS

40% glycerol

20% β-mercaptoethanol

0.02% w/v Bromophenol blue

***SDS-PAGE running buffer, 10x***

30.3 g Tris base

144 g glycine

10 g SDS

Dissolve in 1000 ml $ddH_2O$

***Western blot transfer buffer, 10x***

30 g Tris base

144 g glycine

Dissolve in 1000 ml $ddH_2O$.

To make 1x transfer buffer, 100 ml of 10x transfer buffer are mixed with 200 ml of methanol and 700 ml of $ddH_2O$.

***Tris buffered saline (TBS), 10x***

24 g Tris base

88 g NaCl

Dissolve in 1000 ml $ddH_2O$

Buffered to pH 7.6 with HCl.

To make 1x TBS-T, mix 100 ml 10x TBS with 900 ml $ddH_2O$ and 1 ml of Tween20 (0.1%).

### 5.2.2 Antibiotics and inducers

Ampicillin 100 mg/ml in $ddH_2O$

Kanamycin 50 mg/ml in $ddH_2O$

Chloramphenicol 34 mg/ml in ethanol

IPTG 0.1 M in $ddH_2O$

Cephalexin 10% w/v in $ddH_2O$

A22 200 mg/ml in DMSO

Rifampicin 200 mg/ml in DMSO

DNP 100 mM in $ddH_2O$

## 5.3 Bacterial strains

All strains used in this study are listed in Table 2.

**Table 2.** List of strains used in this study.

| Strain | Relevant genotype | Reference or source |
|---|---|---|
| *E. coli* W3110 | W3110 derivative with functional RpoS [rpoS396(Am)] | (Serra Diego et al. 2013) |
| NB63 | W3110 Δ*clpA* | This work |
| RC111 | W3110 *Δflu, fliC::KanR* | This work |
| DLT1215 | MG1655 *hu-mCherry::frt-kan-frt* | (Le Gall et al. 2016) |

## 5.4 Molecular biology methods

### 5.4.1 Primers

All primers used in this study are listed in Table 3.

**Table 3.** List of primers used in this study.

| Primer name | Sense | Nucleotide sequence | Description |
|---|---|---|---|
| NBp1 | RW | ACCCATGGCACACTCC TTCACTAG | Amplify pTrc99A |
| NBp2 | RW | CTTGGACATGCTACCTC CGCCCCCTTAGTACAA CGGTGACGCCGG | Amplify UbiC gene from K12 genome and fuse it to linker-sfGFP |
| NBp3 | FW | GGGGGCGGAGGTAGCA TGTCCAAGGGTGAAGA GCTATTTAC | Amplify pTrc99A + Gly-Ser linker +sfGFP |
| NBp4 | FW | GTACTAGTGAAGGAGT GTGCCATGGGTATGTC ACACCCCGCGTTAAC | Amplify UbiC gene from K12 genome and fuse it to pTrc promoter |
| NBp5 | FW | TTGACAATTAATCATCC GGCTCG | Sequence pTrc99A insert and sfGFP |
| NBp7 | RW | CTTGGACATGCTACCTC CGCCCCCGTACAACGG TGACGCCGG | Amplify UbiC gene from K12 and fuse it to linker-sfGFP: without STOP codon |
| NBp8 | FW | GTACTAGTGAAGGAGT GTGCCATGGGTATGCG TATCATTCTGCTTGGCG | Amplify Adk gene from K12 genome and fuse it to pTrc promoter |
| NBp9 | RW | CTTGGACATGCTACCTC CGCCCCCGCCGAGGAT TTTTTCCAGATCAG | Amplify Adk gene from K12 and fuse it to linker-sfGFP delete STOP codon |

| | | | |
|---|---|---|---|
| NBp10 | FW | GTACTAGTGAAGGAGT GTGCCATGGGTATGTC GCAGAATAATCCGTT | Amplify mmuM gene from K12 genome and fuse it to pTrc promoter |
| NBp11 | RW | CTTGGACATGCTACCTC CGCCCCCGCTTCGCGCT TTTAACG | Amplify mmuM gene from K12 genome and fuse it to linker-sfGFP; delete STOP codon |
| NBp12 | FW | GTACTAGTGAAGGAGT GTGCCATGGGTATGGA AAACGCTAAAATGAAC TCG | Amplify dsdA gene from K12 genome and fuse it to pTrc promoter |
| NBp13 | RW | CTTGGACATGCTACCTC CGCCCCCACGGCCTTTT GCCAGATATTG | Amplify dsdA gene from K12 genome and fuse it to linker-sfGFP; delete STOP codon |
| NBp14 | FW | GTACTAGTGAAGGAGT GTGCCATGGGTATGTCT GTACAGCAAATCGACT GGG | Amplify HemN gene from K12 genome and fuse it to pTrc promoter |
| NBp15 | RW | CTTGGACATGCTACCTC CGCCCCCAATCACCCG AGAGAACTGCTGC | Amplify HemN gene from K12 genome and fuse it to linker-sfGFP; delete STOP codon |
| NBp16 | FW | GTACTAGTGAAGGAGT GTGCCATGGGTATGAG TCAAACCATAACCCAG AG | Amplify glcB gene from K12 genome and fuse it to pTrc promoter |
| NBp17 | RW | CTTGGACATGCTACCTC CGCCCCCATGACTTTCT TTTTCGCGTAAAC | Amplify glcB gene from K12 genome and fuse it to linker-sfGFP; delete STOP codon |
| NBp18 | RW | GATTTAATCTGTATCAG G | Sequence pTrc insert and sfGFP |
| NBp19 | FW | GTACTAGTGAAGGAGT GTGCCATGGGTATGAC AGTGGCGTATATTGC | Amplify folK gene from K12 genome and fuse it to pTrc promoter |
| NBp20 | RW | CTTGGACATGCTACCTC CGCCCCCCCATTTGTTT AATTTGTCAA | Amplify folK gene from K12 genome and fuse it to linker-sfGFP |
| NBp21 | FW | GTACTAGTGAAGGAGT GTGCCATGGGTATGGC TATCTCAATCAAGACC CC | Amplify map gene from K12 genome and fuse it to pTrc promoter |
| NBp22 | RW | CTTGGACATGCTACCTC CGCCCCCTTCGTCGTGC GAGATTATCG | Amplify map gene from K12 genome and fuse it to linker-sfGFP |
| NBp23 | FW | GTACTAGTGAAGGAGT GTGCCATGGGTATGAA ACTCTACAATCTGAAA G | Amplify thrC gene from K12 genome and fuse it to pTrc promoter |
| NBp24 | RW | CTTGGACATGCTACCTC CGCCCCCCTGATGATTC ATCATCAATTTAC | Amplify thrC gene from K12 genome and fuse it to linker-sfGFP |
| NBp25 | FW | GTACTAGTGAAGGAGT GTGCCATGGGTATGTC AGCTCAAATCAACAAC ATCCG | Amplify prpD gene from K12 genome and fuse it to pTrc promoter |
| NBp26 | RW | CTTGGACATGCTACCTC CGCCCCCAATGACGTA CAGGTCGAGATACTC | Amplify prpD gene from K12 genome and fuse it to linker-sfGFP |
| NBp27 | FW | GTACTAGTGAAGGAGT GTGCCATGGGTATGTT | Amplify malZ gene from K12 genome and fuse it to pTrc promoter |

| | | | |
|---|---|---|---|
| | | AAATGCATGGCACCTGC | |
| NBp28 | RW | CTTGGACATGCTACCTCCGCCCCCGTTCATCCATACCGTAGCCGAAATG | Amplify malZ gene from K12 genome and fuse it to linker-sfGFP |
| NBp29 | FW | GTACTAGTGAAGGAGTGTGCCATGGGTATGTCTGAACCGCAACGTCTG | Amplify thrP gene from K12 genome and fuse it to pTrc promoter |
| NBp30 | RW | CTTGGACATGCTACCTCCGCCCCCTTGCGTTAGCGCCCAGC | Amplify thrP gene from K12 genome and fuse it to linker-sfGFP |
| NBp31 | FW | GTACTAGTGAAGGAGTGTGCCATGGGTATGTCTGTAATTAAGATGACCGATC | Amplify pgk gene from K12 genome and fuse it to pTrc promoter |
| NBp32 | RW | CTTGGACATGCTACCTCCGCCCCCCTTCTTAGCGCGCTCTTCG | Amplify pgk gene from K12 genome and fuse it to linker-sfGFP |
| NBp33 | FW | GTACTAGTGAAGGAGTGTGCCATGGGTATGAGGTATATAGTTGCCTTAACGG | Amplify coaE gene from K12 genome and fuse it to pTrc promoter |
| NBp35 | FW | GTACTAGTGAAGGAGTGTGCCATGGGTATGACGGCAATTGCCCC | Amplify cmk gene from K12 genome and fuse it to pTrc promoter |
| NBp37 | FW | GTACTAGTGAAGGAGTGTGCCATGGGTATGGATACGTCACTGGCTGAG | Amplify entC gene from K12 genome and fuse it to pTrc promoter |
| NBp39 | FW | GTACTAGTGAAGGAGTGTGCCATGGGTATGATTAGCGTAACCCTTAGCC | Amplify murF gene from K12 genome and fuse it to pTrc promoter |
| NBp41 | FW | GTACTAGTGAAGGAGTGTGCCATGGGTATGAAAATTACCGTATTGGGATGCG | Amplify panE gene from K12 genome and fuse it to pTrc promoter |
| NBp53 | FW | TCCAAGGGTGAAGAGCTATTTACTGGG | ATG deletion from dsdA-sfGFP, UbiC-sfGFP, thrC-sfGFP, malZ-sfGFP |
| NBp54 | RW | GCTACCTCCGCCCCCACG | ATG deletion from dsdA-sfGFP |
| NBp55 | FW | TCCAAGGGTGAAGAGCTATTTACTGGGGTTG | ATG deletion from Adk-sfGFP |
| NBp56 | RW | GCTACCTCCGCCCCCGCC | ATG deletion from Adk-sfGFP |
| NBp57 | FW | TCCAAGGGTGAAGAGCTATTTACTGGGG | ATG deletion from mmuM-sfGFP and folK-sfGFP |
| NBp58 | RW | GCTACCTCCGCCCCCGCT | ATG deletion from mmuM-sfGFP |
| NBp59 | RW | GCTACCTCCGCCCCCGTA | ATG deletion from UbiC-sfGFP |
| NBp60 | FW | TCCAAGGGTGAAGAGCTATTTACTGG | ATG deletion from glcB-sfGFP |
| NBp61 | RW | GCTACCTCCGCCCCCATG | ATG deletion from glcB-sfGFP |

| | | | |
|---|---|---|---|
| NBp62 | FW | TCCAAGGGTGAAGAGC TATTTACTG | ATG deletion from HemN-sfGFP, map-sfGFP, prpD-sfGFP |
| NBp63 | RW | GCTACCTCCGCCCCCA AT | ATG deletion from HemN-sfGFP and prpD-sfGFP |
| NBp64 | RW | GCTACCTCCGCCCCCTT C | ATG deletion from map-sfGFP |
| NBp65 | RW | GCTACCTCCGCCCCCCT G | ATG deletion from thrC-sfGFP |
| NBp66 | RW | GCTACCTCCGCCCCCCC A | ATG deletion from folK -sfGFP |
| NBp67 | RW | GCTACCTCCGCCCCCGT T | ATG deletion from malZ-sfGFP |
| NBp68 | FW | GGGGGCGGAGGTAGCT CCAAGGGTGAAGAGCT ATTTACTG | Amplification of backbone flexible linker-sfGFP without ATG |
| NBp81 | RW | GCTCTTCACCCTTGGAG CTACCTCCGCCCCCTGC GAGAGCCAATTTCTGG | Amplify cmk gene from K12 genome and fuse it to linker-sfGFP deleted STOP |
| NBp82 | RW | GCTCTTCACCCTTGGAG CTACCTCCGCCCCCCGG TTTTTCCTGTGAGACAA AC | Amplify coaE gene from K12 genome and fuse it to linker-sfGFP deleted STOP |
| NBp83 | RW | GCTCTTCACCCTTGGAG CTACCTCCGCCCCCATG CAATCCAAAAACGTTC AACAT | Amplify entC gene from K12 genome and fuse it to linker -sfGFP deleted STOP |
| NBp84 | RW | GCTCTTCACCCTTGGAG CTACCTCCGCCCCCACA TGTCCCATTCTCCTGTA AAG | Amplify murF gene from K12 genome and fuse it to linker-sfGFP deleted STOP |
| NBp85 | RW | GCTCTTCACCCTTGGAG CTACCTCCGCCCCCTTG CGTTAGCGCCCAGC | Amplify thrP gene from K12 genome and fuse it to linker-sfGFP deleted STOP |
| NBp86 | RW | GCTCTTCACCCTTGGAG CTACCTCCGCCCCCCCA GGGGCGAGGCAAAC | Amplify panE gene from K12 genome and fuse it to linker-sfGFP deleted STOP |
| NBp87 | RW | GCTCTTCACCCTTGGAG CTACCTCCGCCCCCCTT CTTAGCGCGCTCTTCG | Amplify pgk gene from K12 genome and fuse it to linker-sfGFP deleted STOP |
| NBp88 | FW | GTACTAGTGAAGGAGT GTGCCATGGGTATGGG TTTGTTCGATAAACTG | Amplify Crr from K12 genome and fuse it to pTrc promoter |
| NBp89 | RW | TCACCCTTGGAGCTACC TCCGCCCCCCTTCTTGA TGCGGATAACC | Amplify Crr from K12 genome and fuse it to flexi linker and sfGFP |
| NBp90 | FW | GTACTAGTGAAGGAGT GTGCCATGGGTATGCA AGAGCAATACCGCC | Amplify leuS from K12 genome and fuse it to pTrc promoter |
| NBp91 | RW | TTCACCCTTGGAGCTAC CTCCGCCCCCGCCAAC GACCAGATTGAGG | Amplify leuS from K12 genome and fuse it to flexi linker and sfGFP |
| NBp92 | FW | GTACTAGTGAAGGAGT GTGCCATGGGTATGGC ACTGCCAATTCTGTTAG | Amplify rihA from K12 genome and fuse it to pTrc promoter |

| | | | |
|---|---|---|---|
| NBp93 | RW | TTCACCCTTGGAGCTAC CTCCGCCCCCAGCGTA AAATTTCAGACGATCA G | Amplify rihA from K12 genome and fuse it to flexi linker and sfGFP |
| NBp94 | FW | GTACTAGTGAAGGAGT GTGCCATGGGTATGAC CATTAAAAATGTAATTT GCGATATCG | Amplify nagA from K12 genome and fuse it to pTrc promoter |
| NBp95 | RW | TTCACCCTTGGAGCTAC CTCCGCCCCCGATAAC GTCGATTTCAGCGACT G | Amplify nagA from K12 genome and fuse it to flexi linker and sfGFP |
| NBp96 | FW | GTACTAGTGAAGGAGT GTGCCATGGGTATGGG TAAAACGAACGACTG | Amplify clpS from K12 genome and fuse it to pTrc promoter |
| NBp97 | RW | TTCACCCTTGGAGCTAC CTCCGCCCCCGGCTTTT TCTAGCGTACACAG | Amplify clpS from K12 genome and fuse it to flexi linker and sfGFP |
| NBp98 | FW | GTACTAGTGAAGGAGT GTGCCATGGGTATGGA ATCCCTGACGTTACAA CC | Amplify aroA from K12 genome and fuse it to pTrc promoter |
| NBp99 | RW | TTCACCCTTGGAGCTAC CTCCGCCCCCGGCTGCC TGGCTAATCCG | Amplify aroA from K12 genome and fuse it to flexi linker and sfGFP |
| NBp100 | FW | GTACTAGTGAAGGAGT GTGCCATGGGTATGAG TTTTGTGGTCATTATTC CCG | Amplify kdsB from K12 genome and fuse it to pTrc promoter |
| NBp101 | RW | TTCACCCTTGGAGCTAC CTCCGCCCCCGCGCATT TCAGCGCGAAC | Amplify kdsB from K12 genome and fuse it to flexi linker and sfGFP |
| NBp102 | FW | GTACTAGTGAAGGAGT GTGCCATGGGTATGAA ATACGATCTCATCATTA TTGGCAG | Amplify solA from K12 genome and fuse it to pTrc promoter |
| NBp103 | RW | TTCACCCTTGGAGCTAC CTCCGCCCCCTTGGAA GCGGGAAAGCCTG | Amplify solA from K12 genome and fuse it to flexi linker and sfGFP |
| NBp107 | RW | CACCCTTGGAGCTACCT CCGCCCCCCCATTTGTT TAATTTGTCAAATGCTC | Amplify folK gene from K12 genome and fuse it to linker-sfGFP deleted STOP |
| NBp122 | FW | ACTAGTGAAGGAGTGT GCCATGGGTGTGAGCA GCAAAGTGGAACAAC | Amplify metH from MG1655 and insert it into pTrc99A fused to sfGFP |
| NBp123 | RW | CACCCTTGGAGCTACCT CCGCCCCCGTCCGCGTC ATACCCCAGATTC | |
| NBp124 | FW | ACTAGTGAAGGAGTGT GCCATGGGTATGTCGT CAACCCTACGAG | Amplify acnA from MG1655 and insert into pTrc99A fused to sfGFP |
| NBp125 | RW | CACCCTTGGAGCTACCT CCGCCCCCCTTCAACAT ATTACGAATGACATAA TGC | |

| | | | |
|---|---|---|---|
| NBp126 | FW | ACTAGTGAAGGAGTGT GCCATGGGTATGACAA TATTGAATCACACCCTC | Amplify metE from MG1655 and insert into pTrc99A fused to sfGFP |
| NBp127 | RW | CACCCTTGGAGCTACCT CCGCCCCCCCCCCGAC GCAAGTTC | |
| NBp177 | FW | ACTAGTGAAGGAGTGT GCCATGGGTATGAGCA GAACGATTTTTTGTAC | Amplify yggX from MG1655 and insert into pTrc99A fused to sfGFP |
| NBp178 | RW | CACCCTTGGAGCTACCT CCGCCCCCTTTTTTATC TTCCGGCGTATAG | |
| NBp179 | FW | ACTAGTGAAGGAGTGT GCCATGGGTATGAATC TGATCCTGTTCGG | Amplify adk from Caulobacter and insert into pTrc99A fused to sfGFP |
| NBp180 | RW | CACCCTTGGAGCTACCT CCGCCCCCTCCTGCAGC GACG | |
| NBp181 | FW | CAGACCATGTACTAGT GAAGGAGTGTGCCATG GGTATGACCTTCCGCA CCCTC | Amplify pgk from Caulobacter and insert into pTrc99A fused to sfGFP |
| NBp182 | RW | CACCCTTGGAGCTACCT CCGCCCCCGGATTCGA GCGCCGC | |
| NBp183 | FW | ACTAGTGAAGGAGTGT GCCATGGGTATGGCGT CTGTGGACAGC | Amplify acnA from Caulobacter and insert into pTrc99A fused to sfGFP |
| NBp184 | RW | CACCCTTGGAGCTACCT CCGCCCCCGTCGGCCTT GGCCAGG | |
| NBp185 | FW | ACTAGTGAAGGAGTGT GCCATGGGTATGAACT TAGTCTTAATGGGG | Amplify adk from Bacillus and insert into pTrc99A fused to sfGFP |
| NBp186 | RW | CACCCTTGGAGCTACCT CCGCCCCCTTTTTTTAA TCCTCCAAGAAGATCC | |
| NBp187 | FW | ACTAGTGAAGGAGTGT GCCATGGGTATGAATA AAAAAACTCTCAAAGA CATCG | Amplify pgk from Bacillus and insert into pTrc99A fused to sfGFP |
| NBp188 | RW | CACCCTTGGAGCTACCT CCGCCCCCTTTATCGTT CAGTGCAGCTAC | |
| NBp189 | FW | ACTAGTGAAGGAGTGT GCCATGGGTATGGCAA ACGAGCAAAAAAC | Amplify acnA from Bacillus and insert into pTrc99A fused to sfGFP |
| NBp190 | RW | CACCCTTGGAGCTACCT CCGCCCCCGGACTGCTT CATTTTTTCACG | |
| NBp191 | FW | ACTAGTGAAGGAGTGT GCCATGGGTATGAACC TGATCCTGTTGGGG | Amplify adk from Myxoxoxxus and insert into pTrc99A fused to sfGFP |
| NBp192 | RW | CACCCTTGGAGCTACCT CCGCCCCCGGCCTTGCC CGCAG | |

| | | | |
|---|---|---|---|
| NBp193 | FW | ACTAGTGAAGGAGTGTGCCATGGGTATGATCCGTTACATCGATGATCTGC | Amplify pgk from Myxoxoxxus and insert into pTrc99A fused to sfGFP |
| NBp194 | RW | CACCCTTGGAGCTACCTCCGCCCCCCCGCGTCTCCAGCG | |
| NBp195 | FW | ACTAGTGAAGGAGTGTGCCATGGGTATGACCGACAGTTTCGGC | Amplify acnA from Myxoxoxxus and insert into pTrc99A fused to sfGFP |
| NBp196 | RW | CACCCTTGGAGCTACCTCCGCCCCCGCCCTTGGCCAGTTG | |
| NBp197 | FW | ACTAGTGAAGGAGTGTGCCATGGGTATGCGCATCATTCTTCTCGG | Amplify adk from Vibrio and insert into pTrc99A fused to sfGFP |
| NBp198 | RW | CACCCTTGGAGCTACCTCCGCCCCCAGCCAACGCTTTAGCAATGTC | |
| NBp199 | FW | ACTAGTGAAGGAGTGTGCCATGGGTATGTCTGTAATCAAGATGATTGACCTGG | Amplify pgk from Vibrio and insert into pTrc99A fused to sfGFP |
| NBp200 | RW | CACCCTTGGAGCTACCTCCGCCCCCCGCTTTAGCGCGTGCTTC | |
| NBp201 | FW | ACTAGTGAAGGAGTGTGCCATGGGTATGAACAGTCTGTATCGTAAAGC | Amplify acnA from Vibrio and insert into pTrc99A fused to sfGFP |
| NBp202 | RW | CACCCTTGGAGCTACCTCCGCCCCCCTGCGCCAAAAAGTCTTG | |
| NBp216 | FW | ACTAGTGAAGGAGTGTGCCATGGGTATGCGTATCATTCTGCTGG | amplify adk from Yersinia and insert into pTrc99A fused to sfGFP |
| NBp217 | RW | CACCCTTGGAGCTACCTCCGCCCCCACCGAGAATAGTCGCCAG | |
| NBp218 | FW | CTAGTGAAGGAGTGTGCCATGGGTATGTCTGTAATTAAGATGACCGATCTGG | Amplify pgk from Yersinia and insert into pTrc99A fused to sfGFP |
| NBp219 | RW | CACCCTTGGAGCTACCTCCGCCCCCCTGCTTAGCGCGCTCTTC | |

| | | | |
|---|---|---|---|
| NBp220 | FW | ACTAGTGAAGGAGTGT GCCATGGGTATGTCGTT GGATTTGCGGAAAAC | Amplify acnA from Yersinia and insert into pTrc99A fused to sfGFP |
| NBp221 | RW | CACCCTTGGAGCTACCT CCGCCCCCCAACATTTT GCGGATCACATAATGC | |
| NBp227 | FW | gatggctggacggtagaaaccgaaG ATCGCAGCTTGTCTGCA C | Mutate Lys to Glu in Map |
| NBp228 | RW | ttccatggtgcggatctcttttcACC CGCGTTGACCATTGG | |
| NBp229 | FW | gatggctggacggtagcaaccgcaG ATCGCAGCTTGTCTGCA C | Mutate Lys to Ala in Map |
| NBp230 | RW | tgccatggtgcggatctcttttgcAC CCGCGTTGACCATTGG | |
| NBp231 | FW | ACTAGTGAAGGAGTGT GCCATGGGTATGGGTA AAATAATTGGTATCG | Amplify dnaK from MG1655 and insert into pTrc99A fused to sfGFP |
| NBp232 | RW | CACCCTTGGAGCTACCT CCGCCCCCTTTTTTGTC TTTGACTTCTTC | |
| NBp234 | FW | CCAGTCTGCGtttACCAT CCATG | Mutation V436F in dnaK |
| NBp235 | RW | TTGTCTTCAGCGGTAGA G | |
| NBp240 | FW | ttttcttatgatgtagaacgtgcaacgc aattgatgctcgctgttgcgTACCA GGGGAAGGCCATT | D35A, D36A, H66A in clpS |
| NBp241 | RW | gaatttttgtaacacgtcaataacaaac tccatcggagtgtacgccgcATTG ACTAATATCACTTTATA CATAGATGGC | |
| Eri121 | FW | CAGTCATAGCCG AATAGCCT | Checking insertion of KanR cassette |
| Eri122 | RW | CGGTGCCCTGAA TGAACTGC | |

### 5.4.2 Preparation of genomic DNA (gDNA) for gene amplification by PCR

5 ml of bacterial culture were spun by centrifugation at 8000g for 5 min, resuspended in 350 µl dd$H_2O$ and heated at 95°C for 10 min. gDNA was stored at -20°C.

Strains used as source of gDNA:

- *Escherichia coli* MG1655 (from our strain collection)
- *Yersinia enterocolitica* dHOPEMTasd (gDNA kindly gifted by Dr. Stephan Wimmi)
- *Vibrio cholerae* N16961 (gDNA kindly gifted by Dr. Sanika Vaidya)
- *Myxococcus xanthus* DK1622 (Bacterial culture kindly gifted by Dr. Luis Carreíra)
- *Bacillus subtilis* 168 (from our strain collection)
- *Caulobacter crescentus* CB15N (Bacterial culture kindly gifted by Ying Liu)

### 5.4.3 Polymerase chain reaction (PCR)

PCR was used to either amplify genes and plasmids for cloning (Q5 polymerase) or to verify positive plasmid assembly or genomic knock out (single-colony PCR). The PCR reactions were run in peqSTAR thermocyclers (PEQLAB). Amplified DNA fragments were analyzed using gel electrophoresis in 1% TAE-agarose gels and purified using the GeneJET PCR purification kit. Amplified plasmids were treated with *Dpn*I for plasmid template degradation.

***Single-colony PCR reaction mix***

25 µl DreamTaq Green PCR Master Mix (2x)
1 µl forward primer (10 pmol/ µl)
1 µl reverse primer (10 pmol/ µl)
colony picked from plate
up to 50 µl ddH2O

**Thermocycler settings**

| Step | Temperature [°C] | Time [min] |
|---|---|---|
| 1 | 95 | 10 |
| 2 | 95 | 1 |
| 3 | 45-55 | 0.5 |
| 4 | 72 | 1/kb |
| | Repeat 2-4 35x | |
| 5 | 72 | 15 |

***PCR with Q5 polymerase reaction mix***

10 µl Q5 reaction buffer (5x)

2.5 µl forward primer (25 pmol/ µL)

2.5 µl reverse primer (25 pmol/ µL)

1 µl dNTPs (0.8 mM)

0.5 µl Q5 high fidelity DNA polymerase

1 µl template DNA (~25 ng for plasmid, ~1 mg/ml for genomic DNA)

up to 50 µl ddH2O

**Thermocycler settings**

| Step | Temperature [°C] | Time [min] |
|---|---|---|
| 1 | 98 | 10 |
| 2 | 98 | 1 |
| 3 | 50-72 | 0.5 |
| 4 | 72 | 1/kb |
| | Repeat 2-4 35x | |
| 5 | 72 | 2 |

### 5.4.4 *Dpn*I treatment

In order to remove the methylated template DNA from a PCR reaction and prevent false positive *E. coli* colonies, PCRs were incubated with *Dpn*I prior to any subsequent step. *Dpn*I is a restriction enzyme that cleaves methylated recognition sites on template plasmid DNA while leaving intact PCR amplicon. After *Dpn*I treatment, PCR products were purified using the GeneJET PCR Purification kit.

***DpnI reaction mix***

5 µl CutSmart 10x

1 µl *Dpn*I

44 µl purified PCR product

### 5.4.5 Agarose gel electrophoresis

The size of amplified gene fragments or plasmids were verified by agarose gel electrophoresis. Agarose gel electrophoresis separates DNA fragments according to their size when an electric field is applied. PCR products amplified for downstream cloning were verified by loading 5 µl with 6x loading dye on a 1% agarose TAE gel supplemented with peqGREEN (Peqlab) for visualization of the DNA bands under UV light. For Colony PCR products, 15 µl was loaded on the gel. The gels were run at 135 V in a chamber with TAE buffer for 10-20 min.

### 5.4.6 Gibson assembly

Gibson Assembly is a DNA assembly method, allowing to assemble 2-6 linear DNA fragments with overlapping ends in a one-pot and one-step reaction (Gibson et al. 2009). Overlapping regions were designed to be at least 25 bp long. DNA fragments and the receiver plasmid were amplified by PCR using Q5 polymerase, verified by gel electrophoresis and the plasmid was additionally treated with *Dpn*I. To prepare the Gibson assembly, parts were combined in a 1:3 molar ratio of backbone to insert, with 100 ng backbone.

***Gibson assembly reaction mix***

10 µl Gibson Assembly Mastermix 2x

100 ng backbone

3:1 molar amount of inserts

dd$H_2O$ to 20 µl

| Step | Temperature [°C] | Time [min] |
|---|---|---|
| 1 | 50 | 15 |

### 5.4.7 Site directed mutagenesis

Point mutations on sfGFP-constructs of ClpS, Map and DnaK were obtained by site-directed mutagenesis (NEB). Primers carrying the point mutations were used to amplify the correspondent pTrc99A plasmid with Q5 DNA polymerase. The obtained PCR product was treated with *Dpn*I , phosphorylated and ligated in a one-pot reaction using the KLD enzyme mix and transformed in competent *E. coli*. The presence of the desired mutation(s) was verified by Sanger sequencing (Microsynth).

***Kinase, ligase and DpnI (KLD) reaction mix***

1 µl PCR product

5 µl KLD buffer (2x)

1 µl KLD enzyme mix (10x)

3 µl nuclease-free $H_2O$

| Step | Temperature [°C] | Time [min] |
|---|---|---|
| 1 | RT | 15-30 |

### 5.4.8 Plasmid purification, determination of DNA concentration and sequencing

To obtain plasmid from *E. coli*, overnight cultures grown in LB supplemented with the appropriate antibiotic were used and the plasmid was purified using the GeneJET Plasmid Miniprep Kit. DNA was eluted in dd$H_2O$. The concentration of the purified DNA, as well as its purity, were determined using spectrophotometric estimation (NanoDrop 2000). Newly constructed plasmids were sent for Sanger sequencing (Microsynth) to verify the correct assembly.

### 5.4.9 Plasmids

The plasmids used in this study are listed in Table 4.

| Strain or plasmid | Relevant genotype or phenotype | Reference or source |
|---|---|---|
| pTrc99A | Amp$^r$; expression vector; pBR ori; *trc* promoter, IPTG inducible | (Amann, Ochs, and Abel 1988) |
| pCP20 | Amp$^r$, Cam$^r$; *flp* | (Cherepanov and Wackernagel 1995) |
| pNB1 | Amp$^r$; *sfGFP* in pTrc99A | This work |
| pNB3 | Amp$^r$; *Adk-sfGFP* in pTrc99A | This work |
| pNB4 | Amp$^r$; *CoaE-sfGFP* in pTrc99A | This work |
| pNB5 | Amp$^r$; *Cmk-sfGFP* in pTrc99A | This work |
| pNB6 | Amp$^r$; *Pgk-sfGFP* in pTrc99A | This work |
| pNB7 | Amp$^r$; *MmuM-sfGFP* in pTrc99A | This work |
| pNB8 | Amp$^r$; *PrpD-sfGFP* in pTrc99A | This work |
| pNB9 | Amp$^r$; *DsdA-sfGFP* in pTrc99A | This work |
| pNB11 | Amp$^r$; *GlcB-sfGFP* in pTrc99A | This work |
| pNB13 | Amp$^r$; *HemN-sfGFP* in pTrc99A | This work |
| pNB14 | Amp$^r$; *Map$^{WT}$-sfGFP* in pTrc99A | This work |
| pNB15 | Amp$^r$; *ThrC-sfGFP* in pTrc99A | This work |
| pNB16 | Amp$^r$; *MalZ-sfGFP* in pTrc99A | This work |
| pNB17 | Amp$^r$; *EntC-sfGFP* in pTrc99A | This work |
| pNB18 | Amp$^r$; *ThpR-sfGFP* in pTrc99A | This work |
| pNB19 | Amp$^r$; *AroA-sfGFP* in pTrc99A | This work |
| pNB20 | Amp$^r$; *ClpS$^{WT}$-sfGFP* in pTrc99A | This work |
| pNB21 | Amp$^r$; *Crr-sfGFP* in pTrc99A | This work |
| pNB22 | Amp$^r$; *KdsB-sfGFP* in pTrc99A | This work |
| pNB23 | Amp$^r$; *LeuS-sfGFP* in pTrc99A | This work |
| pNB24 | Amp$^r$; *MurF-sfGFP* in pTrc99A | This work |

| | | |
|---|---|---|
| pNB25 | Amp$^r$; *NagD-sfGFP* in pTrc99A | This work |
| pNB26 | Amp$^r$; *RihA-sfGFP* in pTrc99A | This work |
| pNB27 | Amp$^r$; *SolA-sfGFP* in pTrc99A | This work |
| pNB28 | Amp$^r$; *UbiC-sfGFP* in pTrc99A | This work |
| pNB29 | Amp$^r$; *PanE-sfGFP* in pTrc99A | This work |
| pNB30 | Amp$^r$; *FolK-sfGFP* in pTrc99A | This work |
| pNB39 | Amp$^r$; *AcnA-sfGFP* in pTrc99A | This work |
| pNB40 | Amp$^r$; *MetE-sfGFP* in pTrc99A | This work |
| pNB42 | Amp$^r$; *MetH-sfGFP* in pTrc99A | This work |
| pNB44 | Amp$^r$; *YggX-sfGFP* in pTrc99A | This work |
| pNB45 | Amp$^r$; $Adk^{C.c.}$-*sfGFP* in pTrc99A | This work |
| pNB46 | Amp$^r$; $Adk^{V.c.}$-*sfGFP* in pTrc99A | This work |
| pNB47 | Amp$^r$; $Adk^{M.x.}$-*sfGFP* in pTrc99A | This work |
| pNB48 | Amp$^r$; $AcnA^{M.x.}$-*sfGFP* in pTrc99A | This work |
| pNB49 | Amp$^r$; $AcnA^{V.c.}$-*sfGFP* in pTrc99A | This work |
| pNB51 | Amp$^r$; $Adk^{B.s.}$-*sfGFP* in pTrc99A | This work |
| pNB52 | Amp$^r$; $AcnA^{B.s.}$-*sfGFP* in pTrc99A | This work |
| pNB54 | Amp$^r$; $Adk^{Y.e.}$-*sfGFP* in pTrc99A | This work |
| pNB56 | Amp$^r$; $Pgk^{C.c.}$-*sfGFP* in pTrc99A | This work |
| pNB58 | Amp$^r$; $Pgk^{V.c.}$-*sfGFP* in pTrc99A | This work |
| pNB59 | Amp$^r$; $Pgk^{M.x.}$*sfGFP* in pTrc99A | This work |
| pNB60 | Amp$^r$; $AcnA^{Y.e.}$-*sfGFP* in pTrc99A | This work |
| pNB61 | Amp$^r$; $DnaK^{WT}$-*sfGFP* in pTrc99A | This work |
| pNB62 | Amp$^r$; $Map^{K211E\_K218E\_K224E\_K226E}$-*sfGFP* in pTrc99A | This work |

| | | |
|---|---|---|
| pNB63 | Amp$^r$; *Map*$^{K211A\_K218A\_K224A\_K226A}$-*sfGFP* in pTrc99A | This work |
| pNB64 | Amp$^r$; *DnaK*$^{V436F}$-*sfGFP* in pTrc99A | This work |
| pNB66 | Amp$^r$; *ClpS*$^{D35A\_D36A\_H66A}$-*sfGFP* in pTrc99A | This work |

## 5.5 Preparation of competent cells

For producing competent cells, two different procedures were used: a chemical method and a one-step preparation.

### 5.5.1 Chemical competent cells with calcium chloride

An LB overnight culture was diluted to final $OD_{600}$ = 0.035 in 100 ml fresh LB media and grown at 37 °C to an $OD_{600}$ = 0.6. Cells were harvested by centrifugation for 5 min at 4000 rpm at 4°C and the pellet was resuspended in 50 ml of ice-cold 0.1 M $CaCl_2$ and incubated on ice for 20 min. Cells were centrifuged for 5 min at 4000 rpm and the pellet was resuspended in 50 ml ice-cold 0.1 M $CaCl_2$, and incubated once more on ice for 20 min. Cells were centrifuged once more as previous and resuspended in 5 ml 0.1 M $CaCl_2$ with 20% glycerol and aliquoted. The aliquots were snap-frozen in liquid nitrogen and stored at -80 °C.

### 5.5.2 One-step preparation of competent cells

When just small amounts of competent cells were needed, a one-step procedure for the preparation of competent *Escherichia coli* cells, which use a transformation and storage solution (TSS), was used (Chung, Niemela, and Miller 1989). 100 µl of a LB overnight culture of the cells were diluted in 3 ml fresh LB medium and grown at 37 °C to an $OD_{600}$ = 0.6. Culture was incubated 20 min on ice. 1 ml of

culture was centrifuged at 8000 rpm for 1 min and resuspended in 100 µl of TSS. The cells are then ready for transformation with the desired plasmid.

## 5.6 Transformation

0.5-1 µl of purified plasmid DNA (~100 ng) or 10 µl Gibson assembly reaction were mixed gently with 100 µl competent cells in a 1.5 ml Eppendorf tube and incubated on ice for 30 min. For heat shock, the sample was placed at 42°C for 45 s in a heating block. After the heat shock, the tube was immediately placed on ice for 5 min. 900 µl of LB medium were added and the cells were incubated at 37 °C for 30-45 min. Cells were then plated on LB agar plates with selective antibiotics. Plates were incubated over night at 37 °C.

## 5.7 Gene deletion strains derived from Keio collection

The kanamycin resistant *ΔclpA* deletion strain of the Keio collection (Baba et al. 2006) was used as donor strain for P1 phage transduction (Thomason, Costantino, and Court 2007), into the W3110 $RpoS^+$ background. The resulting transduced strains were tested for correct insertion of the FRT-site flanked kanamycin cassette into the genome, using gene and kanamycin cassette specific primers, ERI121 and ERI122 (Table 3). The kanamycin cassette was removed from the deletion strain using the temperature sensitive pCP20 plasmid encoding a FLP recombinase (Cherepanov and Wackernagel 1995) and tested for the loss of antibiotic resistance after several rounds of growth on LB plates at 42°C. The resulting strains carry an 82-85 nucleotide scar in place of the disrupted gene (Datsenko and Wanner 2000).

## 5.8 Protein diffusion measurements

### 5.8.1 Growth conditions

*E. coli* cultures were grown in M9 minimal medium supplemented with 0.2% casamino acids, 20 mM glucose and 100 μg/ml ampicillin for plasmid selection. The overnight cultures, inoculated from the glycerol stock, were diluted to $OD_{600}$ = 0.035 and grown for 3.5 hours at 37°C and 200 rpm shaking (day culture). Cultures were treated for additional 45 minutes, under the same temperature and shaking conditions, with 100 μg/ml cephalexin and with 0 - 15 μM IPTG (Table 1), to induce expression of the fluorescent protein constructs. Where indicated, cultures were further incubated with 200 μg/ml rifampicin, DMSO as a mock treatment, 200 μg/ml chloramphenicol or 2 mM DNP for 1 hour. When treatment with A22 is performed, 1 μg/ml A22 is added from the inoculation of the day culture.

### 5.8.2 Sample preparation

Cells were harvested by centrifugation at 7000g for 3 minutes and washed 3 times in tethering buffer. When indicated, 1 ml of chloramphenicol-treated cells were stained for 15 minutes with 300 nM SYTOX Orange Nucleic Acid Stain (Invitrogen). The excess of SYTOX Orange was washed in tethering buffer before proceeding with FCS experiments. 2.5 μl of bacterial cells were then spread on a small 1% agarose pad prepared in tethering buffer salts**,** unless differently stated. Imaging was performed on Ibidi 2-well μ-Slides (#1.5H, 170 μm ± 5 μm).

For toluene treatment, 1 ml of culture was harvested by centrifugation at 7000g for 3 minutes and washed 3 times in permeabilization buffer. Toluene was added to a final concentration of 2.5% v/v and cultures were incubated with toluene for 15 min, at 37°C and 700 rpm shaking on an Eppendorf ThermoMixer. Excess of toluene was removed by centrifugation at 7000g for 3 minutes and washed 3 times in permeabilization buffer. Permeabilized cells were then incubated with 15 nM SYTOX Red (Thermo Fischer) for 10 min at the same conditions of temperature and shaking. Stained cells were then

immobilized on the bottom of poly-L-lysine coated Ibidi 8-well μ-Slides (#1.5H, 170 μm ± 5 μm), overlaid with permeabilization buffer supplemented with the same concentration of SYTOX Red and the indicated concentrations of nucleotides.

### 5.8.3 FCS data acquisition

FCS measurements were performed on a LSM 880 confocal laser scanning microscope (Carl Zeiss Microscopy) using a C-Apochromat 40×/1.2 water immersion objective selected for FCS. sfGFP was excited with a 488 nm Argon laser (25 mW) and fluorescence emission was collected from 490 to 580 nm. SYTOX Orange was excited with a 543 nm laser and fluorescence emission was collected from 553 to 615 nm. In order to avoid the partial spectral overlap between the emission spectra of sfGFP and SYTOX Orange, the fluorescence emission of sfGFP in the co-staining experiments was collected from 490 to 535 nm. SYTOX Red was excited with a 633 nm laser and fluorescence emission was collected from 635 to 711 nm. Each sample was equilibrated for at least 20 minutes at 25°C (or 35°C when specified), on the stage of the microscope and measurements were taken at the same temperature. FCS measurements were acquired within 60 minutes from the sample preparation. The pinhole was aligned on a daily basis, by maximizing the fluorescence intensity count rate of an Alexa488 (Invitrogen) solution (35 nM) in phosphate-buffered saline (PBS). Unless differently stated, all measurements were performed with a pinhole size correspondent to 1 Airy unit, to ensure the optimal gathering of fluorescence signal. The coverslip collar adjustment ring of the water immersion objective was also adjusted daily, maximizing the fluorescence intensity signal and the brightness of Alexa 488. The laser power was adjusted in order to obtain molecular brightness (*i.e.* photon counts per second per molecule, cpsm) of 10 kcpsm for Alexa 488, using the ZEN software (Carl Zeiss Microscopy). The brightness of Alexa 488 was used as a daily reference to ensure constant laser power and adjusting it using the software-provided laser power percentage whenever necessary (range over the entire set of measurements was 0.11 – 0.18%). Before

each measurement session, we acquired three sequential FCS measurements of Alexa488 in PBS, to verify the reproducibility of the confocal volume shape and size. The ratio between axial and lateral beam waist $S = \frac{z_0}{\omega_0}$ = 8.0 ± 0.2 (Avg. ± SEM) was obtained from a Brownian fit of the Alexa 488 autocorrelation curves using the ZEN software. For the lateral beam waist, we obtained $\omega_0$ = 0.186 ± 0.001 µm (Avg. ± SEM), calculated from the diffusion time $\tau_D$ = 20.9 ± 0.11 µs (Avg. ± SEM) obtained from the Brownian fit, being

$$D = \frac{\omega_0^2}{4\tau_D} \quad (1)$$

and being $D_{Alexa488}$ = 414 µm$^2$/s at 25°C (Petrov et al. 2006).

For the FCS measurements *in vivo*, the laser was positioned at the center of the short length axis and typically 0.8 - 1 µm from one of the cell poles along the long axis. For each cell, six sequential fluorescence intensity acquisitions of 20 seconds each were performed on the same spot. The laser power used for measurements *in vivo* was fixed to a value about 7 times lower than for Alexa488 in PBS, in order to reduce photobleaching. Confocal images of the selected cell were routinely acquired before and after the FCS measurement to verify focal (*z*) and positioning (*xy*) stability.

### 5.8.4 FCS data analysis

Due to the small size of bacterial cells, fluorescence intensity traces are affected by photobleaching. The effect of photobleaching on autocorrelation curves was corrected by detrending the long-time fluorescence decay of each of the six fluorescence intensity traces using an ImageJ plugin (Jay Unruh, https://research.stowers.org/imagejplugins/index.html, Stowers Institute for Medical Research, USA). The plugin calculates the autocorrelation function (ACF) from each fluorescence intensity trace, correcting it for the photobleaching effect by approximating the decreasing fluorescence intensity trend with a multi-segment line (the number of segments was fixed to two). We obtained almost identical ACFs

correcting for photobleaching effects by local averaging using the FCS-dedicated software package Fluctuation Analyzer (Wachsmuth et al. 2015). In both cases, ACFs were calculated starting at 2 µs, since at times shorter than 2 µsec, ACFs can be significantly affected by the GaAsp photomultipliers afterpulsing.

For each FCS measurement, we fitted all the six ACFs, calculated using the multi-segment detrending method, with a three-dimensional anomalous diffusion model that includes one diffusive component and one blinking component due to the protonation-deprotonation of the chromophore of sfGFP, according to the Equation (2):

$$G(\tau) = G_\infty + \frac{1}{N}\left(\frac{1-F_P+F_P e^{-\frac{\tau}{\tau_P}}}{1-F_P}\right)\frac{1}{1+\left(\frac{\tau}{\tau_D}\right)^{\alpha}\sqrt{1+\frac{1}{S^2}\left(\frac{\tau}{\tau_D}\right)^{\alpha}}}$$

(2)

where $N$ is the average number of particles in the confocal volume, $F_P$ the fraction of particles in the non-fluorescent state, $\tau_P$ the protonation-deprotonation lifetime at pH 7.5, $S = \frac{z_0}{\omega_0}$, the aspect ratio of the confocal volume with $z_0$ and $\omega_0$ being the axial and lateral beam waists, $\tau_D$ the diffusion time in the confocal volume, $\alpha$ the anomalous diffusion exponent, and $G_\infty$ the offset of the autocorrelation function. The protonation-deprotonation lifetime ($\tau_P$) for sfGFP was fixed to 25 µs according to FCS measurements of sfGFP in PBS at pH 7.5 (Cotlet et al. 2006). The aspect ratio of the confocal volume was fixed to $S = 8$ in the fittings to be consistent with the experimental calibration (see above). All other parameters were left free. For each FCS measurement, we calculated the average diffusion time $\tau_D$ and the average anomalous diffusion exponent $\alpha$ based on the autocorrelation curves of the six sequential fluorescence intensity traces. Fitting to the anomalous diffusion model was performed using the Levenberg-Marquardt algorithm in the FCS analysis-dedicated software QuickFit 3.0 developed by Jan Wolfgang Krieger and Jörg Langowski

(Deutsches Krebsforschungszentrum, Heidelberg, https://github.com/jkriege2/QuickFit3). Identical results were obtained when fitting the data with OriginPro.

Alternatively, the autocorrelation functions were fitted by the Ornstein-Uhlenbeck model (Appendix 2) according to Equation (3):

$$G(\tau) = G_\infty + \frac{1}{N}\left(\frac{1-F_P+F_P e^{-\frac{\tau}{\tau_P}}}{1-F_P}\right)\left(1+2\frac{\sigma^2}{\omega_0^2}\frac{1-e^{-\frac{1\omega_0^2}{2\sigma^2}\frac{\tau}{\tau_D}}}{1+\frac{1\omega_0^2}{8\sigma^2}}\right)^{-\frac{1}{2}}\left(1+\frac{\tau}{\tau_D}\right)^{-\frac{1}{2}}\left(1+2\frac{\sigma^2}{S^2\omega_0^2}\frac{1-e^{-\frac{1\omega_0^2}{2\sigma^2}\frac{\tau}{\tau_D}}}{1+\frac{1S^2\omega_0^2}{8\ \sigma^2}}\right)^{-\frac{1}{2}} \quad (3)$$

where $S$ and $\tau_P$ were fixed to the same values mentioned for equation (2), $\omega_0$ was fixed to 0.19 and $\sigma$ was fixed to $d/2$=0.42 μm, being $d$ the typical diameter of an *E. coli* cell (see Ornstein-Uhlenbeck model validation paragraph). Fitting to the Ornstein-Uhlenbeck model was performed with OriginPro.

### 5.8.5 FRAP data acquisition and analysis

Cells for FRAP experiments were grown and prepared for imaging following the same protocol as for the FCS measurements. Due to the higher sensitivity of FCS at low fluorophore concentrations, several fusion constructs required higher induction by IPTG to obtain fluorescence intensity suitable for FRAP. The same LSM 880 confocal microscope, including objective and light path, used for the FCS measurements, was used also for FRAP. The bacterial cell was imaged at 40×40 pixels with 30× zoom (pixel size 0.177 μm) with a pixel dwell time of 3.15 μs. First, 15 pre-bleaching frames were acquired at 2% laser power, subsequently the photobleaching was performed on a 3×3 pixels area on one cell pole with 100% laser power for a total of 48 ms and 584 post-bleaching frames were acquired to monitor the fluorescence recovery. During the data analysis, the bleaching spot, the target cell and a reference area for background subtraction, were defined as ImageJ ROIs (regions of interest). The mobile fractions and the half-times of recovery were obtained using the easyFRAP web tool (Rapsomaniki et al. 2012; Koulouras et al. 2018). The background intensity was subtracted at each time point and the intensity of fluorescence was

normalized for the acquisition bleaching during the course of the experiment. Of note, we used the target cell itself as a reference for the normalization, as done previously (Kumar, Mommer, and Sourjik 2010). This enabled us to achieve the highest possible temporal resolution, by reducing the acquisition area to a single *E. coli* cell. The mobile fractions (*mf*) were calculated as: $mf = \frac{I_\infty - I_a}{1 - I_a}$, where $I_\infty$ is the fluorescence intensity after full recovery (plateau of the curve) and $I_\alpha$ the normalized intensity of the first post-bleach time point. The half-times of fluorescence recovery ($t_{half}$) were computed from the fit of the recovery curves with a single exponential equation $I_{fit} = I_0 - a \cdot e^{-\beta \cdot t}$. $t_{half}$ is computed by solving the exponential equation for the value $I_{fit} = \frac{I_\infty - I_a}{2}$. FRAP diffusion coefficients shown in the results section, were estimated using simFRAP (Blumenthal et al. 2015), an ImageJ plugin based on a simulation approach implemented in a fast algorithm, which bypasses the need of using analytical models to interpolate the data. The simFRAP algorithm simulates two-dimensional random walks in each pixel, using the first image acquired after bleaching to define initial and boundary conditions, and it resolves numerically the diffusion equation by iterative simulation. The frame time and pixel size were fixed respectively to 0.018 s and 0.177 μm. The target cell and the bleached region were defined as the same ImageJ ROIs used for the analysis with easyFRAP. The FRAP derived diffusion coefficient $D_{FRAP}$ was directly obtained as output of the plugin.

## 5.9 Verification of sfGFP-constructs stability

The stability of the fusion constructs was verified by polyacrylamide gel electrophoresis and western blot (immunoblotting).

### 5.9.1 Sample preparation

*E. coli* cultures expressing all plasmid-encoded sfGFP constructs were grown as described in paragraph 5.8.1. 10 ml culture was spun 4000g for 10 min and washed in 5 ml PBS. Cells were then resuspended in 350 µl 1x SDS-PAGE (Laemmli) sample buffer and samples were heated at 95°C for 10 min, briefly vortexed (~10 s) and stored at -20°C overnight.

### 5.9.2 Sodium dodecyl sulfate polyacrylamide gel electrophoresis (SDS-PAGE)

The method of SDS-PAGE allows the separation of proteins depending on their mass. SDS is an anionic detergent that binds proteins in a constant stoichiometry. Proteins bound to SDS are linearized and charged negatively, thus allowing their separation by size depending on the electrophoretic mobility in a polyacrylamide gel. Gels were cast in two steps, starting with the preparation of the 10% resolving gel. Components were used in the amounts indicated below and mixed by inversion before and after addition of TEMED which initiated the polymerization of the gel. The mixture was applied to a gel caster system and isopropanol added on top of the gel in order to flatten the surface and prevent formation of bubbles. In the second step, the 5% stacking gel was prepared under the same conditions and poured on top of the resolving gel after the isopropanol had been discarded. The wells for sample loading were formed by insertion of a comb in the gel caster system. Hardened gels were either stored in moist paper at 4°C or immediately used for gel electrophoresis.

***Resolving 10% gel***

2 ml dd$H_2O$
1.3 ml 1.5 M Tris-HCl, pH 8.8
1.6 ml 30% Acrylamide
100 µl 10 % SDS
50 µl 10% Ammonium Persulfate
5 µl TEMED

***Stacking 5% gel***

ddH$_2$O 1.95 ml

315 µl 1 M Tris-HCl, pH 6.8

165 µl 30% Acrylamide Stock

12.5 µl 10 % SDS

6.25 µl 10% Ammonium Persulfate

1.25 µl TEMED

When loading the gel, 5 µl of protein molecular weight markers (PageRuler Plus Prestained Protein Ladder, 10 to 180 kDa, ThermoScientific) were applied to one of the wells in order to serve as size standard. 8 – 15 µl of samples were applied to the remaining gel wells. The stacking gel was run at 100 V for 30 min, the resolving gel was run at 120V for ~90 min. The run was performed in running buffer. The progress of the gel electrophoresis could be monitored by observation of the tracking dye bromophenol blue which was included in the Laemmli buffer and due to its low molecular weight moved ahead of most of the negatively charged proteins towards the positively charged anode.

**5.9.3 Western blot (immunoblot)**

By using the Western blotting technique, proteins that have been separated by gel electrophoresis are transferred to a nitrocellulose membrane and afterwards detected by incubation with specific antibodies. Proteins were transferred from the respective SDS gel to nitrocellulose membranes by wet blotting procedure. For every gel to be blotted two blotting papers cut to approximate gel size and two blotting sponges were soaked in transfer buffer. A nitrocellulose membrane was cut to gel size and shortly soaked in transfer buffer. The SDS gel was equally incubated in blotting buffer before being assembled into the transfer "sandwich" of blotting papers, sponges and nitrocellulose membrane and placed in the transfer tank. Electroblotting was performed at 100 V for 1 h, or overnight at 30 V. During transfer the negatively charged proteins are pulled from the SDS gel onto the nitrocellulose membrane towards the positively

charged electrode of the blotting tank. To prevent overheat, the transfer was performed in the cold room and a cooling pack was placed in the tank. The efficiency of the protein transfer was controlled by staining of the nitrocellulose membrane in Ponceau Red, a non-permanent and unspecific protein staining dye with low background signal. In order to prevent unspecific antibody binding during the following incubation steps, membranes were first blocked in 5 % skimmed dry milk dissolved in TBS-Tween (TBS-T milk). Incubation was carried out under gentle agitation for 60 min at RT. For specific labeling of sfGFP-tagged proteins, an anti-GFP primary antibody (JL-8 monoclonal, mouse, Takara) was diluted 1:10000 in 5 % TBS-T milk and applied to the blocked membrane. Samples were then incubated at RT for 1 h or at 4°C overnight under gentle shaking. Thereafter, membranes were washed three times in TBS-T to eliminate unbound antibody residues and subsequently incubated with anti-mouse secondary antibody (IRDye® 800CW Rabbit anti-mouse IgG) equally 1:10000 diluted in 5 % TBS-T milk. After incubation at RT for 1 h, membranes were again rinsed three times in TBS-T for residual antibody removal. The membranes were then imaged with an Odyssey Li-Cor imager. The percentage of free sfGFP was estimated from the membrane images with ImageJ.

## 5.10 Growth curves

Measurements of bacterial growth were performed using 96-well plates. Overnight cultures were inoculated at an initial $OD_{600}$ of 0.01 in the same medium as used for growth in other experiments. Each well contained 150 µl of culture and the plate was covered with the plastic cover provided by the producer and further sealed with parafilm that prevents evaporation but allows air exchange. Plates were incubated at 37°C with continuous shaking, alternating between 150 s orbital and 150 s linear, in a Tecan Infinite® 200 PRO plate reader.

## 5.11 Cellular density measurements

Cell cultures were grown following the same protocol as for the FCS and FRAP measurements. Cultures were harvested at 4000g for 5 minutes, and the pellet was resuspended in motility buffer (MB) supplemented with Tween 80, a surfactant that prevents cell-surface adhesion (Nielsen et al. 2016; Schwarz-Linek et al. 2016). Bacterial suspension was adjusted to a high cell density ($OD_{600}$=15) by subsequent centrifugation (4000g, 5 minutes) and resuspension in MB containing 20% iodixanol to match the density of the medium with that of *E. coli* cell (1.11 g/ml) (Martínez-Salas, Martín, and Vicente 1981). Each sample was then loaded in the chamber of a previously fabricated poly-di-methylsiloxane (PDMS) microfluidic device. The chamber consists of an inlet connected to an outlet by a straight channel of 50 μm height, 1 mm width and 1 cm length. The channel was then sealed with grease to prevent fluid flows. After letting the mixtures reach the steady state in the microfluidic device for 40 minutes, cell sedimentation was visualized by acquiring Z-stack images of the whole microfluidic channel using the same microscopy setup as for the FCS and FRAP measurements (1px = 0.2 μm in X and Y, 1px = 1 μm in Z; field of view = 303.64 x 303.64 x 70 $\mu m^3$, 0.35 μs/px exposure). The number of cells in each Z plane was quantified by the connected components labeling algorithm for ImageJ (Legland, Arganda-Carreras, and Andrey 2016). Each experiment was conducted in three technical replicates. Because the height and the tilt of the microfluidic channels slightly varies from sample to sample, the Z position was binned and the mean of the cell fraction over the bins was calculated.

The vertical density profiles were fitted to the theoretical expectation for diffusing particles in a buoyant fluid, $n(z) = n_o \exp(-\frac{z}{z_o})$, in the range $z = [0.25, 0.8] \times 50$ μm to avoid effects of sample boundaries. The fitted decay length is expected to obey $\frac{1}{z_o} = \frac{\Delta\rho V g}{k_B T}$, with $\Delta\rho$ the difference in density between the cells and the suspending fluid, $V$ the average volume of the cells, $g = 9.81$ $m^2/s$ the acceleration of gravity and $k_B T = 4.11$ pN·nm the thermal energy at 25°C. To compute the buoyancy-corrected cell density $\Delta\rho =$

$\frac{k_B T}{V g z_o}$, the cell volume was estimated assuming the cells are cylinders closed by hemispherical caps, $V = \pi d^3/6 + (L-d)\pi d^2/4$. For all conditions, the cell diameter $d$ was evaluated on confocal images taken prior to FCS measurement, and so was the length of cephalexin treated cells (L = 5.5 ± 0.1 (SEM) μm), cephalexin + A22 treated cells (L = 5.8 ± 0.1 (SEM) μm), and untreated cells (L=2.8 ± 0.2 μm). Cell length for 100 mM NaCl, DMSO, rifampicin and chloramphenicol treated cells was kept equal to the one of untreated cells, because cephalexin was not used during culture growth for sedimentation assay for these conditions.

## 5.12 Brownian dynamics simulations

We performed Brownian dynamics simulations of uncorrelated point particles under confinement. The *N* = 50 fluorescent particles performed a random walk with steps taken from a Gaussian distribution of width $\sqrt{2D\Delta t}$, with $D$ the free diffusion coefficient and $\Delta t = 10^{-6}\ s$ the simulation step. Confinement was imposed by redrawing the random steps that moved out of the confinement volume. Imposing elastic reflections on the walls yielded identical results. The confinement volume was assumed to be a cylinder of diameter *d* and length (*L-d*) closed at both ends by hemispheric caps of diameter *d*, idealizing the shape of *E. coli*. The cell length was fixed to *L* = 5 μm. The diameter was varied in the range *d* = [0.7, 1] μm. The collected fluorescence intensity was computed at each time step assuming a Gaussian intensity profile of the laser beam, $I(t) = \sum_{i=1}^{N} I_G(\boldsymbol{r}_i(t) - \boldsymbol{r}_0)$ with $\boldsymbol{r}_i(t)$ the position of particle *i*, $\boldsymbol{r}_0$ the center of the confocal volume and $I_G\big(\boldsymbol{r} = (x,y,z)\big) = \exp\left(-2\left(\frac{x^2+y^2}{\omega_0^2} + \frac{z^2}{z_0^2}\right)\right)$, with $\omega_0 = 200$ nm and $z_0 = 800$ nm the lateral and axial widths of the confocal volume. The normalized intensity autocorrelation $C(dt) = \frac{\langle I(t+dt)I(t)\rangle}{\langle I(t+dt)\rangle\langle I(t)\rangle} - 1$ is computed for logarithmically spaced lag times $dt$, to reflect experimental practices. The center of the confocal volume was chosen in the center of the cell along the *y* and *z* axes and 1 μm

away from the edge of the cell along the longitudinal *x* axis of the cell, similarly to experimental conditions. The intensity autocorrelation function was finally multiplied by an exponential decay, $\left(1 + 0.1 * \exp -\frac{dt}{\tau_H}\right)/1.1$ with $\tau_H = 25$ µs, to mimic the blinking component due to the protonation-deprotonation process of sfGFP, before fitting with the different models of diffusion. The code used for this simulation is available in GitHub (https://github.com/croelmiyn/Simulation_FCS_in_Bacteria) and via DOI: 10.5281/zenodo.5940484.

### 5.13 Validation of fitting by the Ornstein-Uhlenbeck model

We first estimated the relation between the width $\sigma$ of the potential well and the diameter *d* of the bacteria by fitting the ACF of the Brownian simulations with the OU model, fixing all parameters except $\sigma$ to their ansatz values. The best fit was obtained for $\sigma \simeq d/2$ over the whole range of tested parameters. To mimic the fit procedure of experimental data and evaluate the accuracy of the diffusion coefficient estimation by the OU model, we then fixed $\sigma = d/2$, and $\omega_0$ and $z_0$ to their ansatz values, since they are measured independently in experiments, whereas the diffusion coefficient, number of particles *N* in the confocal volume, fraction of triplet excitation and background noise were taken as free parameters.

# References


Agudo-Canalejo, Jaime, and Ramin Golestanian. 2020. 'Diffusion and steady state distributions of flexible chemotactic enzymes', *The European Physical Journal Special Topics*, 229: 2791-806.

Almblad, Henrik, Trevor E. Randall, Fanny Liu, Katherine Leblanc, Ryan A. Groves, Weerayuth Kittichotirat, Geoffrey L. Winsor, Nicolas Fournier, Emily Au, Julie Groizeleau, Jacquelyn D. Rich, Yuefei Lou, Elise Granton, Laura K. Jennings, Larissa A. Singletary, Tara M. L. Winstone, Nathan M. Good, Roger E. Bumgarner, Michael F. Hynes, Manu Singh, Maria Silvina Stietz, Fiona S. L. Brinkman, Ayush Kumar, Ann Karen Cornelia Brassinga, Matthew R. Parsek, Boo Shan Tseng, Ian A. Lewis, Bryan G. Yipp, Justin L. MacCallum, and Joe Jonathan Harrison. 2021. 'Bacterial cyclic diguanylate signaling networks sense temperature', *Nature Communications*, 12: 1986.

Amann, E., B. Ochs, and K. J. Abel. 1988. 'Tightly regulated tac promoter vectors useful for the expression of unfused and fused proteins in *Escherichia coli*', *Gene*, 69: 301-15.

André, Alain A. M. A. U. Spruijt EvanTI Liquid–Liquid Phase Separation in Crowded Environments. 2020. *International Journal of Molecular Sciences*.

Axelrod, D., D. E. Koppel, J. Schlessinger, E. Elson, and W. W. Webb. 1976. 'Mobility measurement by analysis of fluorescence photobleaching recovery kinetics', *Biophysical Journal*, 16: 1055-69.

Baba, T., T. Ara, M. Hasegawa, Y. Takai, Y. Okumura, M. Baba, K. A. Datsenko, M. Tomita, B. L. Wanner, and H. Mori. 2006. 'Construction of *Escherichia coli* K-12 in-frame, single-gene knockout mutants: the Keio collection', *Molecular Systems Biology*, 2: 2006 0008.

Bakshi, Somenath, Benjamin P Bratton, and James C Weisshaar. 2011. 'Subdiffraction-Limit Study of Kaede Diffusion and Spatial Distribution in Live *Escherichia coli*', *Biophysical Journal*, 101: 2535-44.

Bakshi, Somenath, Heejun Choi, Jagannath Mondal, and James C. Weisshaar. 2014. 'Time-dependent effects of transcription- and translation-halting drugs on the spatial distributions of the *Escherichia coli* chromosome and ribosomes', *Molecular Microbiology*, 94: 871-87.

Balbo, Jessica, Paolo Mereghetti, Dirk-Peter Herten, and Rebecca C. Wade. 2013. 'The shape of protein crowders is a major determinant of protein diffusion', *Biophysical Journal*, 104: 1576-84.

Banks, Daniel S., and Cécile Fradin. 2005. 'Anomalous Diffusion of Proteins Due to Molecular Crowding', *Biophysical Journal*, 89: 2960-71.

Ben-Hamida, Fakher, and François Gros. 1973. 'Synthesis and Translation of Ribopolymers in Escherichia coli Made Permeable by Treatment in High Sucrose Concentration', *European Journal of Biochemistry*, 38: 359-64.

Bennett, Bryson D., Elizabeth H. Kimball, Melissa Gao, Robin Osterhout, Stephen J. Van Dien, and Joshua D. Rabinowitz. 2009. 'Absolute metabolite concentrations and implied enzyme active site occupancy in Escherichia coli', *Nature Chemical Biology*, 5: 593-99.

Blumenthal, D., L. Goldstien, M. Edidin, and L. A. Gheber. 2015. 'Universal Approach to FRAP Analysis of Arbitrary Bleaching Patterns', *Scientific Reports*, 5: 11655.

Bouchaud, Jean-Philippe, and Antoine Georges. 1990. 'Anomalous diffusion in disordered media: Statistical mechanisms, models and physical applications', *Physics Reports*, 195: 127-293.

Boye, Erik. 1980. 'DNA Repair and Replication in Cells of Escherichia coli Made Permeable with Hypotonic Buffers', *Radiation Research*, 84: 35-45.

Bruno, L., V. Levi, M. Brunstein, and M. A. Desposito. 2009. 'Transition to superdiffusive behavior in intracellular actin-based transport mediated by molecular motors', *Phys Rev E Stat Nonlin Soft Matter Phys*, 80: 011912.

Buckstein Michael, H., Jian He, and Harvey Rubin. 2008. 'Characterization of Nucleotide Pools as a Function of Physiological State in Escherichia coli', *Journal of Bacteriology*, 190: 718-26.

Bucurenci, Nadia, Hiroshi Sakamoto, Pierre Briozzo, Nicolae Palibroda, Lidia Serina, Robert S. Sarfati, Gilles Labesse, Gilbert Briand, Antoine Danchin, Octavian Bârzu, and Anne-Marie Gilles. 1996. 'CMP Kinase from Escherichia coli Is Structurally Related to Other Nucleoside Monophosphate Kinases (*)', *Journal of Biological Chemistry*, 271: 2856-62.

Cabrera Julio, E., Cedric Cagliero, Selwyn Quan, L. Squires Catherine, and Jun Jin Ding. 2009. 'Active Transcription of rRNA Operons Condenses the Nucleoid in Escherichia coli: Examining the Effect of Transcription on Nucleoid Structure in the Absence of Transertion', *Journal of Bacteriology*, 191: 4180-85.

Cayley, Scott, Barbara A. Lewis, Harry J. Guttman, and M. Thomas Record. 1991. 'Characterization of the cytoplasm of *Escherichia coli* K-12 as a function of external osmolarity: Implications for protein-DNA interactions in vivo', *Journal of Molecular Biology*, 222: 281-300.

Chai, Qian, Bhupender Singh, Kristin Peisker, Nicole Metzendorf, Xueliang Ge, Santanu Dasgupta, and Suparna Sanyal. 2014. 'Organization of Ribosomes and Nucleoids in Escherichia coli Cells during Growth and in Quiescence*', *Journal of Biological Chemistry*, 289: 11342-52.

Chen, Xiaoying, Jennica L. Zaro, and Wei-Chiang Shen. 2013. 'Fusion protein linkers: Property, design and functionality', *Advanced Drug Delivery Reviews*, 65: 1357-69.

Cherepanov, Peter P., and Wilfried Wackernagel. 1995. 'Gene disruption in *Escherichia coli*: TcR and KmR cassettes with the option of Flp-catalyzed excision of the antibiotic-resistance determinant', *Gene*, 158: 9-14.

Chongsiriwatana, Nathaniel P., Jennifer S. Lin, Rinki Kapoor, Modi Wetzler, Jennifer A. C. Rea, Maruti K. Didwania, Christopher H. Contag, and Annelise E. Barron. 2017. 'Intracellular biomass flocculation as a key mechanism of rapid bacterial killing by cationic, amphipathic antimicrobial peptides and peptoids', *Scientific Reports*, 7: 16718.

Chung, C. T., S. L. Niemela, and R. H. Miller. 1989. 'One-step preparation of competent Escherichia coli: transformation and storage of bacterial cells in the same solution', *Proceedings of the National Academy of Sciences*, 86: 2172-75.

Cluzel, Philippe, Michael Surette, and Stanislas Leibler. 2000. 'An Ultrasensitive Bacterial Motor Revealed by Monitoring Signaling Proteins in Single Cells', *Science*, 287: 1652-55.

Colberg, Peter H., and Raymond Kapral. 2014. 'Ångström-scale chemically powered motors', *EPL (Europhysics Letters)*, 106: 30004.

Cotlet, M., P. M. Goodwin, G. S. Waldo, and J. H. Werner. 2006. 'A comparison of the fluorescence dynamics of single molecules of a green fluorescent protein: one- versus two-photon excitation', *Chemphyschem*, 7: 250-60.

Datsenko, Kirill A., and Barry L. Wanner. 2000. 'One-step inactivation of chromosomal genes in Escherichia coli K-12 using PCR products', *Proceedings of the National Academy of Sciences*, 97: 6640-45.

De Smet, Marie Jose, Jaap Kingma, and Bernard Witholt. 1978. 'The effect of toluene on the structure and permeability of the outer and cytoplasmic membranes of escherichia coli', *Biochimica et Biophysica Acta (BBA) - Biomembranes*, 506: 64-80.

de Vries, Renko. 2010. 'DNA condensation in bacteria: Interplay between macromolecular crowding and nucleoid proteins', *Biochimie*, 92: 1715-21.

Deutscher, M. P. 1974. 'Preparation of cells permeable to macromolecules by treatment with toluene: studies of transfer ribonucleic acid nucleotidyltransferase', *Journal of Bacteriology*, 118: 633-39.

Dey, Krishna Kanti, Sambeeta Das, Matthew F. Poyton, Samudra Sengupta, Peter J. Butler, Paul S. Cremer, and Ayusman Sen. 2014. 'Chemotactic Separation of Enzymes', *ACS Nano*, 8: 11941-49.

Di Rienzo, Carmine, Vincenzo Piazza, Enrico Gratton, Fabio Beltram, and Francesco Cardarelli. 2014. 'Probing short-range protein Brownian motion in the cytoplasm of living cells', *Nature Communications*, 5: 5891.

Diepold, A., E. Sezgin, M. Huseyin, T. Mortimer, C. Eggeling, and J. P. Armitage. 2017. 'A dynamic and adaptive network of cytosolic interactions governs protein export by the T3SS injectisome', *Nature Communications*, 8: 15940.

Einstein, Albert 1906. 'On the theory of the Brownian movement', *Annalen der Physik*, 19: 371-81.

Elowitz Michael, B., G. Surette Michael, Pierre-Etienne Wolf, B. Stock Jeffry, and Stanislas Leibler. 1999. 'Protein Mobility in the Cytoplasm of *Escherichia coli*', *Journal of Bacteriology*, 181: 197-203.

Elson, E. L. 2011. 'Fluorescence correlation spectroscopy: past, present, future', *Biophysical Journal*, 101: 2855-70.

English, Brian P., Vasili Hauryliuk, Arash Sanamrad, Stoyan Tankov, Nynke H. Dekker, and Johan Elf. 2011. 'Single-molecule investigations of the stringent response machinery in living bacterial cells', *Proceedings of the National Academy of Sciences of the United States of America*, 108: E365-E73.

Enright, Matthew B., and David M. Leitner. 2005. 'Mass fractal dimension and the compactness of proteins', *Physical Review E*, 71: 011912.

Etoc, Fred, Elie Balloul, Chiara Vicario, Davide Normanno, Domenik Liße, Assa Sittner, Jacob Piehler, Maxime Dahan, and Mathieu Coppey. 2018. 'Non-specific interactions govern cytosolic diffusion of nanosized objects in mammalian cells', *Nature Materials*, 17: 740-46.

Fessler, Mathias, Bertil Gummesson, Godefroid Charbon, Sine Lo Svenningsen, and Michael A. Sørensen. 2020. 'Short-term kinetics of rRNA degradation in Escherichia coli upon starvation for carbon, amino acid or phosphate', *Molecular Microbiology*, 113: 951-63.

Genevaux, P., C. Georgopoulos, and W. L. Kelley. 2007. 'The Hsp70 chaperone machines of *Escherichia coli*: a paradigm for the repartition of chaperone functions', *Molecular Microbiology*, 66: 840-57.

Gennerich, Arne, and Detlev Schild. 2000. 'Fluorescence Correlation Spectroscopy in Small Cytosolic Compartments Depends Critically on the Diffusion Model Used', *Biophysical Journal*, 79: 3294-306.

Gibson, D. G., L. Young, R. Y. Chuang, J. C. Venter, C. A. Hutchison, 3rd, and H. O. Smith. 2009. 'Enzymatic assembly of DNA molecules up to several hundred kilobases', *Nature Methods*, 6: 343-5.

Goins, Aron B., Hugo Sanabria, and M. Neal Waxham. 2008. 'Macromolecular crowding and size effects on probe microviscosity', *Biophysical Journal*, 95: 5362-73.

Goldstein, Byron, Harold Levine, and David Torney. 2007. 'Diffusion Limited Reactions', *SIAM Journal on Applied Mathematics*, 67: 1147-65.

Goltermann, L., M. V. Sarusie, and T. Bentin. 2015. 'Chaperonin GroEL/GroES Over-Expression Promotes Aminoglycoside Resistance and Reduces Drug Susceptibilities in Escherichia coli Following Exposure to Sublethal Aminoglycoside Doses', *Front Microbiol*, 6: 1572.

Goodsell, David S. 2009. 'The machinery of life'.

Grossman, N., E. Z. Ron, and C. L. Woldringh. 1982. 'Changes in cell dimensions during amino acid starvation of Escherichia coli', *Journal of Bacteriology*, 152: 35-41.

Guerra, Paolo, Luc-Alban Vuillemenot, Brady Rae, Valeriia Ladyhina, and Andreas Milias-Argeitis. 2022. 'Systematic In Vivo Characterization of Fluorescent Protein Maturation in Budding Yeast', *ACS Synthetic Biology*, 11: 1129-41.

Guigas, Gernot, and Matthias Weiss. 2008. 'Sampling the Cell with Anomalous Diffusion—The Discovery of Slowness', *Biophysical Journal*, 94: 90-94.

Hallen, Mark A., and Anita T. Layton. 2010. 'Expanding the scope of quantitative FRAP analysis', *Journal of Theoretical Biology*, 262: 295-305.

Horton, Margaret R., Felix Höfling, Joachim O. Rädler, and Thomas Franosch. 2010. 'Development of anomalous diffusion among crowding proteins', *Soft Matter*, 6: 2648-56.

Hou, Jennifer Y., Robert T. Sauer, and Tania A. Baker. 2008. 'Distinct structural elements of the adaptor ClpS are required for regulating degradation by ClpAP', *Nature Structural & Molecular Biology*, 15: 288-94.

Huber, M. L., R. A. Perkins, A. Laesecke, D. G. Friend, J. V. Sengers, M. J. Assael, I. N. Metaxa, E. Vogel, R. Mareš, and K. Miyagawa. 2009. 'New International Formulation for the Viscosity of H2O', *Journal of Physical and Chemical Reference Data*, 38: 101-25.

Humbard, M. A., S. Surkov, G. M. De Donatis, L. M. Jenkins, and M. R. Maurizi. 2013. 'The N-degradome of *Escherichia coli*: limited proteolysis in vivo generates a large pool of proteins bearing N-degrons', *The Journal of Biological Chemistry*, 288: 28913-24.

Illien, Pierre, Xi Zhao, Krishna K. Dey, Peter J. Butler, Ayusman Sen, and Ramin Golestanian. 2017. 'Exothermicity Is Not a Necessary Condition for Enhanced Diffusion of Enzymes', *Nano Letters*, 17: 4415-20.

Jackson Robert, W., and J. A. DeMoss. 1965. 'Effects of Toluene on Escherichia coli', *Journal of Bacteriology*, 90: 1420-25.

Jiang, Yanfei, Bingxian Xu, Artem Melnykov, Guy M. Genin, and Elliot L. Elson. 2020. 'Fluorescence Correlation Spectroscopy and Photon Counting Histograms in Finite, Bounded Domains', *Biophysical Journal*, 119: 265-73.

Joyner, Ryan P., Jeffrey H. Tang, Jonne Helenius, Elisa Dultz, Christiane Brune, Liam J. Holt, Sebastien Huet, Daniel J. Müller, and Karsten Weis. 2016. 'A glucose-starvation response regulates the diffusion of macromolecules', *Elife*, 5: e09376.

Kalwarczyk, Tomasz, Marcin Tabaka, and Robert Holyst. 2012. 'Biologistics--diffusion coefficients for complete proteome of *Escherichia coli*', *Bioinformatics (Oxford, England)*, 28: 2971-78.

Kang, Minchul, Charles A. Day, Anne K. Kenworthy, and Emmanuele DiBenedetto. 2012. 'Simplified Equation to Extract Diffusion Coefficients from Confocal FRAP Data', *Traffic*, 13: 1589-600.

Kapanidis, A. N., S. Uphoff, and M. Stracy. 2018. 'Understanding Protein Mobility in Bacteria by Tracking Single Molecules', *Journal of Molecular Biology*, 430: 4443-55.

Katayama, Y., S. Gottesman, J. Pumphrey, S. Rudikoff, W. P. Clark, and M. R. Maurizi. 1988. 'The two-component, ATP-dependent Clp protease of Escherichia coli. Purification, cloning, and mutational analysis of the ATP-binding component', *Journal of Biological Chemistry*, 263: 15226-36.

Klumpp, Stefan, Matthew Scott, Steen Pedersen, and Terence Hwa. 2013. 'Molecular crowding limits translation and cell growth', *Proceedings of the National Academy of Sciences*, 110: 16754.

Konopka, M. C., I. A. Shkel, S. Cayley, M. T. Record, and J. C. Weisshaar. 2006. 'Crowding and confinement effects on protein diffusion in vivo', *Journal of Bacteriology*, 188: 6115-23.

Konopka, M. C., K. A. Sochacki, B. P. Bratton, I. A. Shkel, M. T. Record, and J. C. Weisshaar. 2009. 'Cytoplasmic protein mobility in osmotically stressed *Escherichia coli*', *Journal of Bacteriology*, 191: 231-7.

Koulouras, Grigorios, Andreas Panagopoulos, Maria A. Rapsomaniki, Nickolaos N. Giakoumakis, Stavros Taraviras, and Zoi Lygerou. 2018. 'EasyFRAP-web: a web-based tool for the analysis of fluorescence recovery after photobleaching data', *Nucleic Acids Research*, 46: W467-W72.

Kumar, M., M. S. Mommer, and V. Sourjik. 2010. 'Mobility of cytoplasmic, membrane, and DNA-binding proteins in *Escherichia coli*', *Biophysical Journal*, 98: 552-9.

Kumar, Mohit, and Victor Sourjik. 2012. 'Physical map and dynamics of the chaperone network in *Escherichia coli*', *Molecular Microbiology*, 84: 736-47.

Lampo, Thomas J., Stella Stylianidou, Mikael P. Backlund, Paul A. Wiggins, and Andrew J. Spakowitz. 2017. 'Cytoplasmic RNA-Protein Particles Exhibit Non-Gaussian Subdiffusive Behavior', *Biophysical Journal*, 112: 532-42.

Le Gall, Antoine, Diego I. Cattoni, Baptiste Guilhas, Céline Mathieu-Demazière, Laura Oudjedi, Jean-Bernard Fiche, Jérôme Rech, Sara Abrahamsson, Heath Murray, Jean-Yves Bouet, and Marcelo Nollmann. 2016. 'Bacterial partition complexes segregate within the volume of the nucleoid', *Nature Communications*, 7: 12107.

Legland, David, Ignacio Arganda-Carreras, and Philippe Andrey. 2016. 'MorphoLibJ: integrated library and plugins for mathematical morphology with ImageJ', *Bioinformatics (Oxford, England)*, 32: 3532-34.

Levin, Petra Anne, and Esther R. Angert. 2015. 'Small but Mighty: Cell Size and Bacteria', *Cold Spring Harbor Perspectives in Biology*, 7.

Lin, Wei-Hsiang, and Christine Jacobs-Wagner. 2022. 'Connecting single-cell ATP dynamics to overflow metabolism, cell growth, and the cell cycle in Escherichia coli', *Current Biology*.

Liu, B., Z. Hasrat, B. Poolman, and A. J. Boersma. 2019. 'Decreased Effective Macromolecular Crowding in *Escherichia coli* Adapted to Hyperosmotic Stress', *Journal of Bacteriology*, 201.

Lobritz, Michael A., Peter Belenky, Caroline B. M. Porter, Arnaud Gutierrez, Jason H. Yang, Eric G. Schwarz, Daniel J. Dwyer, Ahmad S. Khalil, and James J. Collins. 2015. 'Antibiotic efficacy is linked to bacterial cellular respiration', *Proceedings of the National Academy of Sciences*, 112: 8173-80.

Loren, N., J. Hagman, J. K. Jonasson, H. Deschout, D. Bernin, F. Cella-Zanacchi, A. Diaspro, J. G. McNally, M. Ameloot, N. Smisdom, M. Nyden, A. M. Hermansson, M. Rudemo, and K. Braeckmans. 2015. 'Fluorescence recovery after photobleaching in material and life sciences: putting theory into practice', *Quarterly Reviews of Biophysics*, 48: 323-87.

Losa, José, Simeon Leupold, Diego Alonso-Martinez, Petteri Vainikka, Sebastian Thallmair, Katarzyna M. Tych, Siewert J. Marrink, and Matthias Heinemann. 2022. 'Perspective: a stirring role for metabolism in cells', *Molecular Systems Biology*, 18: e10822.

Luby-Phelps, Kate. 2013. 'The physical chemistry of cytoplasm and its influence on cell function: an update', *Molecular Biology of the Cell*, 24: 2593-96.

Luby-Phelps, Katherine. 1999. 'Cytoarchitecture and Physical Properties of Cytoplasm: Volume, Viscosity, Diffusion, Intracellular Surface Area.' in Harry Walter, Donald E. Brooks and Paul A. Srere (eds.), *International Review of Cytology* (Academic Press).

Macháň, Radek, Yong Hwee Foo, and Thorsten Wohland. 2016. 'On the Equivalence of FCS and FRAP: Simultaneous Lipid Membrane Measurements', *Biophysical Journal*, 111: 152-61.

Malchus, N., and M. Weiss. 2010. 'Elucidating anomalous protein diffusion in living cells with fluorescence correlation spectroscopy-facts and pitfalls', *J Fluoresc*, 20: 19-26.

Manzo, Carlo, and Maria F. Garcia-Parajo. 2015. 'A review of progress in single particle tracking: from methods to biophysical insights', *Reports on Progress in Physics*, 78: 124601.

Martínez-Salas, E., J. A. Martín, and M. Vicente. 1981. 'Relationship of Escherichia coli density to growth rate and cell age', *J Bacteriol*, 147: 97-100.

Mayer, Matthias P., Stefan Rüdiger, and Bernd Bukau. 2000. 'Molecular Basis for Interactions of the DnaK Chaperone with Substrates', *Biological Chemistry*, 381: 877-85.

McConkey, E. H. 1982. 'Molecular evolution, intracellular organization, and the quinary structure of proteins', *Proceedings of the National Academy of Sciences*, 79: 3236-40.

McMurry, L. M., M. Hendricks, and S. B. Levy. 1986. 'Effects of toluene permeabilization and cell deenergization on tetracycline resistance in Escherichia coli', *Antimicrobial Agents and Chemotherapy*, 29: 681-86.

Meacci, G., J. Ries, E. Fischer-Friedrich, N. Kahya, P. Schwille, and K. Kruse. 2006. 'Mobility of Min-proteins in *Escherichia coli* measured by fluorescence correlation spectroscopy', *Physical Biology*, 3: 255-63.

Metzler, Ralf, and Joseph Klafter. 2000. 'The random walk's guide to anomalous diffusion: a fractional dynamics approach', *Physics Reports*, 339: 1-77.

Mika, J. T., G. van den Bogaart, L. Veenhoff, V. Krasnikov, and B. Poolman. 2010. 'Molecular sieving properties of the cytoplasm of *Escherichia coli* and consequences of osmotic stress', *Molecular Microbiology*, 77: 200-7.

Mikhailov, Alexander S., and Raymond Kapral. 2015. 'Hydrodynamic collective effects of active protein machines in solution and lipid bilayers', *Proceedings of the National Academy of Sciences*, 112: E3639-E44.

Montecinos-Franjola, Felipe, Brianna L. Bauer, Jason A. Mears, and Rajesh Ramachandran. 2020. 'GFP fluorescence tagging alters dynamin-related protein 1 oligomerization dynamics and creates disassembly-refractory puncta to mediate mitochondrial fission', *Scientific Reports*, 10: 14777.

Montero Llopis, Paula, Oleksii Sliusarenko, Jennifer Heinritz, and Christine Jacobs-Wagner. 2012. '*In vivo* biochemistry in bacterial cells using FRAP: insight into the translation cycle', *Biophysical Journal*, 103: 1848-59.

Mu, Xin, Seongil Choi, Lisa Lang, David Mowray, Nikolay V. Dokholyan, Jens Danielsson, and Mikael Oliveberg. 2017. 'Physicochemical code for quinary protein interactions in *Escherichia coli*', *Proceedings of the National Academy of Sciences*, 114: E4556.

Muddana, Hari S., Samudra Sengupta, Thomas E. Mallouk, Ayusman Sen, and Peter J. Butler. 2010. 'Substrate Catalysis Enhances Single-Enzyme Diffusion', *Journal of the American Chemical Society*, 132: 2110-11.

Mullineaux, C. W., A. Nenninger, N. Ray, and C. Robinson. 2006. 'Diffusion of green fluorescent protein in three cell environments in *Escherichia coli*', *Journal of Bacteriology*, 188: 3442-8.

Munder, M. C., D. Midtvedt, T. Franzmann, E. Nuske, O. Otto, M. Herbig, E. Ulbricht, P. Muller, A. Taubenberger, S. Maharana, L. Malinovska, D. Richter, J. Guck, V. Zaburdaev, and S. Alberti. 2016. 'A pH-driven transition of the cytoplasm from a fluid- to a solid-like state promotes entry into dormancy', *Elife*, 5.

Muramatsu, N., and A. P. Minton. 1988. 'Tracer diffusion of globular proteins in concentrated protein solutions', *Proceedings of the National Academy of Sciences of the United States of America*, 85: 2984-88.

Navarro Llorens, Juana María, Antonio Tormo, and Esteban Martínez-García. 2010. 'Stationary phase in gram-negative bacteria', *FEMS Microbiology Reviews*, 34: 476-95.

Nenninger, A., G. Mastroianni, and C. W. Mullineaux. 2010. 'Size dependence of protein diffusion in the cytoplasm of *Escherichia coli*', *Journal of Bacteriology*, 192: 4535-40.

Nielsen, Christina K., Jørgen Kjems, Tina Mygind, Torben Snabe, and Rikke L. Meyer. 2016. 'Effects of Tween 80 on Growth and Biofilm Formation in Laboratory Media', *Frontiers in Microbiology*, 7.

Oldewurtel Enno, R., Yuki Kitahara, and Sven van Teeffelen. 2021. 'Robust surface-to-mass coupling and turgor-dependent cell width determine bacterial dry-mass density', *Proceedings of the National Academy of Sciences*, 118: e2021416118.

Oleksiuk, Olga, Vladimir Jakovljevic, Nikita Vladimirov, Ricardo Carvalho, Eli Paster, William S Ryu, Yigal Meir, Ned S Wingreen, Markus Kollmann, and Victor Sourjik. 2011. 'Thermal Robustness of Signaling in Bacterial Chemotaxis', *Cell*, 145: 312-21.

Ouzounov, N., J. P. Nguyen, B. P. Bratton, D. Jacobowitz, Z. Gitai, and J. W. Shaevitz. 2016. 'MreB Orientation Correlates with Cell Diameter in *Escherichia coli*', *Biophysical Journal*, 111: 1035-43.

Parry, B. R., I. V. Surovtsev, M. T. Cabeen, C. S. O'Hern, E. R. Dufresne, and C. Jacobs-Wagner. 2014. 'The bacterial cytoplasm has glass-like properties and is fluidized by metabolic activity', *Cell*, 156: 183-94.

Pastor, A., A. K. Singh, P. K. Shukla, M. J. Equbal, S. T. Malik, T. P. Singh, and T. K. Chaudhuri. 2016. 'Role of N-terminal region of Escherichia coli maltodextrin glucosidase in folding and function of the protein', *Biochim Biophys Acta*, 1864: 1138-51.

Patel, Avinash, Liliana Malinovska, Shambaditya Saha, Jie Wang, Simon Alberti, Yamuna Krishnan, and Anthony A. Hyman. 2017. 'ATP as a biological hydrotrope', *Science*, 356: 753-56.

Paul, S., S. Punam, and T. K. Chaudhuri. 2007. 'Chaperone-assisted refolding of Escherichia coli maltodextrin glucosidase', *FEBS J*, 274: 6000-10.

Pédelacq, Jean-Denis, Stéphanie Cabantous, Timothy Tran, Thomas C. Terwilliger, and Geoffrey S. Waldo. 2006. 'Engineering and characterization of a superfolder green fluorescent protein', *Nature Biotechnology*, 24: 79-88.

Persson, Laura B., Vardhaan S. Ambati, and Onn Brandman. 2020. 'Cellular Control of Viscosity Counters Changes in Temperature and Energy Availability', *Cell*, 183: 1572-85.e16.

Petrov, E. P., T. Ohrt, R. G. Winkler, and P. Schwille. 2006. 'Diffusion and segmental dynamics of double-stranded DNA', *Physical Review Letters*, 97: 258101.

Rapsomaniki, Maria Anna, Panagiotis Kotsantis, Ioanna-Eleni Symeonidou, Nickolaos-Nikiforos Giakoumakis, Stavros Taraviras, and Zoi Lygerou. 2012. 'easyFRAP: an interactive, easy-to-use tool for qualitative and quantitative analysis of FRAP data', *Bioinformatics (Oxford, England)*, 28: 1800-01.

Reverey, J. F., J. H. Jeon, H. Bao, M. Leippe, R. Metzler, and C. Selhuber-Unkel. 2015. 'Superdiffusion dominates intracellular particle motion in the supercrowded cytoplasm of pathogenic Acanthamoeba castellanii', *Sci Rep*, 5: 11690.

Riedel, Clement, Ronen Gabizon, Christian A. M. Wilson, Kambiz Hamadani, Konstantinos Tsekouras, Susan Marqusee, Steve Pressé, and Carlos Bustamante. 2015. 'The heat released during catalytic turnover enhances the diffusion of an enzyme', *Nature*, 517: 227-30.

Ries, Jonas, and Petra Schwille. 2012. 'Fluorescence correlation spectroscopy', *BioEssays*, 34: 361-68.

Rocha, J., J. Corbitt, T. Yan, C. Richardson, and A. Gahlmann. 2019. 'Resolving Cytosolic Diffusive States in Bacteria by Single-Molecule Tracking', *Biophysical Journal*, 116: 1970-83.

Roman-Hernandez, G., J. Y. Hou, R. A. Grant, R. T. Sauer, and T. A. Baker. 2011. 'The ClpS adaptor mediates staged delivery of N-end rule substrates to the AAA+ ClpAP protease', *Molecular Cell*, 43: 217-28.

Rotter, D. A. O., C. Heger, L. M. Oviedo-Bocanegra, and P. L. Graumann. 2021. 'Transcription-dependent confined diffusion of enzymes within subcellular spaces of the bacterial cytoplasm', *BMC Biology*, 19: 183.

Rowland, D. J., H. H. Tuson, and J. S. Biteen. 2016. 'Resolving Fast, Confined Diffusion in Bacteria with Image Correlation Spectroscopy', *Biophys J*, 110: 2241-51.

Sabri, Adal, Xinran Xu, Diego Krapf, and Matthias Weiss. 2020. 'Elucidating the Origin of Heterogeneous Anomalous Diffusion in the Cytoplasm of Mammalian Cells', *Physical Review Letters*, 125: 058101.

Saint Girons, I., A. M. Gilles, D. Margarita, S. Michelson, M. Monnot, S. Fermandjian, A. Danchin, and O. Bârzu. 1987. 'Structural and catalytic characteristics of Escherichia coli adenylate kinase', *Journal of Biological Chemistry*, 262: 622-29.

Sanamrad, A., F. Persson, E. G. Lundius, D. Fange, A. H. Gynna, and J. Elf. 2014. 'Single-particle tracking reveals that free ribosomal subunits are not excluded from the *Escherichia coli* nucleoid', *Proceedings of the National Academy of Sciences of the United States of America*, 111: 11413-8.

Sandikci, A., F. Gloge, M. Martinez, M. P. Mayer, R. Wade, B. Bukau, and G. Kramer. 2013. 'Dynamic enzyme docking to the ribosome coordinates N-terminal processing with polypeptide folding', *Nature Structural & Molecular Biology*, 20: 843-50.

Saxton, M. J. 1996. 'Anomalous diffusion due to binding: a Monte Carlo study', *Biophysical Journal*, 70: 1250-62.

Saxton, Michael J. 2007. 'A Biological Interpretation of Transient Anomalous Subdiffusion. I. Qualitative Model', *Biophysical Journal*, 92: 1178-91.

Schavemaker, P. E., W. M. Smigiel, and B. Poolman. 2017. 'Ribosome surface properties may impose limits on the nature of the cytoplasmic proteome', *Elife*, 6.

Schultz, Christian P., Loida Ylisastigui-Pons, Lidia Serina, Hiroshi Sakamoto, Henry H. Mantsch, Jan Neuhard, Octavian Bârzu, and Anne-Marie Gilles. 1997. 'Structural and Catalytic Properties of CMP Kinase fromBacillus subtilis:A Comparative Analysis with the Homologous Enzyme fromEscherichia coli', *Archives of Biochemistry and Biophysics*, 340: 144-53.

Schwartz, Russell, Claire S. Ting, and Jonathan King. 2001. 'Whole Proteome pI Values Correlate with Subcellular Localizations of Proteins for Organisms within the Three Domains of Life', *Genome Research*, 11: 703-09.

Schwarz-Linek, Jana, Jochen Arlt, Alys Jepson, Angela Dawson, Teun Vissers, Dario Miroli, Teuta Pilizota, Vincent A. Martinez, and Wilson C. K. Poon. 2016. 'Escherichia coli as a model active colloid: A practical introduction', *Colloids and Surfaces B: Biointerfaces*, 137: 2-16.

Selinger, Douglas W., Rini Mukherjee Saxena, Kevin J. Cheung, George M. Church, and Carsten Rosenow. 2003. 'Global RNA Half-Life Analysis in Escherichia coli Reveals Positional Patterns of Transcript Degradation', *Genome Research*, 13: 216-23.

Sengupta, Samudra, Krishna K. Dey, Hari S. Muddana, Tristan Tabouillot, Michael E. Ibele, Peter J. Butler, and Ayusman Sen. 2013. 'Enzyme Molecules as Nanomotors', *Journal of the American Chemical Society*, 135: 1406-14.

Sengupta, Samudra, Michelle M. Spiering, Krishna K. Dey, Wentao Duan, Debabrata Patra, Peter J. Butler, R. Dean Astumian, Stephen J. Benkovic, and Ayusman Sen. 2014. 'DNA Polymerase as a Molecular Motor and Pump', *ACS Nano*, 8: 2410-18.

Serra Diego, O., M. Richter Anja, Gisela Klauck, Franziska Mika, Regine Hengge, and Roberto Kolter. 2013. 'Microanatomy at Cellular Resolution and Spatial Order of Physiological Differentiation in a Bacterial Biofilm', *mBio*, 4: e00103-13.

Sinensky, M. 1974. 'Homeoviscous adaptation--a homeostatic process that regulates the viscosity of membrane lipids in *Escherichia coli*', *Proceedings of the National Academy of Sciences of the United States of America*, 71: 522-25.

Śmigiel, Wojciech M., Luca Mantovanelli, Dmitrii S. Linnik, Michiel Punter, Jakob Silberberg, Limin Xiang, Ke Xu, and Bert Poolman. 2022. 'Protein diffusion in Escherichia coli cytoplasm scales with the mass of the complexes and is location dependent', *Science Advances*, 8: eabo5387.

Smilgies, Detlef- M., and Ewa Folta-Stogniew. 2015. 'Molecular weight-gyration radius relation of globular proteins: a comparison of light scattering, small-angle X-ray scattering and structure-based data', *Journal of applied crystallography*, 48: 1604-06.

Solbiati, José, Anne Chapman-Smith, Judith L. Miller, Charles G. Miller, and John E. Cronan. 1999. 'Processing of the N termini of nascent polypeptide chains requires deformylation prior to methionine removal', *Journal of Molecular Biology*, 290: 607-14.

Soundrarajan, Nagasundarapandian, Sriram Sokalingam, Govindan Raghunathan, Nediljko Budisa, Hyun-Jong Paik, Tae Hyeon Yoo, and Sun-Gu Lee. 2012. 'Conjugation of Proteins by Installing BIO-Orthogonally Reactive Groups at Their N-Termini', *PLoS One*, 7: e46741.

Spitzer, Jan, and Bert Poolman. 2013. 'How crowded is the prokaryotic cytoplasm?', *FEBS Letters*, 587: 2094-98.

Stasevich, Timothy J., Florian Mueller, Ariel Michelman-Ribeiro, Tilman Rosales, Jay R. Knutson, and James G. McNally. 2010. 'Cross-validating FRAP and FCS to quantify the impact of photobleaching on in vivo binding estimates', *Biophysical Journal*, 99: 3093-101.

Stracy, M., J. Schweizer, D. J. Sherratt, A. N. Kapanidis, S. Uphoff, and C. Lesterlin. 2021. 'Transient non-specific DNA binding dominates the target search of bacterial DNA-binding proteins', *Molecular Cell*, 81: 1499-514 e6.

Swaminathan, R., C. P. Hoang, and A. S. Verkman. 1997. 'Photobleaching recovery and anisotropy decay of green fluorescent protein GFP-S65T in solution and cells: cytoplasmic viscosity probed by green fluorescent protein translational and rotational diffusion', *Biophysical Journal*, 72: 1900-07.

Terry, B. R., E. K. Matthews, and J. Haseloff. 1995. 'Molecular Characterization of Recombinant Green Fluorescent Protein by Fluorescence Correlation Microscopy', *Biochemical and Biophysical Research Communications*, 217: 21-27.

Thanbichler, Martin, Bernhard Neuhierl, and August Böck. 1999. 'S-Methylmethionine Metabolism in Escherichia coli', *Journal of Bacteriology*, 181: 662-65.

Thomason, Lynn C., Nina Costantino, and Donald L. Court. 2007. 'E. coli Genome Manipulation by P1 Transduction', *Current Protocols in Molecular Biology*, 79: 1.17.1-1.17.8.

Tran, Buu Minh, Haritha Prabha, Aditya Iyer, Conor O'Byrne, Tjakko Abee, and Bert Poolman. 2021. 'Measurement of Protein Mobility in *Listeria monocytogenes* Reveals a Unique Tolerance to Osmotic Stress and Temperature Dependence of Diffusion', *Frontiers in Microbiology*, 12.

Tyn, Myo T., and Todd W. Gusek. 1990. 'Prediction of diffusion coefficients of proteins', *Biotechnology and Bioengineering*, 35: 327-38.

Vámosi, György, Norbert Mücke, Gabriele Müller, Jan Wolfgang Krieger, Ute Curth, Jörg Langowski, and Katalin Tóth. 2016. 'EGFP oligomers as natural fluorescence and hydrodynamic standards', *Scientific Reports*, 6: 33022.

van den Berg, Jonas, Arnold J. Boersma, and Bert Poolman. 2017. 'Microorganisms maintain crowding homeostasis', *Nature Reviews Microbiology*, 15: 309-18.

von Bülow, Sören, Marc Siggel, Max Linke, and Gerhard Hummer. 2019. 'Dynamic cluster formation determines viscosity and diffusion in dense protein solutions', *Proceedings of the National Academy of Sciences*, 116: 9843-52.

von Stetten, David, Marjolaine Noirclerc-Savoye, Joachim Goedhart, Theodorus W. J. Gadella, Jr, and Antoine Royant. 2012. 'Structure of a fluorescent protein from Aequorea victoria bearing the obligate-monomer mutation A206K', *Acta Crystallographica Section F*, 68: 878-82.

Wachsmuth, M., C. Conrad, J. Bulkescher, B. Koch, R. Mahen, M. Isokane, R. Pepperkok, and J. Ellenberg. 2015. 'High-throughput fluorescence correlation spectroscopy enables analysis of proteome dynamics in living cells', *Nature Biotechnology*, 33: 384-9.

Wachsmuth, Malte, Waldemar Waldeck, and Jörg Langowski. 2000. 'Anomalous diffusion of fluorescent probes inside living cell nuclei investigated by spatially-resolved fluorescence correlation spectroscopy11Edited by W. Baumeister', *Journal of Molecular Biology*, 298: 677-89.

Weber, Stephanie, C., Andrew Spakowitz, J., and Julie Theriot, A. 2012. 'Nonthermal ATP-dependent fluctuations contribute to the in vivo motion of chromosomal loci', *Proceedings of the National Academy of Sciences*, 109: 7338-43.

Whitford, Paul C., Osamu Miyashita, Yaakov Levy, and José N. Onuchic. 2007. 'Conformational Transitions of Adenylate Kinase: Switching by Cracking', *Journal of Molecular Biology*, 366: 1661-71.

Wickner, Reed B., and Jerard Hurwitz. 1972. 'DNA replication in Escherichia coli made permeable by treatment with high sucrose', *Biochemical and Biophysical Research Communications*, 47: 202-11.

Wlodarski, Michal, Leonardo Mancini, Bianca Raciti, Bianca Sclavi, Marco Cosentino Lagomarsino, and Pietro Cicuta. 2020. 'Cytosolic Crowding Drives the Dynamics of Both Genome and Cytosol in Escherichia coli Challenged with Sub-lethal Antibiotic Treatments', *iScience*, 23: 101560.

Wojcieszyn, J. W., R. A. Schlegel, E. S. Wu, and K. A. Jacobson. 1981. 'Diffusion of injected macromolecules within the cytoplasm of living cells', *Proceedings of the National Academy of Sciences*, 78: 4407-10.

Wong, Felix, Jonathan M. Stokes, Bernardo Cervantes, Sider Penkov, Jens Friedrichs, Lars D. Renner, and James J. Collins. 2021. 'Cytoplasmic condensation induced by membrane damage is associated with antibiotic lethality', *Nature Communications*, 12: 2321.

Xiang, Limin, Kun Chen, Rui Yan, Wan Li, and Ke Xu. 2020. 'Single-molecule displacement mapping unveils nanoscale heterogeneities in intracellular diffusivity', *Nature Methods*, 17: 524-30.

Xu, Mengqi, Jennifer L. Ross, Lyanne Valdez, and Aysuman Sen. 2019. 'Direct Single Molecule Imaging of Enhanced Enzyme Diffusion', *Physical Review Letters*, 123: 128101.

Yaginuma, Hideyuki, Shinnosuke Kawai, Kazuhito V. Tabata, Keisuke Tomiyama, Akira Kakizuka, Tamiki Komatsuzaki, Hiroyuki Noji, and Hiromi Imamura. 2014. 'Diversity in ATP concentrations in a single bacterial cell population revealed by quantitative single-cell imaging', *Scientific Reports*, 4: 6522.

Yeates, Todd O., Michael C. Thompson, and Thomas A. Bobik. 2011. 'The protein shells of bacterial microcompartment organelles', *Current Opinion in Structural Biology*, 21: 223-31.

Yu, Hua, Kyubong Jo, Kristy L. Kounovsky, Juan J. de Pablo, and David C. Schwartz. 2009. 'Molecular Propulsion: Chemical Sensing and Chemotaxis of DNA Driven by RNA Polymerase', *Journal of the American Chemical Society*, 131: 5722-23.

Yu, Shi, Julian Sheats, Pietro Cicuta, Bianca Sclavi, Marco Cosentino Lagomarsino, and Kevin D. Dorfman. 2018. 'Subdiffusion of loci and cytoplasmic particles are different in compressed Escherichia coli cells', *Communications Biology*, 1: 176.

Zhao, Xi, Krishna K. Dey, Selva Jeganathan, Peter J. Butler, Ubaldo M. Córdova-Figueroa, and Ayusman Sen. 2017. 'Enhanced Diffusion of Passive Tracers in Active Enzyme Solutions', *Nano Letters*, 17: 4807-12.

Zhao, Xi, Henri Palacci, Vinita Yadav, Michelle M. Spiering, Michael K. Gilson, Peter J. Butler, Henry Hess, Stephen J. Benkovic, and Ayusman Sen. 2018. 'Substrate-driven chemotactic assembly in an enzyme cascade', *Nature Chemistry*, 10: 311-17.

Zhou, Huan-Xiang. 2013. 'Influence of crowded cellular environments on protein folding, binding, and oligomerization: Biological consequences and potentials of atomistic modeling', *FEBS Letters*, 587: 1053-61.

Zimmerman, Steven B., and Stefan O. Trach. 1991. 'Estimation of macromolecule concentrations and excluded volume effects for the cytoplasm of *Escherichia coli*', *Journal of Molecular Biology*, 222: 599-620.

# Acknowledgements

First and foremost, my warmest thanks go to Prof. Dr. Victor Sourjik. This work would have not been possible without his constant supervision, guidance, mentoring, motivation, and support over the four years of my PhD.

The second big thanks go to the members of my thesis advisory committee, Prof. Dr. Martin Thanbichler and Dr. Andreas Diepold, for the fruitful discussions and helpful suggestions during our annual meetings.

I would like to also thank my examiners: Prof. Dr. Martin Thanbichler, which was also so kind to revise this thesis, Dr. Andreas Diepold, and Prof. Dr. Michael Bölker.

I take this opportunity to also thank Prof. Dr. Ramin Golestanian and Dr. Jaime Agudo-Canalejo, from the MPI for Dynamics and Self-Organization in Göttingen. Their fruitful collaboration improved dramatically the quality of this work by putting our experimental results into a robust theorical framework.

Special thanks go to Dr. Gabriele Malengo for sharing his great expertise and experience through the whole process of the experiments on protein diffusion: from the planning, through the execution and ultimately on the analysis of the data. I want to also thank Dr. Remy Colin for his great work with the Brownian diffusion simulations and the help with the measurements of the cell density. I want to also thank them both for the invaluable work of proofreading on our manuscript and on this thesis.

I would also like to thank the technicians in our lab: Ali, Melissa, Sarah, Sebastian, Inka, Claudia, that allowed the work in this thesis to run smoothly by always providing fresh media, clean plastic- and glassware, and every necessary reagent. A great thank also to Manuel, that has always been helpful when I was having “arguments” with my PC.

A very warm thanks go to all the fellow PhDs and post-docs, current and past, of AG Sourjik for creating a chill and welcoming place to work, for all the useful suggestions during the lab meetings and for the help with the everyday lab work. Particularly, I would like to thank Giovanni, for the help with the growth curves experiments, and Silvia E.B. for the experimental and analytical help with the cell density experiments.

Finally, I would like to thank the LoFi girl, Yuka Kitamura, and Christopher Larkin for providing the soundtracks used during the writing of this thesis.

# Erklärung

Hiermit erkläre ich, dass ich die vorliegende Dissertation mit dem Titel:

**“ Protein diffusion in the cytoplasm of *Escherichia coli* “**

selbstständig verfasst, keine anderen als die im Text angegebenen Hilfsmittel verwendet und sämtliche Stellen, die im Wortlaut oder dem Sinn nach anderen Werken entnommen sind, mit Quellenangaben kenntlich gemacht habe.

Die Arbeit wurde in dieser oder ähnlicher Form noch keiner Prüfungskommission vorgelegt.

Marburg, den _____._____._____

_____

Nicola Bellotto